Functional and mechanistic insights into cytokine induced macrophage polarization

dissertation to obtain PhD Degree of Natural Sciences

submitted to Faculty 14, Biochemistry, Chemistry and Pharmacy,

Johann Wolfgang Goethe University in Frankfurt am Main

from

Sahil Gupta

(from Dehradun, India)

Frankfurt am Main (2018)

(D30)

Accepted from the faculty 14 of the

Johann Wolfgang Goethe - University as dissertation.

Dean: Prof. Dr. Clemens Glaubitz

Supervisor: PD Dr. Dmitry Namgaladze

Reviewer: Prof. Dr. Dieter Steinhilber

Date of the disputation:

Abbreviations

ChIP: Chromatin Immunoprecipitation

Co-IP: Co immunoprecipitation

CRISPRi: clustered regularly interspaced short palindromic repeats-interference

dCas9: dead CRISPR associated protein 9 (catalytically inactive)

IL: Interleukins

STAT: Signal transducer and activator of transcription

BATF: Basic leucine zipper transcription factor, ATF-like

CCL18: Chemokine (C-C motif) ligand

TGFA: Transforming growth factor alpha (TGF-α)

CD274/PDL-1: Cluster of differentiation 274/ Programmed death-ligand 1 (PD-L1)

NGS: Next generation sequencing

hMDMs: human monocyte derived macrophages

GRR: Genome regulatory regions

Index

Project I: IL-6 augments IL-4-induced polarization of primary human macrophages through synergy of STAT3, STAT6 and BATF transcription factors

1. Summary

Macrophages in the tumor microenvironment respond to complex cytokine signals. How these responses shape the phenotype of tumor-associated macrophages (TAMs) is incompletely understood. Here we explored how cytokines of the tumor milieu, interleukin (IL)-6 and IL-4, interact to influence target gene expression in primary human monocyte-derived macrophages (hMDMs). We show that dual stimulation with IL-4 and IL-6 synergistically modified gene expression. Among the synergistically induced genes are several targets with known pro-tumorigenic properties, such as CC-chemokine ligand 18 (CCL18), transforming growth factor alpha (TGFA) or CD274 (programmed cell death 1 ligand 1 (PD-L1)). We found that transcription factors of the signal transducer and activator of transcription (STAT) family, STAT3 and STAT6 bind regulatory regions of synergistically induced genes in close vicinity. STAT3 and STAT6 co-binding further induces the basic leucine zipper ATF-like transcription factor (BATF), which participates in synergistic induction of target gene expression. Functional analyses revealed increased MCF-7 and MDA-MB 231 tumor cell motility in response to conditioned media from co-treated hMDMs compared to cells incubated with media from single cytokine-treated hMDMs. Flow cytometric analysis of T cell populations upon co-culture with hMDMs polarized by different cytokines indicated that dual stimulation promoted immunosuppressive properties of hMDMs in a PD-L1-dependent manner. Analysis of clinical data revealed increased expression of BATF together with TAM markers in tumor stroma of breast cancer patients as compared to normal breast tissue stroma. Collectively, our findings suggest that IL-4 and IL-6

cooperate to alter the human macrophage transcriptome, endowing hMDMs with pro-tumorigenic properties.

Zusammenfassung

Makrophagen in der Tumor-Mikroumgebung reagieren auf komplexe Zytokinsignale. Wie diese Signale den Phänotyp tumorassoziierter Makrophagen (TAMs) prägen, ist jedoch nicht vollständig geklärt. Es wurde beschrieben, dass IL-4 und IL-6 synergistisch in Knochenmarks-Makrophagen der Maus (mBMDM) über die Aktivierung von *inositol-requiring enzyme 1* (IRE-1α), einem Marker der *unfolded protein response* (UPR), wirken. Diese Aktivierung steigert die Cathepsin-Freisetzung in mBMDMs durch Hochregulierung der in Golgi-Vesikeln angereicherten Faktoren *X-box binding protein* 1 (XBP1) und *activating transcription factor 6* (ATF6). Die Autoren beobachteten erhöhte Konzentrationen von sXBP1 in Wildtyp (WT) mBMDM im Vergleich zu STAT6 $^{-/-}$ oder STAT3 $^{-/-}$ BMDMs, was für sie ein Indiz war, dass Zytokin-induzierte nicht-kanonische UPR durch den IRE1α / XBP1-Signalweg die Sekretion von lysosomalen Proteasen fördert. Jedoch hat bisher keine Studie einen synergistischen Einfluss der Zytokine IL-4 und IL-6 auf die Zielgenexpression in primären, humanen, aus Monozyten generierten Makrophagen (hMDMs) unter Verwendung von *next-generation RNA sequencing* (RNA-Seq) untersucht.

In meiner Doktorarbeit konnte ich durch RNA-Seq-Experimente zeigen, dass die Stimulation mit IL-4 und IL-6 synergistisch die Genexpression beeinflusst. Die mit dieser Methode ermittelten Reads wurden auf das humane hg19-Genome ge*mappt* und mittels des DEseq2-Pakets in ‘R’ analysiert. Unter den synergistisch induzierten Genen befanden sich mehrere mit bekannten pro-tumorigenen Eigenschaften, wie CC-Chemokin-Ligand 18 (CCL18), transformierender Wachstumsfaktor-alpha (TGFA) CD274 (*programmed cell death 1 ligand 1* (PD-L1)) sowie andere Chemokine wie CCL8, CCL17 und CCL23. Um den Mechanismus dieser Synergie zu charakterisieren, untersuchten wir die Veränderungen in der Phosphorylierung und der nukleären

Translokation der Transkriptionsfaktoren *signal transducer and activator of transcription* (STAT)3/6. Wie beobachteten jedoch keine signifikanten Veränderungen in der Proteinphosphorylierung. Als nächstes testeten wir IRE-1α-abhängige (z.B. HERPUD1, XBP1s) sowie -unabhängige Stressmarker des endoplasmatischen Retikulums (ER) (GRP78, ATF6, ERJD4) in mBMDMs . Unsere Daten zeigen, dass die Expression von ER-Stress-abhängigen Genen nach IL-4/IL-6 Kosttimulation in hMDMs unverändert blieb, was auf eine speziesspezifische Diskrepanz verglichen mit mBMDMs hinweist.

In einem nächsten Schritt untersuchten wir, ob die Bindung von STAT3 und STAT6 in regulatorischen Regionen der synergistisch induzierten Gene nach dualer Zytokinstimulation ansteigen. Obwohl sich die STAT3- und STAT6-Bindung quantitativ nicht signifikant änderte, beobachteten wir, dass STAT3/STAT6 in enger Nachbarschaft (5-500 bp voneinander) an die jeweiligen regulatorischen Regionen binden. Nach einem Knockdown von STAT3 beobachteten wir eine Hemmung der Ko-Induktion von synergistisch induzierten Genen, was deutlich macht, dass die synergistische Induktion tatsächlich über STAT3-abhängige Mechanismen erfolgt. Wir stellten die Hypothese auf, dass die gleichzeitige Bindung von STAT3 und STAT6 andere Proteine induziert, die an der synergistischen Regulation beteiligt sein könnten. Um weiter zu überprüfen, ob STAT3- und STAT6-Bindung tatsächlich für die Zielgenexpression verantwortlich waren, blockierten wir die STAT3- und STAT6-Bindung durch CRISPRi Technologie spezifisch durch eine Modifikation der oben genannten Bindungsstellen. Darüber hinaus untersuchten wir, ob die alleinige Bindung von STAT3 und STAT6 an die Enhancer-Sequenz im CCL18-Gen eine verstärkte Genexpression fördert. Zu diesem Zweck klonierten wir den CCL18-Kernpromotor (-147 bp von der TSS) mit oder ohne Enhancer-Bindungsstellen in den

pGL3-basic Luciferase-Reportervektor und bestimmten die Firefly-Luciferase-Aktivität normalisiert auf Aktivität der kotransfizierten Renilla-Luciferase-Aktivität (SV40-pRL) als interne Kontrolle. Die Firefly-abhängige Luciferase-Expression war im Vergleich zum Core-Promotor allein signifikant erhöht, wenn gleichzeitig die Enhancer-Bindungsstellen vorhanden waren. Dies impliziert, dass die Enhancer-Sequenzen zur CCL18-Genexpression beitragen. Es gab jedoch keinen weiteren Anstieg in IL-4 versus IL-4/IL-6-stimulierten Proben. Wir nehmen an, dass dies höchstwahrscheinlich auf das Fehlen der epigenetischen Histonacetylierung zurückzuführen ist, da klonierten Vektoren die epigenetische Maschinerie fehlt und die Vektor-DNA in einem linearen und nicht in einem chromosomalen Zustand (wie er *in vivo* vorkommt) vorliegt. Da die epigenetische Modifikation stark mit der Transkriptionsfaktorbindung assoziiert ist, untersuchten wir H3K9ac-Spiegel nach Zytokinstimulation und fanden heraus, dass H3K9ac an den STAT3- und STAT6-Bindungsstellen nach dualer Stimulation ansteigt. Diese Experimente zeigten, dass unsere STAT3/STAT6-Bindungsstellen bei der synergistischen Induktion der Zielgenexpression funktionell relevant waren.

Um Mechanismen der synergistischen Genexpression weiter zu validieren, identifizierten wir Gene, die nach IL-4/IL-6- im Vergleich zur IL-4-Stimulation (| log2FC |> 1, p≤0.5) differentiell exprimiert waren. Wir beobachteten, dass der *basic leucine zipper ATF-like transcription factor* (BATF) synergistisch nach dualer Stimulation induziert wurde. Wir untersuchten mRNA- und Proteinspiegel von BATF, die unsere Ergebnisse bestätigten. Anschließend beobachteten wir eine erhöhte STAT3-, aber unveränderte STAT6-Bindung (2-10bp auseinander) nach dualer Stimulation (IL-4/IL-6) in regulatorischen Regionen des BATF Gens via ChIP, sowie eine reduzierte BATF-Expression auf mRNA-Ebene nach einem Knockdown von STAT3. Somit bestätigten

wir, dass die BATF-Induktion tatsächlich von der STAT3-Bindung abhängig war. Um zu untersuchen, ob BATF tatsächlich an der synergistischen Genregulation nach IL-4/IL-6-Stimulation beteiligt war, verwendeten wir eine BATF-siRNA-Knockdown-Strategie und zeigten, dass via IL-4/IL-6-Stimulation synergistisch induzierte Gene nach BATF-Knockdown gehemmt waren. Weiterhin identifizierten wir BATF-Bindungsstellen in den regulatorischen Elementen der Gene für CD274, CCL18 und PD-L1, mittles existierender ChIP-Seq-Daten (andere Zelllinien) und Online-Vorhersage-Tools (Jaspar). Eigene ChIP Analysen zeigten ebenfalls eine erhöhte BATF-Bindung in diesen Elementen sowie eine Erhöhung von H3K9ac nach dualer Stimulation im Vergleich zur alleinigen Stimulation mit IL-4. Ferner konnten wir zeigen, dass die Blockade von BATF-Bindungsstellen mittels CRISPRi die synergistische Induktion von CCL18 hemmte, was die Rolle von BATF bei der synergistische Geninduktion bestätigte.

Der durch IL-4 und IL-6 ko-induzierte BATF-Transkriptionsfaktor, der weiterhin mit STAT3 und STAT6 synergiert, könnte in vivo durch BATF3- oder IRF4-Bindung komplementiert werden. Wir stützen diese Hypothese auf unsere Beobachtung, dass BATF3 und IRF4 nicht nur synergistisch durch duale Zytokinstimulation induziert werden, sondern auch durch STAT3 und BATF reguliert werden, was wir durch siRNA-Knockdown-Experimente zeigen konnten. Darüber hinaus wurde zuvor gezeigt, dass BATF und IRF4 einen Komplex bilden können.

Funktionelle Analysen unserer Zielgene zeigten eine erhöhte MCF-7- und MDA-MB 231 Tumorzellmotilität in 3D-Chemotaxis-Assays als Reaktion auf konditionierte Medien von ko-behandelten (IL-4 und IL-6) hMDMs im Vergleich zu Tumorzellen, die mit Überständen von mit den einzelnen Zytokinen behandelten hMDMs inkubiert wurden. Durchflusszytometrische Analysen von T-Zellpopulationen nach Co-Kultur

mit hMDMs, die durch verschiedene Zytokine polarisiert wurden, zeigten, dass die duale Stimulation mit IL-4 und IL-6 immunsuppressive Eigenschaften von hMDMs föderte, was PD-L1-abhängig war. Wir stellten darüber hinaus fest, dass hMDMs nach dualer Stimulation die Aktivierung von ko-kultivierten $CD8^+$ -T-Zellen hemmten, was durch eine verringerte IFNγ-Sekretion und eine reduzierte Anzahl von $CD8^+$ aktivierten T-Zellen angezeigt wurde. Dieser Effekt war PD-L1-abhängig, da die Verwendung PD-L1-blockierender Antikörper die oben beschriebenen Phänotypen aufhob. Von Interesse war eine unerwartete, erhöhte IFNγ-Freisetzung bei Co-Kultur von T-Zellen mit IL-4-polarisierten hMDMs. Wir spekulieren, dass die erhöhte Expression von co-stimulatorischen Immunrezeptoren (CD40, CD80, CD86) und die mäßige Induktion von PD-L1 in IL-4-polarisierten hMDMs den Makrophagen-Phänotyp in Richtung Aktivierung von T-Zellen verschiebt. Dieser Effekt kehrte sich nach der dualen Zytokinbehandlungen durch synergistische Induktion von PD-L1 um, dessen immunsuppressive Effekte den co-stimulatorischen hMDM-Phänotyp, wie nach alleiniger Stimulation mit IL-4 beobachtet, außer Kraft setzen. Dies führt in Konsequenz zu einer verminderten IFNγ-Sekretion durch aktivierte $CD8^+$ T-Zellen und TH1-Zellen.

Im Anschluss analysierten wir klinische Daten von gesundem Gewebe im Vergleich zu Tumorstroma aus publizierten, öffentlichen GEO-Datensätzen. Deren Analyse zeigte eine erhöhte Expression von BATF zusammen mit dem TAM-Marker CD163 im Tumorstroma von Brustkrebspatienten im Vergleich zu normalem Brustgewebsstroma. Zusammenfassend legen unsere Ergebnisse nahe, dass IL-4 und IL-6 zusammenwirken um das Transkriptom humaner Makrophagen so zu verändern, dass sie pro-tumorigene Eigenschaften erhalten.

2. Introduction

Tumor is defined through its unrestrained proliferation marked by increased genome instability. A few hallmarks of cancer are defined by (I) prolonged proliferative signals by growth factor ligands or deregulating growth factor receptor structure or downstream signaling, (II) evading growth repressors, (III) invasion and metastasis activation (IV) indefinite replication potential, (V) induction of angiogenesis, and (VI) enabling apoptosis resistance[1, 2]. Apart from these classical hallmarks of cancer, a few emerging hallmarks include pro-tumorigenic inflammatory environment and avoiding immune cell mediated checkpoints through e.g. upregulation of immune inhibitory receptors. This helps the tumor resist the recognition and elimination by the adaptive immune system.

Crosstalk of tumor and immune cells is critical to promote tumor progression and metastasis [3-5]. A major outcome of this crosstalk is reshaping of gene expression landscapes and functional properties of tumor-resident and infiltrating myeloid cells, such as myeloid derived suppressor cells (MDSCs) or tumor-associated macrophages (TAMs) [6, 7]. MDSC are $CD33^{+}CD11b^{+}HLADR^{lo}$, lacking markers for mature hematopoietic cells[8]. MDSCs are derived from CMP (common myeloid progenitors) or GMP (granulocyte to monocyte progenitors) and may suppress both innate or adaptive immune responses by inhibiting T effector cells through arginase-1 , reactive oxygen species (ROS) or nitric oxide synthase (iNOS) expression and expanding T regulatory (Tregs) by releasing interleukin (IL-10) and transforming growth factor (TGFβ)[9-11]. As a result tumor myeloid cells promote tumor growth and invasiveness, support angiogenesis and help tumor cells evade immune surveillance mechanisms [12]. TAMs and MDSCs share many characteristics but are yet are two separate cell types. TAMs are sustained via circulating inflammatory monocytes

(CCR2^{+}CD14^{+}CD16^{-}) and are distinct from vessel patrolling monocytes (CD14^{dim}CD16^{-}CX3CR1^{hi}) in human tumors[6]. Although, MDSC (CD45^{+}CD11b^{+}CD33^{+}) and TAMs (CD45^{+}CD68^{+}CD115^{+}HLA-DR^{+}CD205^{+}) differ in their surface expression for receptor genes as measured by fluorescent activated cell sorting (FACS), they do share similar functional characteristics for tumor promoting phenotype. On one hand while MDSC suppress the innate and adaptive immune responses, TAMs share a tumor promoting phenotype via direct or indirect processes and are generally associated with poor patient prognosis. Interestingly MDSC also employ the CCR2/CCL2 signaling pathway as TAMs for their recruitment from bone marrow to the tumor site. TAMs and MDSCs can mediate tumor cell progression via (i) immune dysfunction, i.e. impairing T cell functions through inducing T cell apoptosis or anergy as well as recruiting Tregs or (ii) non-immune related mechanisms. These include induction of angiogenesis by releasing VEGF and MMP9, promotion of metastasis via release of cathepsins, chemokines, metalloproteases or induction of chemotherapy resistance via increasing expression of latency/tumor-stemness genes with distinct pro-tumorigenic properties [13, 14] (Fig. 1). TAMs may also promote malignant cell evasion from the antibody-dependent cell-mediated phagocytosis by activating inhibitory immunoglobulin Fc receptors (FCGR2B/ CD32b) or inhibiting activation receptors (FCGR1A/CD16, FCGR3A/CD64) [15]. Among immunosuppressive mechanisms exerted by tumor myeloid cells, surface expression of a T-cell inhibitory receptor, programmed cell death 1 ligand 1 (PD-L1) (synonym CD274), is prominent in TAMs, MDSCs as well as in tumor cells. PD-L1 expression is induced by IFNγ or under hypoxic conditions [16, 17 18]. Induction of PD-L1 induces T cell anergy or inhibits cytotoxic T lymphocyte activation[19-22], thereby facilitating tumor progression.

Pro-tumorigenic phenotype remodeling of tumor-infiltrating myeloid cells is greatly influenced by soluble factors secreted by tumor and stromal cells, such as chemokines, cytokines, and metabolites. For instance, breast tumor cells release high amounts of lactate and GM-CSF, switching TAMs towards a pro-metastatic phenotype characterized by high levels of CCL18 secretion [13, 23]. Another prominent cytokine of the tumor microenvironment is interleukin-6 (IL-6) [24], which acts either pro- or anti-inflammatory in a context-dependent manner. IL-6 binds to the IL-6 receptor α chain and transduces downstream signaling via gp130 receptor that recruits Jak2 tyrosine kinases and signal transducer and activator of transcription 3 (STAT3) transcription factors. Activated STAT3 induces IL-6 target genes, such as suppressor of cytokine signaling 3, in human monocyte-derived macrophages (hMDMs). IL-6 is released in the tumor microenvironment by tumor as well as stromal cells, including fibroblasts, endothelial cells, and macrophages [25-28]. The mode of IL-6 action is influenced by its cooperation with other cytokines. For example, cooperation of IL-6 with IL-1β and TNFα potentiates pro-inflammatory outcomes, whereas complementing IL-6 with IL-4/IL-13 is anti-inflammatory [24, 29, 30]. Similarly, the cytokines IL-4 and IL-13, released by adipose tissue, Th2 T cells as well as tumor cells in breast, pancreatic, and glioblastoma cancers [31, 32] can polarize TAMs towards an anti-inflammatory phenotype to support tumor progression and metastasis [33-35].

The exact mechanisms of cytokine-cytokine interactions are only recently being explored. How combinations of cytokines and other soluble factors of the tumor microenvironment shape the TAM phenotype is poorly understood. Investigating different cytokine polarization patterns gives insights into designing effective therapies to reprogram TAMs towards anti-tumor phenotypes [36]. Recently, a study investigating the mechanism for IL-4 and IL-6 synergy in mBMDMs reported [37] that these cytokines

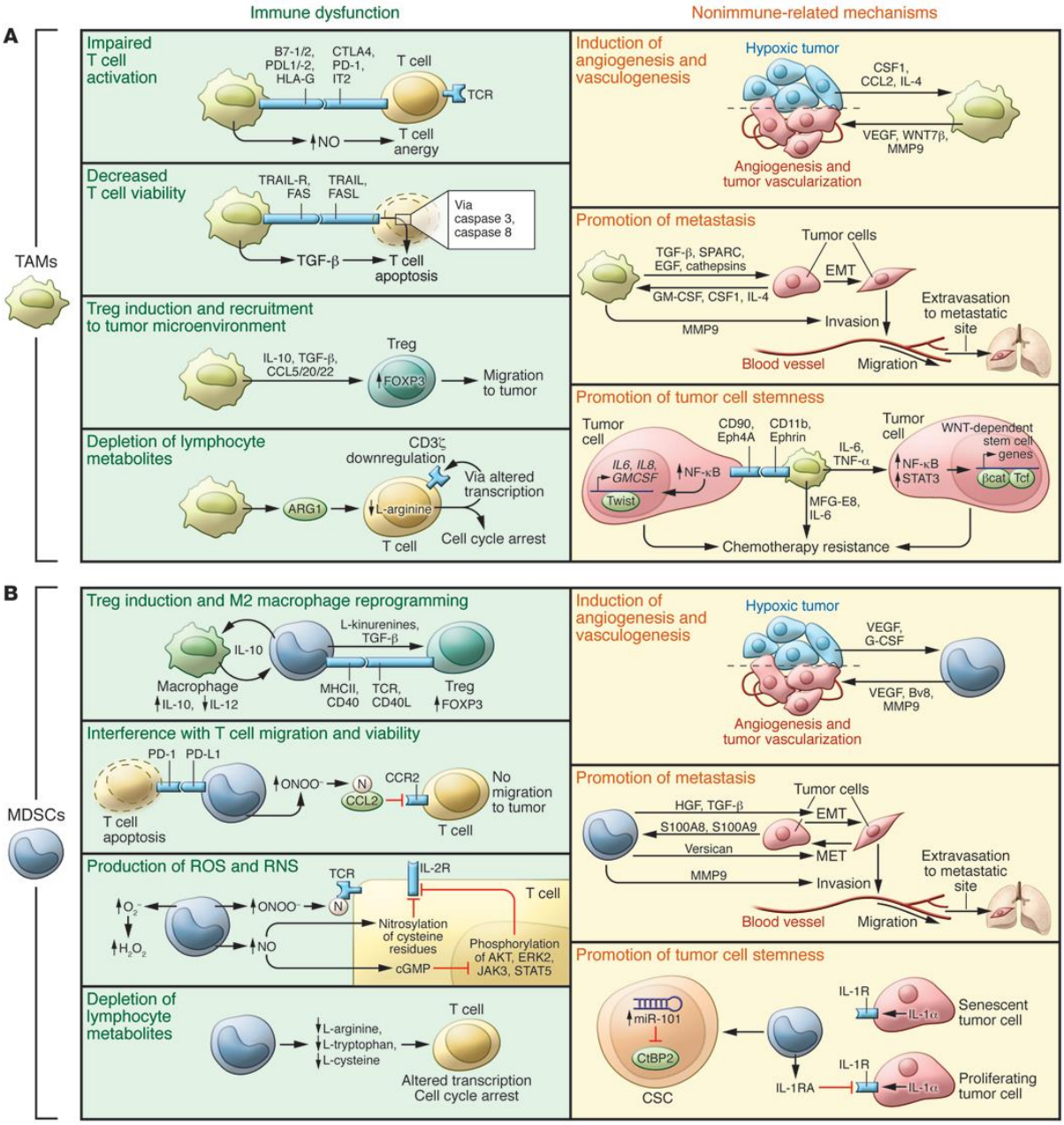

Figure 1: Mechanism governing (A)TAMs and (B) MDSCs mediated tumor progression (adapted from Ugel S et.al, JCI, 2015)

synergize via activation of inositol-requiring enzyme 1 (IRE-1α), a marker of unfolded protein response (UPR). This activation promoted cathepsin secretion in mouse BMDMs by upregulation of golgi vesicle enriched XBP1 and ATF6. During classical UPR activation, release of ER-resident GRP78 chaperone from IRE-1α promotes its

oligomerization and auto-phosphorylation. This allows IRE-1α to catalyze the excision of a 26-nucleotide intron XBP1 RNA, resulting in spliced 33KDa (sXBP1) variant, which is an active transcription factor regulating the expression of multiple UPR target genes. The authors found increased levels of sXBP1 in wild type (WT) compared to $STAT6^{-/-}$ or $STAT3^{-/-}$ BMDMs. Yan et.al suggested that cytokine-induced non-canonical UPR through IRE1α/XBP1 pathway promotes the secretion of lysosomal proteases by re-routing the pro-form of cathepsins through ER.

Another example of cytokine interactions as commonly seen in tumor microenvironment was depicted by antagonism of IFNγ-stimulated transcriptional response by IL-4 and vice versa in BMDMs [38]. It was demonstrated that the cytokines of opposing polarizations IL-4 and IFNγ show extensive epigenomic and cross transcriptional inhibition. The responses were stratified based on IFNγ sensitive (IFNγ target genes inhibited by IL-4), IFNγ resistant (IFNγ target genes unaffected by IL-4), IL-4 sensitive (IL-4 target genes inhibited by IFNγ) and IL-4 resistant (IL-4 target genes unaffected upon IFNγ stimulation). STAT1 and IRF1 were associated with IFNγ resistant response to IL-4, however when co-bound with auxiliary factory such as AP-1, were sensitive to IL-4 mediated inhibition. Through further computational and functional analysis, the authors conclude that IFNγ resistant regulatory elements were enriched for IFNγ induced *MafB* motifs whereas that of IL-4 resistant regulatory elements for IL-4 induced Myc transcription factor binding motif [38]. The authors argue that the inhibitory effects of IL-4 on IFNγ sensitive enhancers are explained IL-4 induced MafB transcription factor that combats IFNγ induced inhibitory effects on enhancers at IL-4 target genes. Nevertheless, Myc and STAT6 levels were comparatively higher to *MafB* in IL-4 resistant enhancers. Furthermore, the authors found that IL-4 stimulated Myc levels were relatively constant and not inhibited after

IFNγ co-stimulation in IL-4 resistant group. This suggested that Myc rather than MafB might confer resistance to antagonistic signals by IFNγ. In another study, authors extracted macrophages from rheumatoid arthritis (RA) patients reported the role of IFNγ mediated disassembly of enhancers bound by transcription factor Maf. IFNγ stimulation displaces Maf bound on anti-inflammatory (M2-like genes) macrophages. This underlies that IFNγ induced inflammatory signals in RA patients displace Maf TF further correlating low *Maf* levels with a negative and inflammatory signature in rheumatoid arthritis patients compared to control group[39].

Goldstein I et.al highlights the importance of transcription factor (TF) assisted loading by IL1β induced NF-κB binding. IL1β and IL-6 can activate or inhibit genes upon co-stimulation during acute phase response. IL1 βinduced NF-κB binds and primes a subset of enhancers for efficient STAT3 binding upon IL-6 stimulation in primary mice hepatocytes [40], thereby mediating synergistic gene expression.

However, the mechanism of how IL-6 enhances inflammatory (TNFα, IL1β, LPS) or anti-inflammatory (IL-4, IL-13) phenotypes in a context dependent mannerduring hMDMs polarization remains unclear. In this study, we address the mechanistic and functional aspects of how IL-6 interacts with IL-4 in hMDMs, explore co-regulated target genes and reveal the differences between murine and human macrophages.

3. Aims of the study

Complex cytokine signals can shape polarization and activation status of stromal and immune cells in tumor microenvironment. Here, we study the effects of two such cytokines that are established M(IL-4) and M(IL-6) macrophage polarization cytokines. Recently IL-6 has been shown to be a context specific cytokine that can enhance the inflammatory M1(TNF-α, IL1β, LPS) or anti-inflammatory phenotype M2(IL-4, IL-13) phenotype of macrophages[41]. However, no report has yet established the mechanism of cytokine synergism in IL-4/IL-6 polarized hMDMs. Therefore, we planned to explore the mechanism and functional consequence of IL-4 and IL-6 mediated hMDMs polarization via high throughput RNA seq, ChIP, CRISPRi and in vitro activity assays.

4. Materials and Methods

4.1 Materials

4.1.1 Cells

Primary human macrophages: Buffy coats of healthy donors were collected from a local blood donation facility (Deutsche Rotes kreuz-Blutspendedienste) and cultured in RPMI-1640, 3% heat-inactivated human serum.

MDA-MB-231, adenocarcinoma metastatic breast, mesenchymal like, cancer epithelial cells and MCF-7, adenocarcinoma metastatic breast, luminal like, cancer epithelial cells were grown in RPMI, 10% FCS, 1% penicillin/streptomycin, non-essential amino acids (1%) and sodium pyruvate (1%)

SKBR3: adenocarcinoma metastatic breast cancer epithelial cells were grown in DMEM, 10% FCS, 1% penicillin/streptomycin, non-essential mino acids (1%) and sodium pyruvate (1%), 1% glutamax.

4.1.2 Bacteria

For CRISPR-Cas9 cloning DH-5α strains were used. XL-10 super-competent cells used for cloning Luciferase firefly >200bp deletion constructs. Stellar cells were used for Agilent Quick site-directed mutagenesis Kit II 10bp deletions.

4.1.3 Plasmids

pGL3 luciferase reporter basic vector (Promega, E1751) was used to clone CCL18 core promoter (147bp upstream of transcription start site (TSS) and enhancer (7.4-8.5

Kb upstream of TSS) with STAT3 and STAT6 binding sites (873bp length between sites).

1. Core promoter: CCL18 core promoter was cloned in pGL3 basic vector
2. Core prom. +enhancer: 147 bp CCL18 core promoter cloned with 873 bp enhancer
3. CE_S3del(10bp): 10bp of STAT3 binding in the enhancer were deleted from core+ enhancer cloned vector
4. CE_S6del(10bp): 10bp of STAT6 binding in the enhancer were deleted from core+ enhancer cloned vector
5. CE_ S3del (280bp): 280bp of region around STAT3 biding was deleted from core+ enhancer cloned vector
6. CE_S6del (358bp): 358 bp of region around STAT3 biding was deleted from core+ enhancer cloned vector
7. pRen-SV40: Renilla luciferase vector was used as transfection control under transcriptional control of T7 promoter and late SV40 poly(A) signal sequence. (#E2231, Promega)

   For CRISPR interference we used following plasmids
8. sg-MS2: Empty sgRNAs cloning vector (Addgene #61424)
9. pHAGE EF1α dCas9-KRAB plasmid (Addgene #50919): Vector expressing dead Cas9 fused with KRAB repressor domain

4.1.4 Primers

Primers were bought from biomers.net GmbH (Ulm). Complete list of primers is available in the Tables 1-4.

Table 1: List of Chromatin immunoprecipitation (ChIP) primers		
Gene_TF binding	**Forward Primer**	**Reverse primer**
CCL18_STAT3	GGTGTAATAACACGTTGAGAGGCAGAG	CTGCACTCTAGCTTCAGTGACAGAG
CCL18_STAT6	GCTGGGATTATAGGCCTGAGACAC	GCAGCCTAGAAAGCCAAAACTGAAG
TGFA_ STAT3 STAT6	ACAGTACTCGAGGTTTCTGGAAATGG	GCAACTGTGGCATCTTTTTGCGT
CD274_STAT3 STAT6	GAGCTTCCCAACTCAGGGAAGTAG	GGTGAGTAAACTCCTGTGGGGA
BATF_STAT3 STAT6	ATGAGTCTGGGTGGAGACCTCTA	TGTGGTAGGAGGTCATTGGCATAG
CCL18_BATF-1	ACAGTCTAGCAAGGACTCCTTACCT	GTAAATCCACTTCTCTGGCCACAAAG
CCL18_BATF-2	TTCAGAGGCACTGCAACTCCG	AGTGCTGTGCTGGAAGAGACG
CD274_BATF-1	TGTGAATTAAAGTTGTGCCAGC	ACTGACGTGAGAGACCTAGATGA
CD274_BATF-2	GAGGCAGAAGGAAGGATGGTACTG	TGTCCTCAGGTGAGTCATGTTCAC
TGFA_BATF-1	CCTTGAAGCTGGGGAACAGTCA	CCCCGGTGTCATCCTTGAACAC

TGFA_BATF-2	ATGTTCTGACTTCGCTGGCACT	GGCAGTTTGTGACAGGCAAGTC

Table 2: List of Real time primers		
Gene	Forward	Reverse
CCL18	CCCAGCTCACTCTGACCACT	GTGGAATCTGCCAGGAGGTA
CCL17	TTCTCTGCAGCACATCCACG	TGTTGGGGTCCGAACAGAT
TGFA	AGGTCCGAAAACACTGTGAGT	AGCAAGCGGTTCTTCCCTTC
CD274	TGGCATTTGCTGAACGCATTT	TGCAGCCAGGTCTAATTGTTTT
CCL8	ACTTGCTCAGCCAGATTCAGTT	TGACCCATCTCTCCTTGGGG
CCL23	TCTCATGCTGCAGGATTCCAT	TTGGTGAGGAAGATGACACCC
FCGR2B	AGCCAATCCCACTAATCCTGA	GGTGCATGAGAAGTGAATAGGTG
FCGR1A	AGCTGTGAAACAAAGTTGCTCT	GGTCTTGCTGCCCATGTAGA
FCGR3A	CCTCCTGTCTAGTCGGTTTGG	TCGAGCACCCTGTACCATTGA
BATF	CCCTGGCAAACAGGACTCAT	TCTGGGCGGCAATACGATTT
CTS B	CTCCTGCTGGCTGTAATGGT	GGATGGAGTACGGTCTGCAC
CTS C	CAAACTGGCCATGAACAGACG	CTGCCTTGGAGGTAGGTCAC
CTS L	GAACCCAGACCCGAGGTTTT	CTGGTGCACACCTACTCGAC
CTS Z	CCAAGGACCAGGAGTGTGAC	ATTCGGCATAGATGCCTCCG

HERPUD 1	CCAAAGCAGGAAAAACGGCA	CCTCAGGATACTGTCCCCGA
XBP1s	CTGAGTCCGCAGCAGGTG	GGCTGGTAAGGAACTGGGTC
XBPU	AGTTAAGACAGCGCTTGGGG	TGCACGTAGTCTGAGTGCTG
GRP78	ACTCCTGCGTCGGCGTGTTC	ACGGGTCATTCCACGTGCGG
ATF6	ACGGAGTATTTTGTCCGCCT	CCAGCCTGTGAAAGAGTCCC
ERDJ4	GTCGGAGGGTGCAGGATATT	CTTCAGCATCCGGGCTCTTA

Table 3: List of luciferase gene primers	
Gene	Primer
XhoI_Fw	CGTGCTAGCCCGGGCGGCTGTGACCACTCATTTCTGAGAAATATCT GTCA
HindIII_Rv	CCGGAATGCCAAGCTCTCCTGGCCTCCTTCTGGGGTATGAG
RT Luci Fw	ATTTATCGGAGTTGCAGTTGCGCC
RT Luci Rv	GCTGCGAAATGCCCATACTGTTGA
Kpni Fw	TCTATCGATAGGTACTGACCTGGCTGATTGGAACCAGAATGC
Saci Rv	GCTAGCACGCGTAAGCAGGCCTTACAATGGAGATAGCAGCCTAGA
S6DelVr-F1	TCTTAACTCATATTACTTGACTTATTTTTTAAAAAAGTAAAGATGCA
S6DelVr-R1	TAATATGAGTTAAGAACTTTCGTGTATTGGCTCAT
S3DelVr-F1	TTAAATCTGTTCTAGCTTAACTCATATTAACTTCTCTATAAATTTAAG TC
S3DelVr-R1	CTAGAACAGATTTAACCTGACATTTCCTGTTCC

S310bpDel Fw	CCCACCACTGCTAATTATAGATTCTGTAAACTCTCCAGACTC
S310bpDel Rv	GAGTCTGGAGAGTTTACAGAATCTATAATTAGCAGTGGTGGG
S610bpDel Fw	CTTTTTTAAAAAATAAGTCAAGACGAAGCTGGGCGCAGTGTCT
S610bpDel Rv	AGACACTGCGCCCAGCTTCGTCTTGACTTATTTTTTAAAAAAG

Table 4: List of CRISPRi sgRNAs		
Gene_TF binding	**sgRNA against TF binding sites**	**Genomic locations of 20bp sgRNAs targeting TF binding (hg 38)**
CCL18 STAT3	CCACTGCTAATTATAGAGTT	chr17:36056227-36056246
CCL18 STAT6-1	GCCCTCTGGGAGACTGAGAT	chr17:36056647-36056666
CCL18 STAT6-2	TTTCTTCAGAACAACTTGAA	chr17:36059471-36059490
CD274 STAT3 STAT6-1	CCATATGCAAATGATTTCAC	chr9:5459473-5459492
CD274 STAT3 STAT6-2	TAACCTGACTTCCTGGAAAA	chr9:5490291-5490310
TGFA STAT3 STAT6-1	GTACTCGAGGTTTCTGGAAA	chr2:70516058-70516077

TGFA STAT3 STAT6-2	GCGATTTCTTGCATCATCAT	chr2:70479954-70479973
TGFA STAT3 STAT6-3	ATCCAAATTCCTGGAATTTC	chr2:70524460-70524479
CCL18 BATF	TTACAGCCCACAGTCTAGCA	chr17:36074500-36074519

4.1.5 Antibodies

Table 5: List of Antibodies		
Antibodies	**Provider**	**Catalogue number**
WB/IP/Co-Immunoprecipitation		
p-STAT6	Cell signaling Technologies (CST)	9361
STAT6	CST	5397
pSTAT3	CST	9131
STAT3	CST	9139
Nucleolin	Santa Cruz	sc-13057
BATF (WW8)	Santa Cruz	sc-100974
Goat α-rabbit IRdye 800	LI-COR	925-32211
Goat α-mouse IRDye 800	LI-COR	925-32210
β-Actin	Sigma-Aldrich	A5316
Histone 3	Merck Millipore	06-755
Tubulin	Sigma-Aldrich	T9026

Human/Mouse/Rat Cathepsin X/Z/P	R&D Systems	AF934-SP
Cathepsin S	R&D Systems	AF1183-SP
Cathepsin L	R&D Systems	MAB9521-SP
Cathepsin B	R&D Systems	AF953-SP
MMP12 [EP1261Y]	Abcam	Ab52897
FACS		
CD16 (BV650)	BD Biosciences	563692
CD32 (PE)	BD Biosciences	303205
CD64(BV605)	BD Biosciences	305033
PD-L1 (APC)	BD Biosciences	329707
CD3 (BV605)	BD Biosciences	563219
CD4 (BV650)	BD Biosciences	563737
CD127 (PerCP-Cy-5.5)	BD Biosciences	560551
CD8 (APC-H7)	BD Biosciences	641400
CD44 (Alexa Fluor 700)	Biolegend	103025
CD279/PD-1 (Brilliant Violet 421)	Biolegend	329919
CD152/ CTLA-4 (PE)	Biolegend	369603
CD366/TIM3(APC)	Biolegend	345011
CD223/LAG3 (Alexa Fluor 488)	Biolegend	369325
CD25(PE-Cy7)	BD Pharmigen	557741
Cytometric Bead Array		

IL-10	BD Biosciences	#558274
IL-4	BD Biosciences	#558272
IL-6	BD Biosciences	#558276
IFNγ	BD Biosciences	#558450
Chromatin Immunoprecipitation		
STAT6	Santa Cruz	sc-981
STAT3	Santa Cruz	sc-482
BATF	CDI/ Neo-biotechnologies	m14-108
H3K9acetylation	Merck Millipore	06-942
Activity Assays		
α-PD-L1 Atezolizumab Humanized Antibody	Biovision	A1305-100
Trastuzumab/Herceptin (25µg/µl)	Roche	Order through MTA

4.1.6 Cytokines

Table 6: List of cytokines		
IL-4	ImmunoTools	11340043
IL-6	ImmunoTools	11340064
IL-10	ImmunoTools	11340103
IL-13	ImmunoTools	11340133
IL-2	ImmunoTools	11340025

4.1.7 Chemicals, reagents, plastic and kits

Table 7: List of kits and reagents		
Kits and Reagents	**Company**	**Catalogue**
iQ custom SYBR green Supermix	Biorad	172-5006CUST
Maxima First Strand cDNA Synthesis Kit for RT-qPCR	ThermoFisher Scientific	K1642
QIA Ampure purification kit	Qiagen	28106
DC Protein Assay Reagent A	Biorad	500-0113
DC Protein Assay Reagent B	Biorad	500-0114
Nitrocellulose membranes	GE Healthcare	10600002
Whatman Gel blotting paper	Sigma	10426892
Human IFNγ CBA Flex set Kit	BD Biosciences	558269
PfuUltra II Fusion HS DNA Polymerase	Agilent	600670
5X passive luciferase lysis buffer	Promega	E1500
Pan-CD3 T cell isolation kit (MACS)	Miltenyi Biotec	130-096-535
Dynabeads (protein G)	Thermofisher Scientific	10003D
NucleoSpin RNA extraction kit	Macherey-Nagel	740955.250
Qubit HS RNA Assay Kit	Thermofisher Scientific	Q32852
Qubit dsDNA HS Assay Kit	Thermofisher Scientific	Q32854
TruSeq Stranded mRNA LT - SetB library preparation kit	Illumina	RS-122-2102

NextSeq 500/550 High Output Kit v2	Illumina	FC-404-2005
A/G agarose beads	Santa Cruz	sc-2003
CL4B Sepharose beads	Sigma-Aldrich	CL4B200-100ml
NucleoSpin RNA extraction kit	Macherey-Nagel	740955.250
Qubit HS RNA Assay Kit	Thermo Fisher Scientific	Q32852
TruSeq Stranded mRNA LT - SetB	Illumina	RS-122-2102
Qubit dsDNA HS Assay Kit	Thermo Fisher Scientific	Q32854
NextSeq using 500/550 High Output Kit v2, 75cycles	Illumina	FC-404-2005

Table 8: List of Enzymes and buffers

Enzymes and Buffer	**Company**	**Catalogue**
XhoI	New England Biolabs (NEB)	R0146S
HindIII	NEB	R0104S
KpnI	NEB	R0142S
ScaI	NEB	R0122
DpnI	NEB	R0176S
BbsI-HF	NEB	R3539S
T4 Ligation Buffer	NEB	B0202S
T4 PNK	NEB	M0201S
10X Tango Buffer	Thermofisher Scientific	BY5

T7 DNA ligase	NEB	M0318S
Plasmid-Safe™ ATP-Dependent DNase (Exonuclease)	Epicentre/Lucigen	E3101K
5X Infusion HD Enzyme	Clonetech Takara	638909
PfU Ultra HF DNA Polymerase (2.5U/µl)	Agilent	600380
Rnase A (100µg/µl)	Qiagen	19101
Proteinase K (20µg/µl)	Qiagen	19131
DMEM	Sigma-Aldrich	D5546
RPMI	Sigma-Aldrich	R0883
Fetal bovine serum	Capricon	FBS-11A
Sodium Pyruvate	Thermofisher Scientific	11360070
MEM Non-Essential Amino acids	Thermofisher Scientific	11140035

Table 9: List of Chemicals		
Chemicals	**Company**	**Catalogue**
Tris	Sigma-Aldrich	T1503
$(MgCO_3)_4Mg(OH)_2.5H2O$	Sigma	M5671
$MgSO_4.7H_2O$	Carl Roth	P027.1
EDTA	Applichem	A3553
DTT	Applichem	A1101
Coenzyme A	Sigma	C3019
Luciferin	Sigma	L9504
ATP	NEB	P0756S

NaOH	Sigma-Aldrich	A1551
$NaHCO_3$	Fluka	71628
Collagen	ibidi	50201
Bis/Acrylamide	Carl Roth	T802.1
SDS pellets	Carl Roth	CN30.3
APS	Sigma-Aldrich	A3678
TEMED	Carl Roth	2367.1
NaCl	Sigma	EC 201-064-4
Glycerol	Sigma-Aldrich	G5516
Bromophenol Blue	Applichem	A2331
NP-40	Applichem	A1694
NaF	Applichem	A3904
Na_3VO_4	Applichem	A2196
Triton X-100	Carl Roth	3051.4
LiCl	Carl Roth	3739.1
Sodium deoxycholate	Sigma-Aldrich	D6750
KCl	Sigma-Aldrich	P9541
HEPES	Sigma-Aldrich	H3375
Tween-20	Carl Roth	9127
Chloroform	Sigma-Aldrich	3211
Methanol	Fischer Scientific UK	M14000/PC17
Ethanol	Sigma-Aldrich	32205
Propanol-2	Fischer Scientific UK	A416P-4
Paraformaldehyde	Merck	1040051000

PMSF	Applichem	A0999.0100
$CaCl_2$	Carl Roth	6751.1
Milk powder	Carl Roth	T145.2
DEPC	Applichem	A0881

Table 10: List of Instruments	
Instruments	**Company**
Biorad Transblot Turbo transfer system	Biorad
PowerPac™ HC High-Current Power Supply	Biorad
Mithras LB 940 (Luciferase)	Berthold
Apollo 11 LB 913 Absorbance Reader	Berthold
Nanodrop ND-1000	Thermo fisher Scientific
BD LSRFORTESSA (FACS)	BD Biosciences
CFX96 Touch™ Real-Time PCR	Biorad
Branson Digital Sonifier® Cell Disruptor	Branson Ultrasonic
Centrifuge 5415 R, 5424 R and 5810 R	Eppendorf
Master Cycler Nexus Gradient	Eppendorf
Bacteria Shaker	Innova® S44i
Odyssey Infrared Imaging	LI-COR Biosciences

Table 11: List of softwares	
Software	**Company**
Corel Draw Graphic Suite 17	Core Corporation
R package	R Foundation for Statistical Computing

Graph Pad Prism	GraphPad Software, Inc.
Endnote	Thomas Reuters Endnote
Fastqc	Babraham Bioinformatics
Image Studio Lite	LI-COR Biosciences
CFX Manager	Biorad
Xcelligence	Roche, Acea Bio

4.1.8 Buffers

Table 12: Reverse transcription buffer	
5X reaction mix (K1642) buffer	2µl
Maxima Enzyme mix (K1642)	1µl
RNA	1µg
Nuclease-free water	Adjust to final reaction volume of 10µl

Table 13: Chromatin Immunoprecipitation buffers	
Farnham Lysis Buffer (Cell Lysis)	
HEPES pH8	5mM
KCl	85mM
NP-40	0.5%
Add PI and PMSF before use	
RIPA Buffer (Nuclear Lysis)	
NP-40	1%
Sodium deoxycholate	0.5%

SDS	0.1%
PBS	1X
Tris-EDTA (TE)	
Tris-HCl pH7.5	100mM
Na_2EDTA	0.1mM
Magnetic Dyna beads	
Dynabeads (protein G) Novex Life Technologies #10003D	
PBS/BSA	1X PBS, 5mg/ml BSA (fresh)
IP Elution buffer	
SDS	1%
$NaHCO_3$	0.1M
Reversion Mix (Decrosslinking) per sample	
Chemical	Working concentration
NaCl	1.9M
Tris/HCl pH 6.8	0.38M
EDTA	100mM
RNase A	10µg
Proteinase K	10µg
Total Volume	42µl
Dilution buffer	
0.01% SDS, 1.1% Triton X 100, 1.1mM EDTA, 20mM Tris-HCl pH 8.0, 167mM NaCl	
Low salt buffer	
0.1% SDS, 1% Triton-X100, 2mM EDTA, 20mM Tris-HCl pH 7.4, 150mM NaCl	
High salt buffer	

0.1% SDS, 1% Triton-X100, 2mM EDTA, 20mM Tris-HCl pH 7.4, 500mM NaCl
LiCl wash buffer
250mM LiCl, 10mM Tris-HCl, pH7.4, 1% NP-40, 1% sodium deoxycholate, 1mM EDTA

Table 14: Co-immunoprecipitation buffer
CoIP buffer
1 % Triton-X 100
20 mM HEPES, pH 7,5
150 mM NaCl
10 % Glycerin
1 mM EDTA

Table 15: Total cell lysis buffer
Components
50mM Tris/HCL
150mM NaCl
5mM EDTA
10mM NaF
1mM Na_3VO_4
0.5% NP-40
Add Phenylmethylsulfonyl fluoride (1mM PMSF and 1mM complete EDTA free protease inhibitor.

Table 16: Nuclear translocation lysis buffer		
Component	**Lysis Buffer A**	**Lysis Buffer B**
Tris (pH 8)	20mM	20mM
NaCl	10mM	400mM
EDTA	5mM	5mM
NP-40	0.5% (with A+ or without A-)	0.5%
Add PMSF (1:500) and PI (1:50) before use		

Table 17: Polyacrylamide gel electrophoresis (PAGE) buffers		
10X SDS Running Buffer		
Components	Working Solution	For 1L
Glycine	1.92M	144g
Tris	250mM	30,3g
SDS	35mM	10g
Dilute to 1X with ddH_2O		
5X Dye Loading buffer		
Component (Stock)	Working solution	
Tris pH 6.8 (0.5M)	5ml	
SDS (10%)	10ml	
Glycerin	5ml	
Bromophenol blue	10mg	
DTT	50mM (7.7mg/ml)	
Dilute to 1X in cell lysate before loading		

10X Blotting Buffer, pH 8.3				
Tris		30,3g		
Glycine		144g		
1X Blotting Buffer				
10X blotting buffer		100ml		
Methanol		200ml		
H_20		700ml		
10X TBS Buffer, pH 7.4		Working Solution (1L)		
Tris HCL pH 7.4		100mM, 12.11g		
NaCl		9%, 90g		
1X TTBS Washing buffer				
10X TBS		100ml		
Tween20 (20%)		5mL		
ddH_20		900ml		
Blocking Buffer		Working solution, 250ml		
Milk/BSA		5% (12.5g)		
1X TTBS		250ml		
Sodium Azide (10%)		0.1%		
Running Gel				
Component	6.5%	8%	10%	15%
Water	5.665 ml	5.4 ml	4.9 ml	3.65 ml
1.5M TrisHcL (pH8.8)	2.5 ml	2.5 ml	2.5 ml	2.5 ml
40% Bis/Acrylamide	1.625 ml	2 ml	2.5 ml	3.75 ml
10% SDS	100µl	100µl	100µl	100µl

10% APS	100µl	100µl	100µl	100µl
TEMED	10µl	10µl	10µl	10µl
Stacking Gel (1x)				
Water	3.2 ml			
0.5M TrisHcL (pH8.8)	1.25 ml			
40% Bis/Acrylamide	500 µl			
10% SDS	50 µl			
10% APS	50 µl			
TEMED	5 µl			

Table 18: List of firefly luciferase reaction buffers		
Recipe for D Luciferase (1L)		
20 mM Tricine	MW: 179.2	3.6g
1.07 mM $(MgCO_3)4Mg(OH)_2.5H2O$	MW: 485.7	.52g
2.67 mM $MgSO_4$	MW: 485.7	.66g
0.1 mM EDTA	MW: 372.24	37.224mg
33.3 mM DTT	MW:154.25	5.136g
270 µM Coenzyme A	MW: 767.53	.2072g
470 uM Luciferin	MW: 280.32	.132g
530 uM ATP	MW: 605.2	.320g
Renilla Substrate Recipe		
Tris-HCL (25mM), NaCl(100mM) $CaCl_2$ (1mM), pH 7.8 in 500ml		

4.2 Methods

4.2.1 Cell Culture and Stimulations:

Peripheral blood mononuclear cells (PBMCs) were isolated from buffy coats supplied by DRK-Blutspendedienst Baden-Württemberg-Hessen (Frankfurt, Germany) using Ficoll density centrifugation. 15ml Ficoll was centrifuged in LeucoSep Falcons. Approximately 20ml of blood was aliquoted in each falcon and volume was refilled with PBS/EDTA (2mM) up to 50ml. The buffies were then centrifuged at 440g, for 35mins, 9 accelerations, 2 brakes at room temperature to separate erythrocytes, granulocytes, PBMCs and plasma. The PBMC layer was carefully transferred into new 50ml falcons and washed twice with PBS/EDTA. The pellet was resuspended in 50ml serum-free RPMI-1640 media and plated on Cell^{+} (Starstedt, 83.3920.300) coated plates. PBMCs were cultured for 1-2h in serum-free RPMI media and differentiated for 7-8d in RPMI-1640 medium containing 3% heat-inactivated AB-positive human serum, with media changed every 2-3 days. Differentiated hMDMs were stimulated for 24h with 20ng/ml of IL-4 and/or IL-6 (Immunotools).

Studies conform to the principles outlined in the Declaration of Helsinki and were approved by the ethics committee of the faculty of medicine at Goethe-University Frankfurt.

4.2.2 Real Time PCR

Total RNA from hMDMs was isolated using PeqGold RNAPure kit (PeqLab). 1ml of Peqgold was added to hMDMs for 15mins and vortexed with 200µl of chloroform for 15secs. The mix was incubated on ice for 5mins and centrifuged at 12,000g for 15mins at 4^{o}C. The top aqueous layer was carefully transferred to a new tube and vortexed with 500µl of isopropanol. The mixture was incubated on ice for 15mins or -20^{o}C

overnight to precipitate the RNA. The mixture was again centrifuged to pellet the RNA at 12,000g for 15mins at 4^{o}C. The white pellet was washed twice with 70% ethanol at 12,000g for 10mins at 4^{o}C. The supernatant was decanted, and the pellet was dried by incubating at 70^{o}C. The pellet was resuspended in 20µl of DEPC-treated water by shaking at 65^{o}C. The RNA was then quantified using Nanodrop and 1µg of RNA was reverse transcribed using cDNA Synthesis kit with following protocol

Table 19: PCR reaction cycles of reverse transcription		
cDNA Synthesis	Temperature (^{o}C)	Time (min)
	25	10
	50	15
Terminate reaction	85	5
Hold	4	

The cDNA was diluted 1:10 in autoclaved water and 2µl of cDNA was mixed in duplicates with 5µl iQ custom SYBR green Supermix,0.4µl primer (10pmol/µl) and 2.6µl water per well followed by quantitative real time PCR analysis on the CFX96 system from Biorad. Expression levels were normalized to β2-microglobulin (β2-MG) to get absolute gene expression→ $2^{-(Mean\_GeneCT - Mean\_\beta 2MGCT)}$

Table 20: PCR reaction cycles for quantitative real time PCR				
Number	Step	Temperature (^{o}C)	Time (min)	Cycles
1		50	2	x1
2	Initial Denaturation and enzyme activation	95	3	x1

3	Denaturation	95	0:15	
4	Annealing	60	0:30	
5	Extension	72	0:30	
Read the plate				
Go to Step 1 for 40 cycles				
6		95	1:00	x1
7		65	1:00	x1
8	Melt Curve analysis	65-95 with 0.5 increment	0:05	Read the plate after every 0:05 sec
END				

4.2.3 Chromatin Immunoprecipitation

On day 1, Differentiated hMDMs were fixed in 1% paraformaldehyde for 10mins, quenched with 0.125M glycine for 5min and washed in ice-cold PBS twice for 5min each on shaker at ambient temperature. Cells were lysed in buffer I to release cytosolic proteins and debris for 10mins and centrifuged at 13000 rpm for 5min at 4^{o}C. The nuclear pellet was lysed in 200µl nuclei lysis buffer for 10mins and sonified with Branson sonifier at 10% amplitude, 20sec burst (0.5sec ON/1sec OFF) for 6 cycles with at least 1-2 mins pause between each cycle. Soluble chromatin was diluted with dilution buffer to 2ml i.e. for a final SDS concentration of 0.1%. Higher SDS concentration prevents binding of antibody to the proteins. The lysate was pre-cleared with sepharose CL-4B beads for 1h and 1% of input was stored at 4°C. The rest of soluble chromatin was pulled down overnight at 4°C using following 4µg of primary

antibodies. Protein A/G beads were blocked in dilution buffer overnight and used the next day to precipitate antibody-protein complexes for 2h at 4°C.

Blocking of Agarose and CL4B sepharose beads

3,5 ml aliquots of protein A sepharose CL-4B beads in 15 ml falcons were washed twice with 3,5 ml of dilution buffer and centrifuged at 1200g, 4°C. Beads were resuspended in 3,5 ml of dilution buffer with PI, 1 g/l BSA (50 µl 10% BSA in 1 ml solution) and 0,4 g/l sonicated salmon sperm DNA (stock: 10 mg/ml → 5 µl Salmon sperm in 1ml solution) to avoid unspecific binding. Beads were rotated overnight at 4°C and stored at 4ºC for further use.

50µl of A/G agarose beads per IP were aliquoted and centrifuged at 3000rpm twice at 4ºC in dilution buffer. Beads were then resuspended in dilution buffer and diluted to 1:20 of 10% BSA (22µl) and 1:100 of salmon sperm (stock: 10µg/µl, 1µl) per 100µl beads. The A/G beads were rotated and blocked overnight and used to pull down protein at 4ºC.

Washing and purification

On day2, the beads were washed once with low salt buffer, once with high salt buffer and twice with LiCl buffer at 4˚C and followed by a final wash with TE (Tris-EDTA) - buffer at room temperature. The beads were then eluted in two rounds of 100µl elution buffer at 55˚C by shaking. The eluate was reverse crosslinked with RNAse and proteinase K at 65˚C for 4h using 42µl of reversion mix solution.

The decrosslinked DNA was then purified using Qiagen QIAquick PCR Purification Kit (Cat No.: 28106) and eluted in 2x40µl of prewarmed elution buffer at 55ºC.

BATF ChIP protocol

The BATF ChIP was performed according to the company's protocol using BATF-antibody coupled to Dynabeads and magnetic isolation.

5x 10^6 cells were lysed in 1ml Farnham Lysis buffer for 10mins at 4^{o}C followed by centrifugation at 2000rpm, 5mins at 4^{o}C. The pellet was resuspended in 300µl RIPA buffer and sonified in Bioruptor (Diagenode) for 2x10 minutes rounds at 'High voltage' settings for 60sec ON/30 sec OFF. The sonicated mixture was diluted to 1ml with RIPA buffer and centrifuged at 13000 rpm for 5min at 4^{o}C. The soluble chromatin was aliquoted and stored on ice but was not blocked because magnetic beads pull down do not need blocking.

Antibody coupling to magnetic beads.

200 µl of re-suspended magnetic bead slurry was added to a 1.5 ml microfuge tube on ice containing 1 ml PBS/BSA and vortexed briefly. The tubes were then fixed on the magnet and supernatants removed. The beads were then resuspended in 1 ml PBS/BSA and washed thrice. 1 ml PBS/BSA was added to beads and incubated with 3µg primary antibody (BATF, m14-108) overnight. Antibody-bound beads must not be vortexed. Beads were gently mixed on a rotator platform for at least 2 hours at 4°C and washed thrice to remove unbound antibody. The bead mix was resuspended in 100 µl PBS/BSA and added to each 1 ml chromatin preparation (from Sonication protocol) followed by incubation on a rotator for 1h at room temperature and 1h at 4°C. From here on all steps were performed at 4°C. Beads containing immuno-bound chromatin were placed on the microfuge tube on the magnet and supernatant discarded. Beads were then washed and mixed twice in LiCl wash buffer for 3 minutes on a rotator followed by 1 ml TE buffer wash and mixing for 1 minute on rotator. Beads were then fixed on the magnet separator, supernatant was discarded, and the bead

pellet was resuspended in 200 µl IP Elution Buffer to elude DNA at 65^{o}C for 1hr with shaking. The eluted DNA was reverse crosslinked as defined previously and purified using QIAmp DNA purification kit.

4.2.4 Co-Immunoprecipitation

Cells grown in 10cm dishes were washed with PBS/0.5 mM EDTA and lysed by scraping in 200 µl Co-IP lysis buffer. Benzonase was added to 1:1000 dilution. The lysate was incubated for 10mins and transferred to reaction tubes and spun for 10 min at 4°C for 16000 g. 3µl of antibody was added to 1 mg of total protein (i. e. roughly 1:50 dilution or use recommended dilution of antibody) and 10% of the mixture was kept as input. The input was sonified and centrifuged at 16,000 g, 4^{o}C. 1X Laemmli buffer was added and input was heated at 95^{o}C and stored at -20^{o}C for next day. The lysate was incubated with antibody under rotation at 4 °C overnight. Next day, 25 µl protein A/G agarose beads per IP were washed thrice with an equal amount of CoIP buffer (1000 rpm, 4 °C, 1 min). 25µl of beads were added to each IP sample and rotated for 2 h at 4 °C. The beads were spun down and the supernatant was kept as flowthrough. Beads were washed thrice with 250 µl CoIP buffer. The protein was eluted in 40 µl 2x SDS laemmli buffer for 5 min at 95 °C. Beads were then spun at 1000 rpm for 1 min and supernatant was loaded on SDS-polyacrylamide gels along with input from previous step.

4.2.5 Western Blot Analysis

4.5.1 Total Cell Lysis

Media was aspirated from primary hMDMs and cells were washed with ice- cold PBS. Cells were then scraped in 100µl of Lysis buffer and sonified using Branson sonifier for 3 seconds (0.6 sec ON/0.3 sec OFF) at 10% amplitude in ice-cold water beaker.

The sonified fragments were then centrifuged at 16100g for 10mins at 4^{o}C and supernatant was collected as total cell lysate.

4.5.2 Cell Fractionation for nuclear translocation analysis

Media was aspirated, and cells washed in ice-cold PBS. Cells were scraped in PBS and centrifuged at 12,000g for 30secs at 4^{o}C. Cells were lysed for 3mins in 100µl of lysis buffer A with detergent (A+) to lyse the cytoplasm. The lysate was spun down at 16100g for 20secs and the cytosolic supernatant fragment was collected. Cells were washed in 1ml lysis buffer A without detergent, NP-40 (A-) at 16,100 g for 20secs. Supernatant was discarded, and the pellet re-suspended in 100µl of nuclear lysis buffer B. Nuclear lysate was then sonicated using Branson sonifier for 3 seconds (0.6 sec ON/0.3 sec OFF) at 20% amplitude in ice-cold water beaker. Following centrifugation for 16,100g at 4^{o}C the supernatants were collected. Nuclear and cytoplasm protein concentration was quantified using Biorad DC^{TM} Protein Assay.

2.5µl of protein cell lysate was loaded in duplicates on a 96-well plate along with 5µl of BSA standards. 25µl of DC^{TM} Protein Assay Reagent A (Biorad, Catalog#500-0113) followed by 200µl of DC^{TM} Protein Assay Reagent B (Biorad, Catalog#500-0114) was pipetted onto samples and shaked at room temperature for at least 20mins. The protein was quantified via measuring absorbance at 750nm using Berthold Apollo 11 LB 913 Absorbance Reader and using BSA standards to plot a standard curve.

80µg of protein was mixed with 5X SDS loading dye to give protein a negative charge and heated at 95^{o}C for 5mins. Denatured samples were then loaded on 7.5-15% polyacrylamide gels in 1X SDS Running Buffer and blotted in 1X blotting buffer on nitrocellulose membranes using Biorad Transblot Turbo transfer system. Gel was blotted in following order, two soaked Whatman papers followed by nitrocellulose

membrane, gel followed by 2 Whatman papers in blotting buffer. Membranes were blocked for 1hr at room temperature followed by overnight incubation in primary antibodies. The next day unbound primary antibody was washed away with 1xTTBS buffer thrice and incubated for 1hr at room temperature in blocking buffer with species-specific IRDye 700/800-coupled secondary antibodies. Unbound secondary antibody was washed away using washing buffer thrice for 10mins, scanned and quantified using Odyssey imaging system (LI-COR Bioscience).

4.6 ELISA

$2x10^5$ hMDMs were stimulated with cytokines for 48h in 1ml serum-free medium, and the cell-free supernatant was processed for TGFA or CCL18 ELISA using kits from RayBiotech (ELH-TGFα-1 and ELH-PARC-1) according to manufacturer's instructions. For TGFA ELISA, the supernatant was diluted to 1:1 whereas for CCL18 ELISA it was diluted 1:5 serum-free media.

4.7 Flex Set CBA

IFNγ and IL-10 were quantified from 25µl of supernatants of macrophage-T cell coculture using BD CBA Human CBA Flex set Kits.

CBA buffer: 0.5% (w/v) BSA, 0.09% (v/v) sodium azide in PBS

The assay was performed according to manufacturer's instructions.

4.8 NGS Library Preparation and RNA Sequencing Analysis

RNA from cytokine-treated hMDMs from three different donors was extracted using NucleoSpin RNA extraction kit, followed by quantification with Qubit HS RNA Assay Kit. 4µg of RNA was used for library preparation and mRNA was extracted using polyA pulldown and converted to cDNA using TruSeq Stranded mRNA LT - SetB library

preparation kit. cDNA library was quantified with Qubit dsDNA HS Assay Kit and prepared for single paired sequencing on NextSeq using 500/550 High Output Kit v2 for 75 cycles.

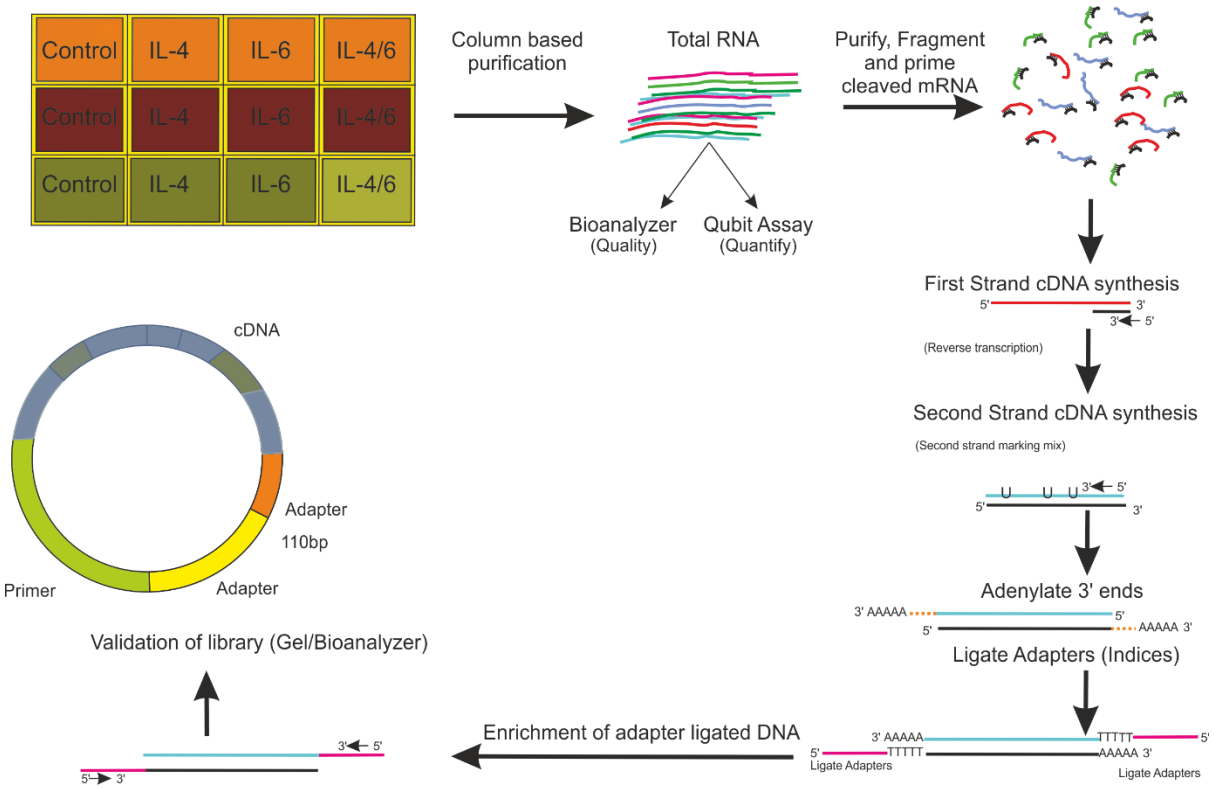

Figure 2: Graphical representation of RNA seq library preparation

Summary statistics of the individual RNA sequence data sets were generated with FastQC [42] analysis that showed a quality score of >93%. Quality trimming of the sequence reads was performed using the Trimmomatic module [43] from Trinity [44] with the following parameter settings: ILLUMINACLIP:/~Trimmomatic-0.32/adapters/TruSeq3-SE.fa:2:30:10 LEADING:5 TRAILING:5 SLIDING WINDOW :4:15. Quality-trimmed reads were mapped to the human genome hg19 with the STAR aligner [45] using the following parameters: --outFilterMultimapNmax 1 --outSAMtype BAM SortedByCoordinate. More than 91>% of reads were uniquely mapped to the

hg19 genome browser. The mapping results were summarized with FeatureCounts [46], and Principal Component Analysis (PCA) of the feature counts was done with the prcomp module in R. Differential Gene Expression (DGE) analysis was performed in R using DESeq2 package [47]. For downstream bioinformatics characterization, we selected differential expressed genes with an absolute log2 fold change (log2FC) ≥ 1 and a p-value < 0.05 for all four test conditions (single cytokine treated versus control (IL-4/-6, IL-4, IL-6 vs Control) and IL-4/-6 vs IL-4) and plotted the heatmap from log2 normalized read counts. Venn diagrams and heat maps were generated in R using the venn.plot and ggplot2 modules, respectively. For every stimulation condition (IL-4, IL-6 and IL-4/-6), we identified antagonistic and synergistic genes according to the procedure described in [40]. Precisely, we identified a gene as antagonistic if the ratios of changes met the following conditions: (IL-4 or IL-6)/Ctr. > 2 and (IL-4+IL-6)/Ctr. < 1.5, where Ctr. denotes untreated control macrophages. Likewise, genes were identified as synergistic, if [(IL-4+IL-6)/Ctr.] / [(IL-4/Ctr.) +(IL-6/Ctr.)] > 1.2. The individual cutoff values were modified from [40].

We calculated the fold changes between two stated conditions for every gene in biological replicates (i.e. matched observations from each donor). Fold changes were either calculated in IL-4, IL-6 or IL-4/-6 versus the control (untreated) condition or between individual (IL-4/-6 versus IL-4) stimulations for each biological replicate (A, B , C). For instance, Gene X will have three changed expression values (CE) in sample A ($X\_CE_{IL\text{-}4A}$), sample B ($X\_CE_{IL\text{-}4B}$) and sample C ($X\_CE_{IL\text{-}4C}$) for IL-4 stimulation. Next, we calculated the standard deviation between the fold changes in $X\_CE_{IL\text{-}4A}$, $X\_CE_{IL\text{-}4B}$ and $X\_CE_{IL\text{-}4C}$ versus control ($X\_CE_{controlA}$, $X\_CE_{controlB}$, $X\_CE_{controlC}$) or between two stimulation conditions using SD function in R. Next, a density plot of all standard deviation values was plotted using ggplot2 function in R.

4.9 Data Analysis

Microarray data from Yan et.al [37] linear coefficient models for mouse BMDMs for synergized genes were compared to synergized genes in human macrophages (Table 36). Data sets GSE14548[48] ,GSE90505[49], GSE83591[50] and GSE9014[51] were analysed using GEO2R web tool (NCBI). Datasets were divided in GEO2R analysis tool at NCBI into two groups (normal/tumor stroma). Gene ID was obtained from respective platform; the dataset was uploaded (e.g. GPL1352 platform) and values were extracted through Profile graph tool online. The respective sample expression values were imported in Excel and analysed through graph Prism software.

4.10 Transfection

Macrophages were transfected for RNA silencing experiments using HiPerFect transfection reagent (Qiagen) and siGenome STAT3 (Dharmacon, M-003544-02-0005) for 72h or BATF for 24h ON-TARGETplus siRNA pools (Dharmacon, 20µM) before stimulation with indicated cytokines.

Table 21: Reaction setup for siRNA knockdown

	siRNA	**HiPerFect**	**medium-FCS**		**final volume**
	3,75µl/well	16,8µl/well	482µl/well		
siControl	12	53,76	1542,4	µl	1608,16
siSTAT3	12	53,76	1542,4	µl	1608,16

The components were added into reaction tubes, vortexed and incubated for 15mins at room temperature. Cells were incubated with 500µl of siRNA for 6hrs, followed by addition of 1ml of serum-containing medium and overnight incubation. The medium

was changed next day, and cells were further incubated for 24 or 72 hrs before treatment with cytokines.

For CRISPRi, hMDMs were transfected using Viromer Red transfection reagent (Lipocalyx). HMDMs were incubated in serum-free medium overnight and transfected with sgR1NAs targeting STAT3/STAT6 or BATF binding sites cloned into sgRNA-MS2 vector (Addgene #61424)[52] and pHAGE EF1α dCas9-KRAB plasmid (Addgene #50919) [53] for 24h followed by stimulation with cytokines for further 24h.

4.11 Cloning, Transformation and vectors

4.11.1 sgRNA-cloning steps in sgRNA-MS2 vector

Primers were designed such that the sgRNAs do not contain any BbsI enzyme site (i.e. the nucleotide sequence 'GAAGAC' or 'GTCTTC'), due to simultaneous digestion-ligation step. The most important step was to add the complementary base pairs (marked in red) after BbsI digestion into the primers ordered sgRNAs i.e. for oligosense1 and antisense 1. sgRNA were designed from http://www.e-crisp.org/E-CRISP/

For example

CCL18crpi S3 (sense 1)	5' -caccgCCACTGCTAATTATAGAGTT-3'
CCL18crpi S3 (antisense 1)	5'-aaacAACTCTATAATTAGCAGTGGc-3'

CRISPRi sgRNAs	
CCL18 STAT3	CCACTGCTAATTATAGAGTT
CCL18 STAT6	GCCCTCTGGGAGACTGAGAT
CCL18 BATF	TTACAGCCCACAGTCTAGCA

After the primer design for sgRNA the following steps were performed to clone sgRNA into sgRNA-MS2 backbone.

1. Phosphorylate and anneal each pair of oligos in a single-step reaction:

Table 22: Reaction setup for template phosphorylation and annealing	
Volume (µl)	**Components**
1	Oligo sense 1 (100µM)
1	Oligo sense 2 (100µM)
1	10X T4 Ligation Buffer (NEB)
6.5	ddH2O
0.5	T4 PNK (NEB)
10µl	Total Volume

The above reaction was annealed in a thermocycler using the following parameters at 37°C for 30 min followed by 95°C for 5 min and then ramped down to 25°C at 5°C/min. The resulting gRNA was diluted to 1:250.

2. Set up digestion-ligation reaction in a single-step reaction:

Table 23: Reaction setup for plasmid digestion and sgRNA ligation	
Volume	**Components**
X µL	sgRNA-MS2 vector or other backbone vector (100ng)
2 µL	phosphorylated and annealed oligo duplex from **step 1** (1:250 dilution)
2 µL	10X Tango buffer (or FastDigest Buffer)

1 µL	DTT (10mM to a final concentration of 0.5mM)
1 µL	ATP (10mM to a final concentration of 0.5mM)
1 µL	FastDigest *Bbs*I (Thermo Fisher Fermentas)
0.5 µL	T7 DNA ligase
Y µL	ddH2O
20 µL	total

The above reaction was incubated for digestion and parallel ligation in a thermocycler at 37°C for 5 min followed by 23°C for 5 min. The cycle was repeated 6 times for a total run time of 1h and reaction was cooled down to 4°C.

3. PlasmidSafe exonuclease treatment

The ligation reaction was treated with exonuclease to prevent unwanted recombination events

Table 24: Reaction setup for exonuclease digestion of unannealed DNA	
Volume	**Reaction Mix**
11 µL	ligation reaction from **step 2**
1.5 µL	10X PlasmidSafe Buffer
1.5 µL	10mM ATP
1 µL	PlasmidSafe exonuclease
15 µL total	

The reaction was incubated at 37°C for 30 min. 1-2µl of the final product was heat shock transformed into competent cells (DH5α). Colonies were picked, followed by plasmid DNA isolation and sequencing to verify the right clones.

4.11.2 Luciferase reporter cloning and transfection

A descriptive cloning procedure in shown in Fig. 3

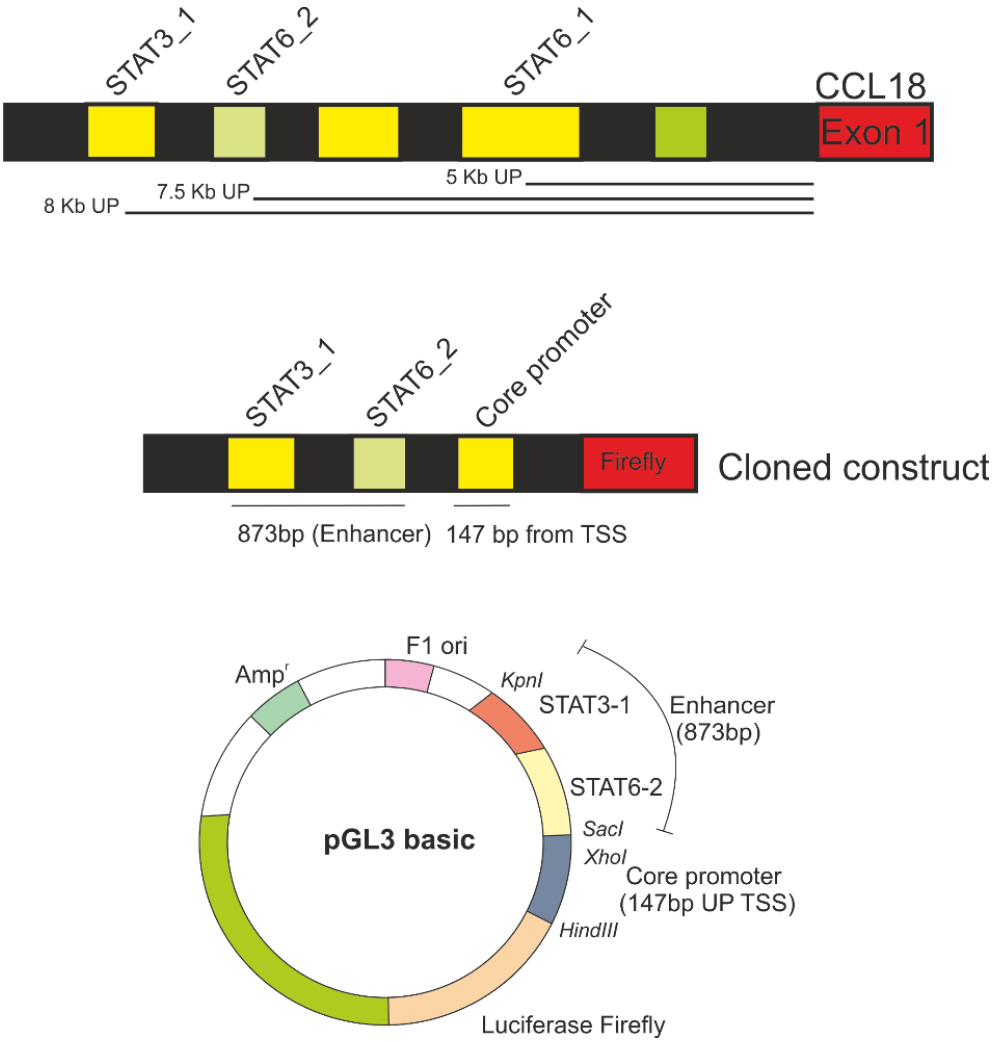

Figure 3: Cloning scheme for pGL3basic vector containing CCL18 core promoter (147bp) and STAT3/STAT6 binding enhancer region (873bp)

4.11.2.1 Cloning core promoter and CCL18 enhancer into pGL3-basic vector

CCL18 core promoter (defined from European promoter database (EPD), 147bp upstream of TSS) was amplified using forward and reverse primers flanked with 15bp homologous fragments for insertion into pGL3-basic (Promega, E1751) vector. The CCL18 core promoter was amplified using genomic DNA from hMDMs and primers

listed in Table 3. Nucleotides marked in yellow below are 15bp homologous sequences to XhoI and HindIII restriction digestion sites in pGL3basic vector and in black are the primer sequences to amplify the CCL18 genomic region. The genomic DNA was amplified using CloneAmp HiFi Premix (CloneTech) with following amplification cycles.

XhoI_Fw

:CGTGCTAGCCCGGGCGGCTGTGACCACTCATTTCTGAGAAATATCTGTCA

HindIII_Rv: CCGGAATGCCAAGCTCTCCTGGCCTCCTTCTGGGGTATGAG

Table 25: PCR Amplification of Genomic DNA

Temperature (ºC)	Time	Cycles
96	5min	1X
98 60 72	10sec 15sec 15sec	30X
72	5min	
4	Hold	

5µg of pGL3 vector was double digested with XhoI (NEB, #R0146S) and HindIII (NEB, #R0104S) restriction enzyme. The PCR insert and the double digested pGL3 vector were gel purified and set-up for infusion reaction as mentioned below.

Table 26: Infusion reaction to infuse amplified core promoter into pGL3basc double digested vector.	
Reaction	Amount
PCR fragment	30ng
Linearized vector	30ng
5X Infusion HD enzyme	2µl
Deionized H_2O	As needed
Total reaction	10µl

The reaction was incubated for 20mins at 50^{o}C. 2µl of reaction was used to transform super competent Stellar *E. coli* cells. Colonies were picked, and DNA was extracted using miniprep kit (Macherey Nagel). The DNA was amplified using following forward and reverse primers to check if the insert was cloned.

rt luci for: ATTTATCGGAGTTGCAGTTGCGCC

rt luci rev: GCTGCGAAATGCCCATACTGTTGA

Following runs on Agarose gels positive PCR bands containing inserts as compared to empty pgL3basic control vectors were sent for sequencing.

Similarly, the CCL18 enhancer region (7.6-8.3Kb upstream of TSS, 500bp in length with both STAT3 and STAT6 sites) was cloned into pGL3 vector with previously inserted CCL18 core promoter (as a template, in Step I) using the same protocol as listed above. In summary, genomic enhancer was amplified with primers (black), cloned CCL18 promoter-pGL3basic vector was double digested using KpnI and SacI restriction sites, both fragments were gel purified and the reaction was set up for Infusion (15bp homology arms in red) and then used to transform to Stellar cells.

Kpni Fw: TCTATCGATAGGTACTGACCTGGCTGATTGGAACCAGAATGC

SacI Rv: GCTAGCACGCGTAAGCAGGCCTTACAATGGAGATAGCAGCCTAGA

4.11.2.2 Deleting STAT3/STAT6 binding regions in cloned enhancer + core promoter vector

The cloned enhancer region was 853 bp in length with STAT3 and STTA6 binding sites. STAT3 and STAT6 binding sites were deleted for a total length of 208bp and 358bp respectively. For this, the pGL3-core+enhancer plasmid was amplified using sequences marked in black color underneath (Tm, 55^{o}C) with PfuUltra II Fusion HS DNA Polymerase (Agilent, Catalog#600670) using listed protocol.

1. S6DelVr-F1:

TCTTAACTCATATTACTTGACTTATTTTTTAAAAAAGTAAAGATGCA

2. S6DelVr-R1: TAATATGAGTTAAGAACTTTCGTGTATTGGCTCAT

3. S3DelVr-F1:

TTAAATCTGTTCTAGCTTAACTCATATTAACTTCTCTATAAATTTAAGTC

4. S3DelVr-R1: CTAGAACAGATTTAACCTGACATTTCCTGTTCC

Table 27: PCR steps for plasmid amplification

Cycles	Temperature (^{o}C)	Duration
1	95	2 min
30	95	10 secs
	T_m-5 (50)	20 secs
	72	1.5-2 mins, (15sec/Kb, Vector 6Kb)
1	72	3 mins

Table 28: PCR reaction steps for plasmid amplification	
Component	**Amount**
Distilled H_2O	40.5µl
10X Pfu Ultra II reaction buffer	5µl
dNTP mix(25mM)	0.5µl
pGL3basic+core+enhancer	30ng
Primer Fw (10µM)	1µl
Primer Rv (10µM)	1µl
PfuUltra II fusion HS DNA Polymerase	1µl
Total volume	50µl

The amplified vector was DpnI-digested at 37^{o}C for 1hr to remove non-amplified DNA template and gel-purified to isolate the single plasmid band at 6Kb. 30ng of purified vector construct was infused using HD-Infusion kit (CloneTech) as mentioned above with 15bp complementary overhangs designed at 5'-end of deletion primers. The reactions were used to transform Stellar competent *E. coli* cells. The deleted enhancer fragment plasmid was sequenced using a pGL3basic-primer and insert was confirmed.

4.11.2.3 Deleting 10bp STAT3/STAT6 binding sites in cloned enhancer + core promoter vector

10bp of STAT3 and STAT6 binding sites were deleted from cloned enhancer and core promoter plasmid using Quick site mutagenesis protocol (Agilent). The following primer sequences were designed from Agilent website https://www.genomics.agilent.com/primerDesignProgram.jsp?toggle=uploadNow&mutate=true&_requestid=403674

S310bpDel Fw: 5'-cccaccactgctaattatagattctgtaaactctccagactc-3'

S310bpDel Rv: 5'-gagtctggagagtttacagaatctataattagcagtggtggg-3'

S610bpDel Fw: 5'-ctttttttaaaaaataagtcaagacgaagctgggcgcagtgtct-3'

S610bpDel Rv: 5'-agacactgcgcccagcttcgtcttgacttatttttttaaaaaag-3'

These primers were used to synthesize a new cDNA strand of the entire pGL3-basic plasmid with core promoter and enhancer cloned together as mentioned below.

Table 29: PCR reaction buffers and steps		
Components		
10X Reaction buffer	5µl	
pGL3basic-core-enhancer DNA	50ng	
Primer 1	125ng	
Primer 2	125ng	
dNTPmix	1µl	
PfU Ultra HF DNA polymerase (2.5U/µl)	1µl	
ddH_20		
Total volume	50µl	
PCR reaction cycles		
Cycles	Temperature (^oC)	Duration
1	95	30 secs
18 cycles	95	30 secs
	55	1min
	68	1min/Kb plasmid length (6min)

The PCR-amplified vector was DpnI digested at 37ºC for 1hr and 2µl was used to transform 50µl of XL-1 Blue supercompetent cells. Colonies were processed to isolate DNA using mini-preps, and the deletions were confirmed by sequencing using Luciferase vector sequencing primers described above.

4.11.2.4 Quantification of Firefly and Renilla luciferase activities

The cells were lysed in 100µl of 1X Passive lysis buffer (Luciferase Cell Culture Lysis 5X Reagent, Promega, Catalog # E1500) in 24 well plate or 200µl per 6 well plate. Plates were frozen in liquid nitrogen and transferred to -80ºC. Samples were thawed for 20mins at room temperature and 20µl lysate was aliquoted in one 96well plate (Greiner Bio-one™ 655075, Catalog #07-000-130) in duplicates for every sample and the remaining lysate was stored at -80ºC for repeated measurements, if necessary. Firefly/Renilla expression was measured separately for 10secs each with Mithras Multimode Microplate Reader LB 940 from Berthold technologies.

4.12 Flow Cytometry Analysis

Cells were centrifuged for 5min at 500g at 4˚C, and the supernatant was discarded. Cells were re-suspended in 80µl PBS/BSA (0.5%) with 2µl of Fc Block (BD Biosciences). Cells were incubated on ice for 15-20min with 1-2µl of antibodies centrifuged and re-suspended in 300µl of FACS flow buffer before analysis on a LSRII/Fortessa flow cytometer (BD Biosciences).

4.13 T Cell Activation Assay

T cells from human buffy coats were isolated using Pan CD3-Tcell extraction kit (Miltenyi Biotec). PBMCs were isolated as described in Section 4.1. The pellet was rigorously re-suspended in 12ml ice-cold water and incubated for 20secs on ice. 4ml of hypoosmotic lysis buffer was then added to lyse platelets. The solution was then

diluted with cold PBS to 50ml and centrifuged at 1300rpm for 6 mins at 4^{o}C. This step was repeated until no erythrocytes and platelets remained. The pellet was resuspended in 500µl of running buffer (1XPBS, 2mM EDTA, 25ml of 10% BSA) buffer and incubated with 80µl of $CD3^{+}$ MACS beads for 30mins on ice. The beads were washed with 2-4ml of running buffer, centrifuged at 4^{o}C and resuspended in 500µl of running buffer. Cell suspension was passed through LS/MACS magnetic columns equilibrated with running buffer, followed by 3x3ml washes and elution in 5ml buffer. After counting $1x10^{6}$ $CD3^{+}$ T cells were expanded using 5µl/10^{6} T cells of ImmunoCult Human CD3/CD28/CD2 T cell activator (STEMCELL Technologies), 100ng/ml human IL-2 and 50µM β-mercaptoethanol, and cultured in RPMI with 5% heat inactivated FCS, 5mM sodium pyruvate, and 5mM non-essential amino acids. hMDMs from the same buffy coats were differentiated with human plasma for 7d in a 24-well plate. On day 7, hMDMs were stimulated for 48h with IL-4 or/and IL-6. On day 8 T cells were reactivated as described earlier. On day 9 hMDMs and T cells were cocultured (1:5) for the next 3d. On day 12, supernatants were centrifuged, and cell pellet was analyzed for surface marker expression, whereas culture media were probed for IFNγ or IL-10 secretion using CBA Flex assays.

4.14 3D Chemotaxis Assay

We collected serum-free conditioned media from hMDMs 48h post-treatment with different cytokines. 20000 MCF-7 or MDA-MB 231 cells were seeded onto collagen-coated µ-slide chemotaxis slides (ibidi, #80326). The cells were then incubated and tracked via Cell Observer (Zeiss) at 37˚C with 5% CO_2 for 16h with images taken every 10min. A total of 90 cells were tracked per condition (30 cells, n=3) and quantified via manual tracking protocol in Image J.

4.14.1 Protocol for Cell preparation

The following protocol is modified from ibidi Application Note 26

https://ibidi.com/img/cms/support/AN/AN26_CollagenI_protocols.pdf

Table 28: Reaction components for 3D collagen and cell preparation for chemotaxis assay	
Final Collagen I concentration in gel (mg/ml) = 0.5	
Component	Volume (µl)
10X DMEM	10
1M NaOH	2
H_2O	71
$NaHCO_3$ 7.5%	2.5
1XDMEM (+FCS)	25
Collagen I, 5mg/ml	15
Cell Suspension	50
Cell ingredients were mixed in a 1.5ml eppendorf tube in exact order at 4^{o}C ensuring no air bubbles.	

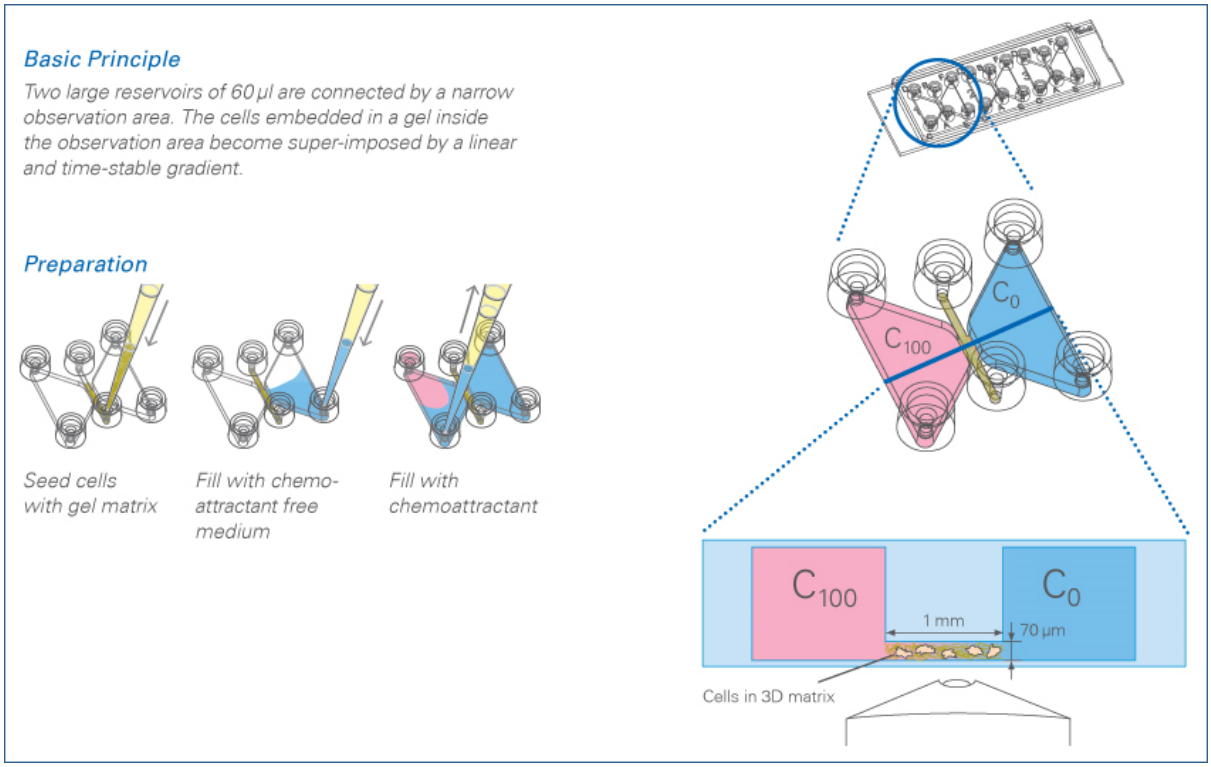

Figure 4: 3D chemotaxis assay design adapted from ibidi ***https://ibidi.com/channel-slides/9--slide-chemotaxis-ibitreat.html***

6µl of above mix with a final concentration of 20,000 MDA-MB 231 cells was seeded onto collagen-coated µ-slide chemotaxis slides (ibidi, #80326) according to manufacturer's recommendations (Fig. 4). At this step, it was ensured that no air bubbles are blocking the microscope acquisition area. 6µl of mix was then incubated in a 10cm dish with wet tissues to prevent evaporation for 30mins, allowing cells to seed. The chamber was washed with 6µl of serum free media thrice to ensure no FCS blocks the chemotaxis of MDA-231 cells. After 30mins chemoattractant free (serum free RPMI) was added on the right chamber and the diluted condition media (1:1 in 1% FCS) was added in the left chamber. Collagen concentrations were tested from 1.5-0.5 mg/ml and the autoclaved sterile water volume was adjusted accordingly.

4.15 Statistical Analysis

Statistical analysis was performed using GraphPad5 Prism. One-way ANOVA analysis with Bonferroni post hoc test was applied for multiple group comparisons with significance levels indicated in figure graphs (*, $p<0.05$, **, $p<0.01$, ***, $p<0.005$). Results are presented as means±SD for at least three independent biological replicates.

5. Results

5.1. Human macrophage transcriptome changes in response to IL-4 and IL-6

To explore how the human macrophage transcriptome changes in response to single and combined IL-4/IL-6-treatments we performed RNA sequencing of human hMDMs stimulated for 24h with IL-4 and IL-6 alone and in combination. The sequencing reads passed the QC quality test with an average %Q30 score (i.e. a Phred quality score of 30 with a probability of an incorrect base call being 1 in 1000) for 93% of the sequences read (A QC score above >75% is generally accepted as a permissible sequencing quality) (Fig. 5).

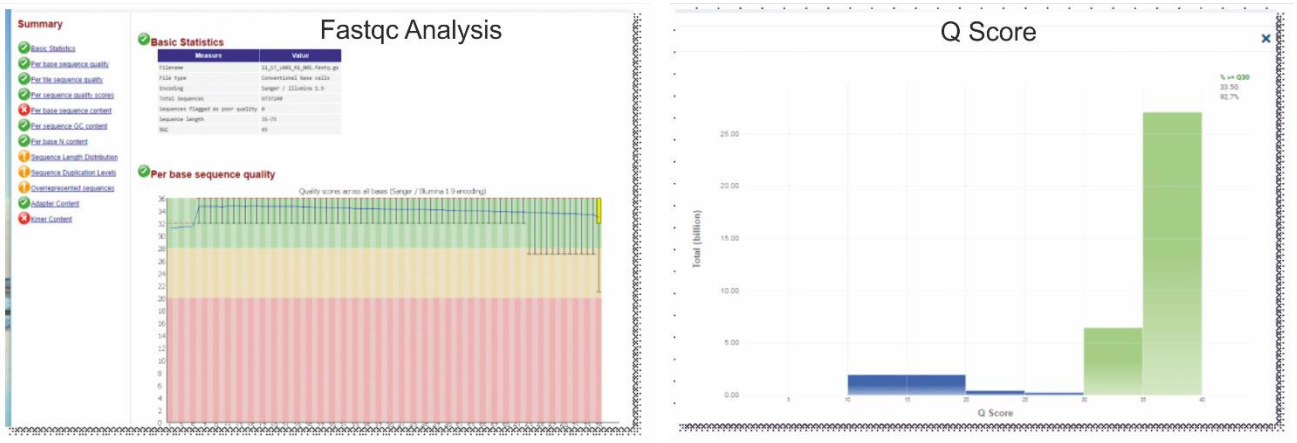

Figure 5: Sequencing quality analysis via Fastqc and Q score

We performed principal component analysis (PCA) of the data, which uses orthogonal transformation to convert a set of possibly correlated values into linearly uncorrelated variables called principal components in fewer dimensions such that each preceding component reflects highest to lowest variance distribution in a correlation matrix[54]. PCA showed that transcriptomes of IL-4 and IL-4/IL-6 co-stimulation are widely

clustered compared to IL-6-treated and unstimulated hMDMs that clustered closely together (Fig. 6).

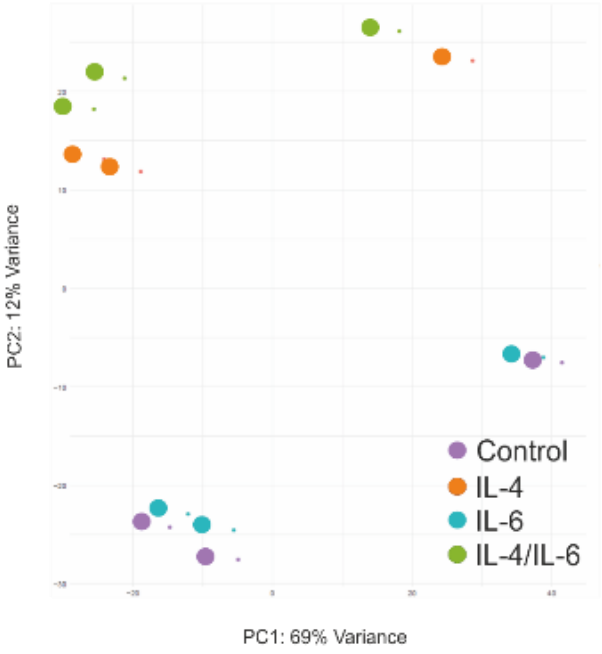

Figure 6: Principal component analysis (PCA) of three biological replicates for each treatment condition

We note the divergence of biological replicates in IL-4 and IL-4/IL-6 co-stimulation reflects a naturally occurring variance in the extent of response (gene induction) to upstream cytokines similar to previous reports with different levels of basal expression in untreated macrophages from different donors [55, 56]. This variation was also not sex mediated as all donors were females as validated by curating a gene count matrix for Y- linked genes which was mostly zero under all treatment conditions. However, genes expressed in untreated condition and IL-6 do not differ substantially and cluster closely because IL-6 alone induces only a small repertoire of STAT3 inducible genes[54]. We analyzed fold changes of mRNA expression across different treatments for each differentially expressed genes and plotted the distribution of standard deviations for

replicate measurements, showing that most of standard deviations are close to zero. This implies little variation of hMDM responses to cytokines between biological replicates (Fig. 7).

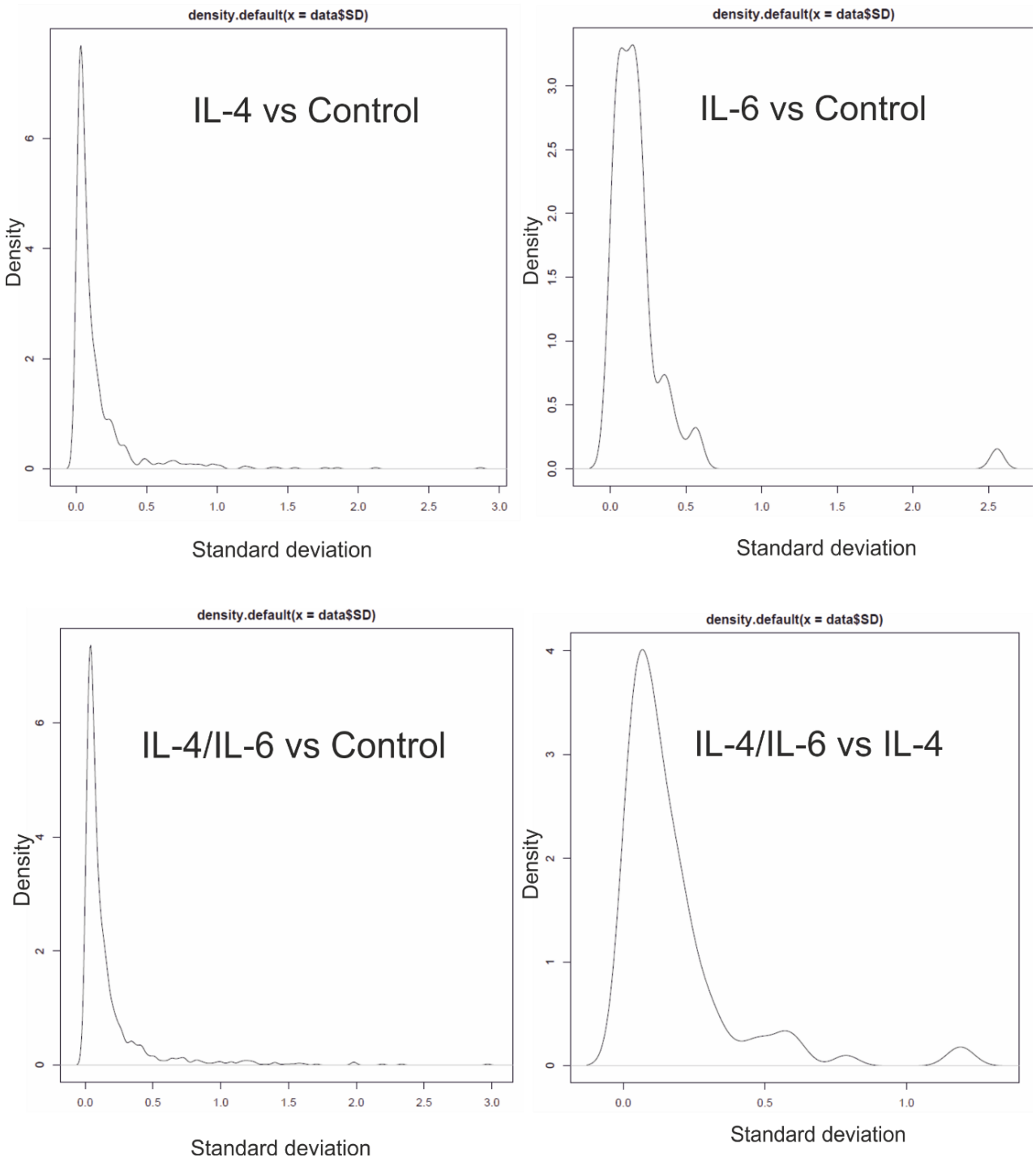

Figure 7: Standard deviations of biological replicates for RNA sequencing

dataset were plotted for fold changes in RNA expression comparing different treatment conditions.

We mapped our reads to hg19 genome and generated normalized raw read counts using DESeq2 package (Table 31, available in soft copy). We next generated a list of differentially expressed genes with $|\log2FoldChange| \geq 1$ relative to the untreated control (Table 32, soft copy). Fig. 8A and Table 33 (soft copy) shows the overlap between the upregulated genes (log2FoldChange≥1) upon treatments with IL-4, IL-6, and IL-4/IL-6 in Venn diagram. Of the 722 genes upregulated in co-stimulated (IL-4/IL-6) macrophages, 60% were also upregulated upon IL-4 stimulation (438), but only 3% were upregulated by IL-6 alone (21).

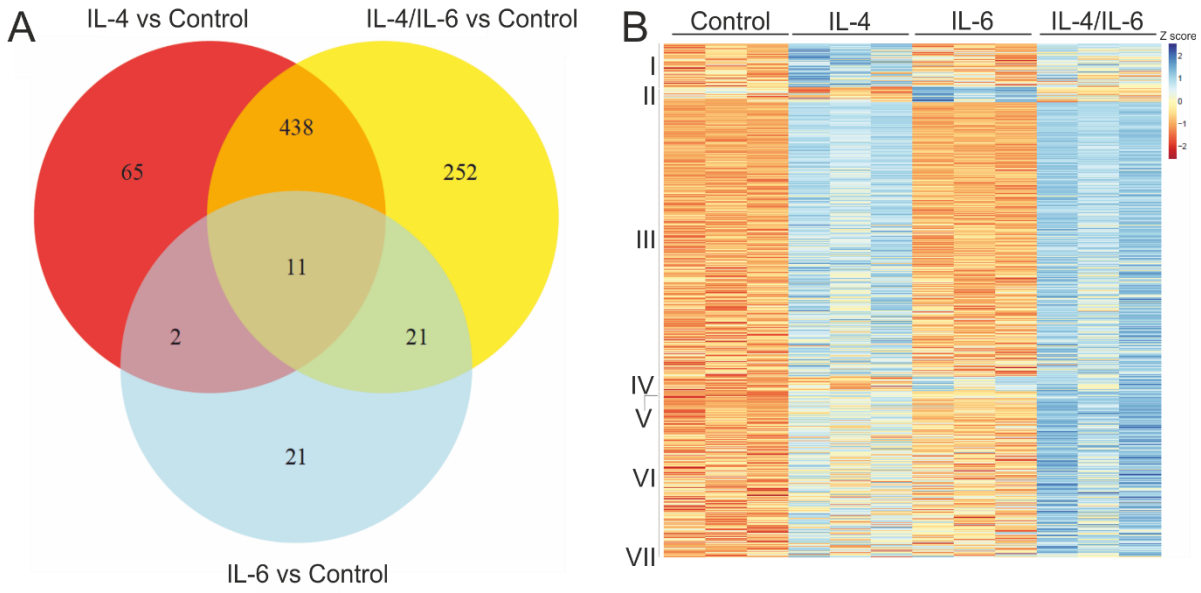

Figure 8: (A)Venn diagram displaying numbers of upregulated genes in IL-4, IL-6, and IL-4/IL-6 co-stimulations relative to control. (B) Heat map representing different patterns of gene induction upon respective stimulus.

We summarized the pattern of induction upon cytokine stimulation in a heat map (Fig. 8B), and categorized the genes into seven categories, depending on their response

across different treatments: Class I (IL-4-unique genes), Class II (IL-6-unique genes), Class III (genes induced by IL-4 and IL-4/IL-6) , Class IV (genes induced by IL-6 and IL-4/IL-6), Class V (genes upregulated by single as well as combined cytokine treatments) , Class VI (genes induced only upon IL-4/IL-6 co-treatment), Class VII (genes upregulated by IL-4 and IL-6, but not their combination). We found 252 genes uniquely upregulated when hMDMs were co-stimulated with both IL-4 and IL-6. Considerably fewer genes are uniquely upregulated upon either IL-6 (21) or IL-4 (65) treatment. The 252 genes are neither individual IL-4 or IL-6 targets, but their expression is induced at least 2-fold relative to the control upon dual stimulation. We find amongst these genes membrane receptors, cytokines and immune activation receptors (Table 33). A Gene Ontology (GO) analysis[57, 58] of these 252 genes using online Panther tool's GO biological process annotation revealed enrichment of IFNγ-signaling pathways as well as extracellular cell matrix and adhesion pathways (Fig. 9).

GO biological process complete	N of genes in the term	N of genes in the list	Fold Enrichment	raw P value	FDR
protein kinase B signaling	46	5	13.22	5.90E-05	3.84E-02
interferon-gamma-mediated signaling pathway	71	6	10.28	3.96E-05	3.25E-02
protein O-linked glycosylation	121	8	8.04	1.10E-05	1.22E-02
response to interferon-gamma	179	11	7.47	4.75E-07	1.48E-03
cellular response to interferon-gamma	157	9	6.97	9.16E-06	1.19E-02
response to molecule of bacterial origin	332	14	5.13	1.01E-06	2.62E-03
glycoprotein biosynthetic process	312	13	5.07	2.82E-06	4.89E-03
response to lipopolysaccharide	313	13	5.05	2.92E-06	4.55E-03
positive regulation of cell-cell adhesion	257	10	4.73	7.09E-05	4.42E-02
extracellular matrix organization	315	11	4.25	7.87E-05	4.39E-02
glycoprotein metabolic process	378	13	4.18	2.04E-05	1.88E-02

Figure 9: List of top 10 significantly enriched GO biological processes for 252 uniquely induced genes in dual IL-4/IL-6 stimulation.

In addition, we identified genes that are controlled by IL-4 and IL-6 in an antagonistic or in a synergistic fashion upon co-stimulation (Fig. 10A, Table 34, soft copy) according to previously described criteria[40]. Apparently, IL-6 has almost no opposing

effects on the IL-4-induced genes, however, IL-4 co- stimulation does antagonize 25% (14 out of 55) of IL-6 target genes. Remarkably, 262 out of 722 upregulated genes upon IL-4/IL-6 co-treatment were synergistically induced.

A

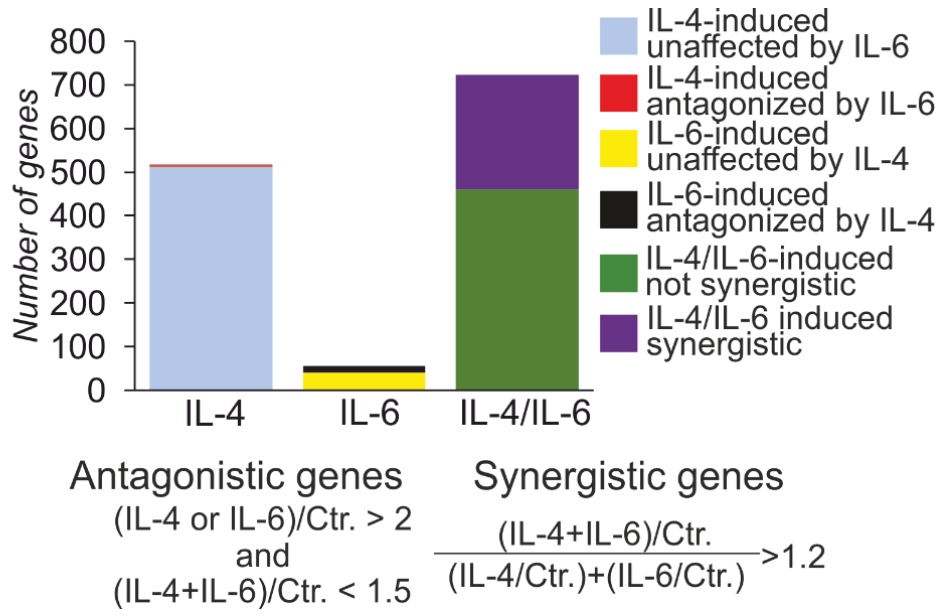

B

GO biological process term	N of genes in the term	N of genes in the list	Fold Enrichment	raw P value	FDR
lymphocyte chemotaxis	43	6	12.49	1.60E-05	1.13E-02
regulation of heart rate by cardiac conduction	36	5	12.44	8.53E-05	3.01E-02
monocyte chemotaxis	41	5	10.92	1.49E-04	4.54E-02
lymphocyte migration	57	6	9.43	6.84E-05	2.72E-02
T cell costimulation	76	8	9.43	4.16E-06	4.61E-03
lymphocyte costimulation	77	8	9.3	4.55E-06	4.71E-03
cellular response to interferon-gamma	139	11	7.09	9.14E-07	4.72E-03
protein O-linked glycosylation	109	8	6.57	4.77E-05	2.38E-02
response to interferon-gamma	160	11	6.16	3.31E-06	3.94E-03
multicellular organismal signaling	128	8	5.6	1.37E-04	4.35E-02

Figure 10: (A) Visualization of numbers of synergistically and antagonistically regulated genes. (B) List of top 10 significantly enriched GO biological processes for synergistically induced IL-4/IL-6 target genes.

Further GO analysis of synergistically induced genes revealed significantly enriched pathways associated with immune cells (Fig. 10B). Importantly, lymphocyte and

monocyte chemotaxis as well as lymphocyte co-stimulation and the response to IFNγ were among top 10 significantly enriched biological processes.

Our analyses reveal that whereas IL-6 on its own induces relatively few genes, it has a bigger impact on IL-4-induced transcriptome. We analyzed IL-6 mediated changes upon co-stimulation by performing differential gene expression analysis between IL-4/IL-6 and IL-4-treated conditions ($|\log2FoldChange| \geq 1$, $p \leq 0.05$). According to these criteria we observed that 109 genes were differentially regulated between IL-4/IL-6 and IL-4 stimulations as depicted in the heat map (Fig. 11, Table 35). Amongst these 109 differentially regulated genes, 23 IL-4 target genes (e.g. CCL18, CCL8, CCL17, CCL23, TGFA) were upregulated and 2 downregulated (BCL11B, INPP4B) upon co-stimulation. In addition, 11 IL-6 target genes (e.g. FAM20A, AQP3, SOCS3) were upregulated and 4 were downregulated (FPR, FPR2, GPR85, KCNK15). 61 of the 109 differentially regulated targets were neither IL-4 nor IL-6 targets, being unique to co-stimulation and 8 genes were not only differentially expressed under IL-4/IL-6 relative to IL-4-treatment conditions but were also differentially expressed in IL-4 vs control and IL-6 vs control (e.g. TGFB1, ENPP2, EHF, GGT5).

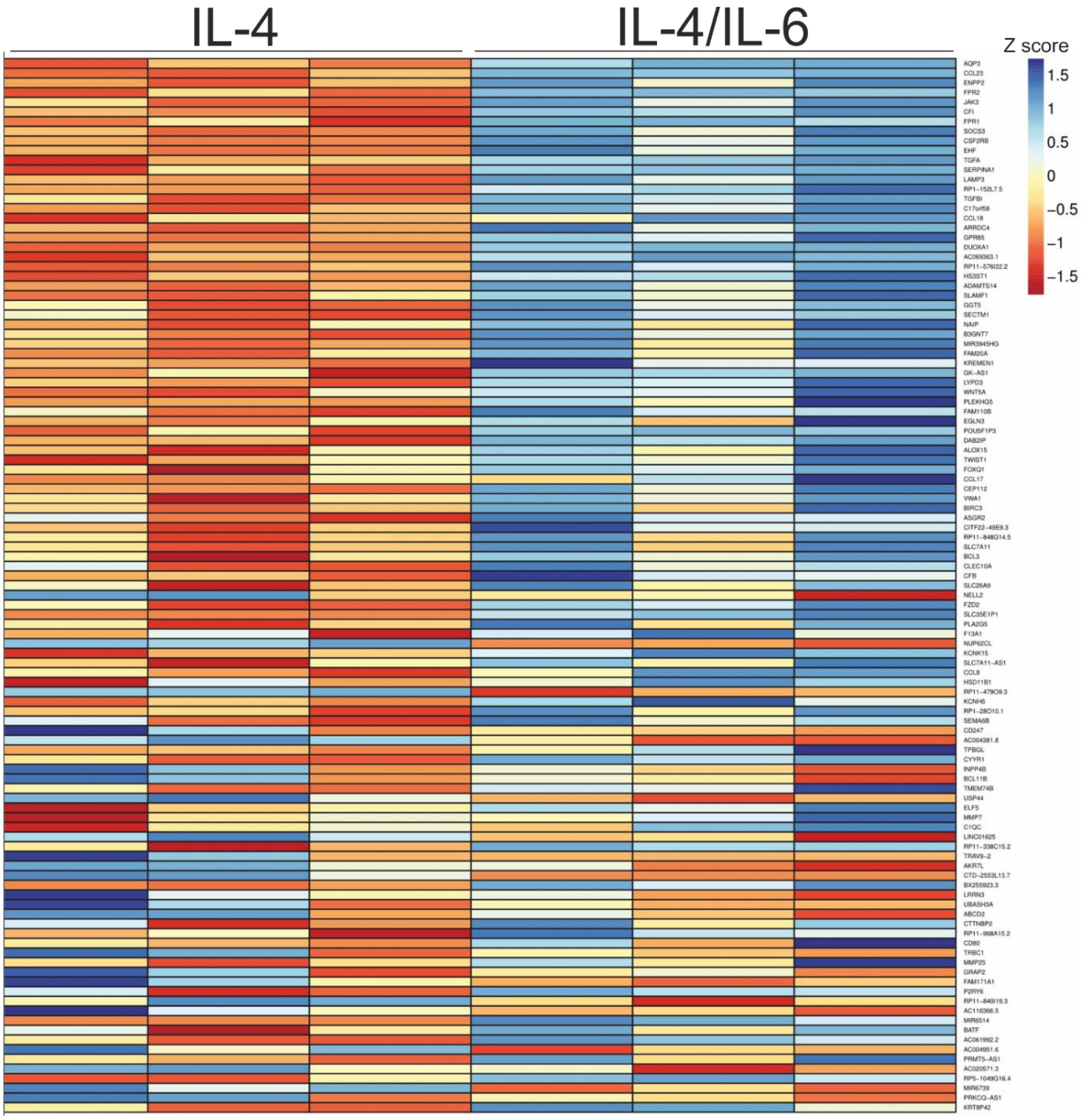

Figure 11: Heat map of 109 differentially regulated genes between IL-4/IL-6 and IL-4 treatments.

We validated transcriptome changes revealed by RNA sequencing for selected synergistically induced genes with known functions in macrophages by Q-PCR and protein expression analyses. Particularly, dual stimulation enhances the expression of several chemokines targeted by IL-4 (CCL17, CCL18, CCL23 and CCL8). We observed induction of TGFA gene encoding an EGF receptor ligand as well as

upregulation of CD274, coding for an immunosuppressive PD-L1 cell surface receptor at mRNA (Fig. 12A) and protein levels (Fig. 12B, C).

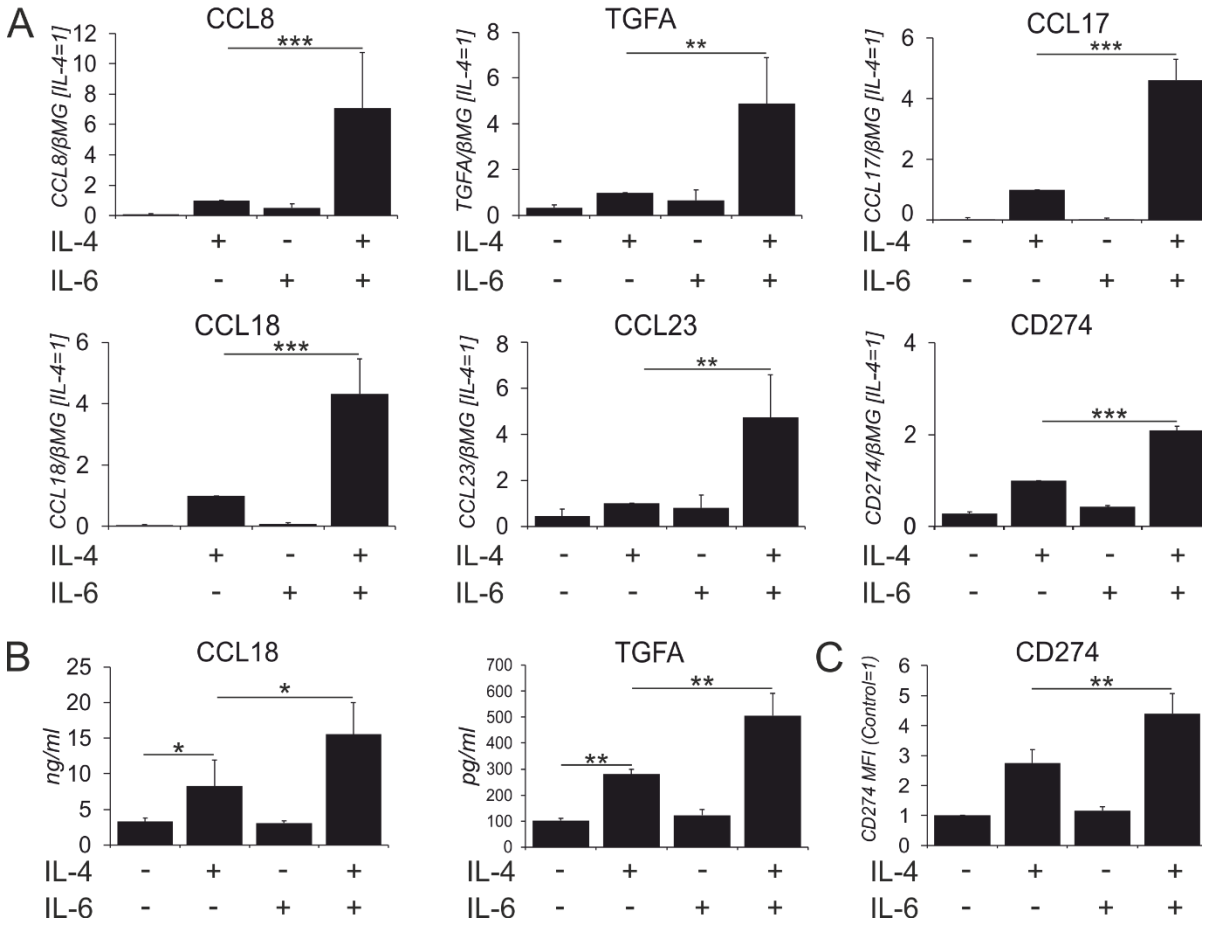

Figure 12: In vitro validation of synergistically induced IL-4/IL-6 target genes. *(A) mRNA expression analysis for indicated genes in macrophages treated for 24h with IL-4 and IL-6 alone or in combination. (B) Protein secretion of CCL18 and TGFα determined by ELISA and (C) surface expression of CD274 determined by flow cytometry in macrophages treated for 48h with IL-4 and IL-6 alone or in combination. Data are presented as mean±SD. *, p<0.05, **, p<0.01, ***, p<0.005.*

We also validated genes uniquely induced by dual stimulation (Fig. 13A), including membrane receptors (CFI, CLEC7A) and chemokines (CCL2, CXCL13). In addition, we confirmed that IL-4 stimulation antagonized some IL-6 target genes (e.g. CD163

and FCGR1A) (Fig. 13B-C). Since the inhibitory immunoglobulin receptor FCGR2B was synergistically upregulated after IL-4/IL-6 co-treatment (Table 34), we measured the expression levels of IgG Fc receptors and found upregulation of the inhibitory receptor FCGR2B at mRNA and protein level, whereas the activation receptors, FCGR1A and FCGR3A were downregulated in IL-4- and IL-4/IL-6-treated cells (Fig. 13 C-E). Analysis of typical markers associated with anti-inflammatory macrophage polarization revealed that CD206 mRNA expression was enhanced but there were no alterations of IL-10 and TGFB1 mRNA expression (Fig. 13F).

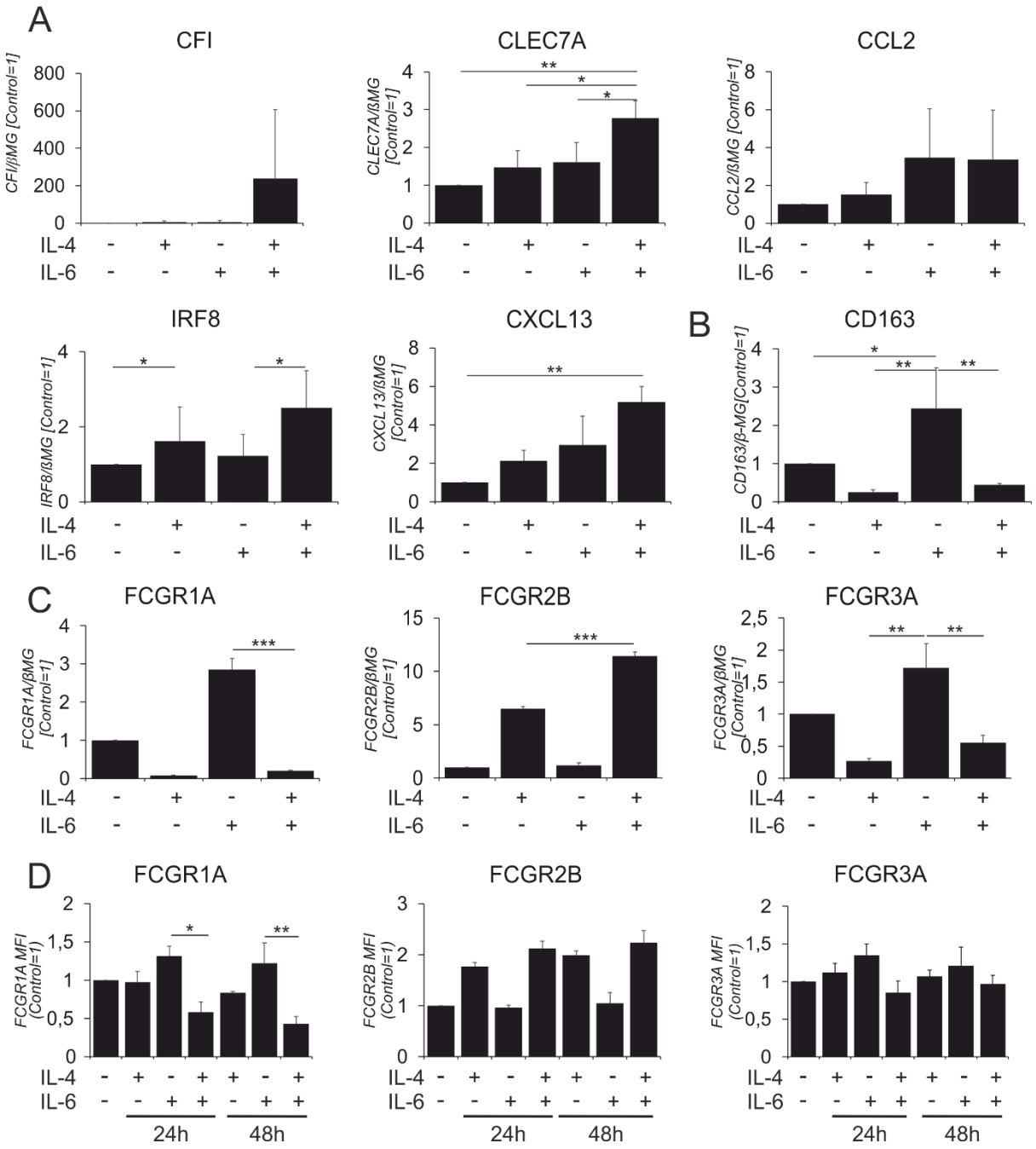
A
CFI
CFI/ßMG [Control=1]
CLEC7A
CLEC7A/ßMG [Control=1]
CCL2
CCL2/ßMG [Control=1]
IRF8
IRF8/ßMG [Control=1]
CXCL13
CXCL13/ßMG [Control=1]
B
CD163
CD163/ß-MG[Control=1]
C
FCGR1A
FCGR1A/ßMG [Control=1]
FCGR2B
FCGR2B/ßMG [Control=1]
FCGR3A
FCGR3A/ßMG [Control=1]
D
FCGR1A
FCGR1A MFI (Control=1)
FCGR2B
FCGR2B MFI (Control=1)
FCGR3A
FCGR3A MFI (Control=1)
IL-4
IL-6
24h
48h

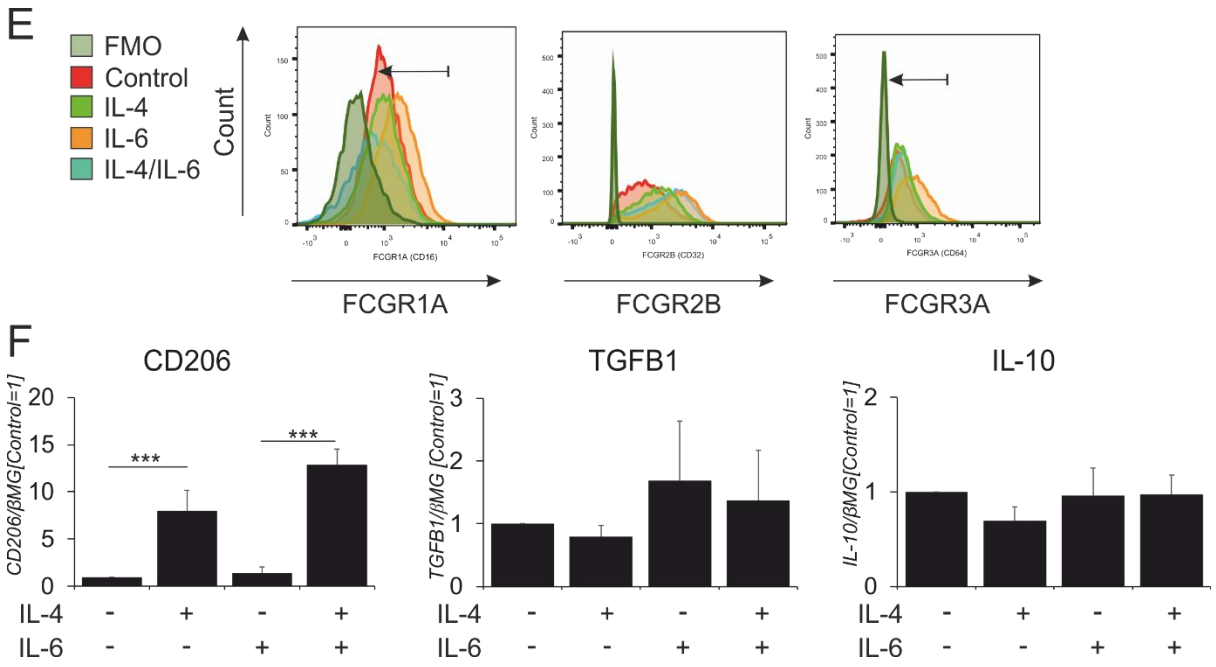

Figure 13: Gene expression defining differences in expression patterns of synergized or antagonized genes *(A) mRNA expression of uniquely induced genes in dually stimulated hMDMs. (B) mRNA expression of IL-6 target gene CD163 antagonized upon dual stimulation. (C-E) mRNA (C) and surface protein (D-E) expression of FcγRs in hMDMs treated for 24h (C) or indicated times (D) with cytokines. (F) mRNA expression of macrophage anti-inflammatory markers CD206, TGFB1 and IL-10. Error bars indicate Mean±SD (*, p<0.05, **, p<0.01, ***, p<0.005).*

Comparing our data with a recent analysis of IL-4/IL-6 co-stimulated murine macrophages [37] revealed considerable differences. The previous study suggested that the synergism of IL-4 and IL-6 was regulated by inositol requiring enzyme-1α (IRE-1α) activation. Therefore, we validated the downstream targets of IRE-1α-dependent (e.g. HERPUD1, XBP1s) as well as -independent endoplasmic reticulum (ER) stress markers (GRP78, ATF6, ERJD4). Our data show that expression of ER-stress-related genes remained unaltered after co-stimulation in hMDMs thus, indicating discrepancies to mBMDMs (Fig. 14A).

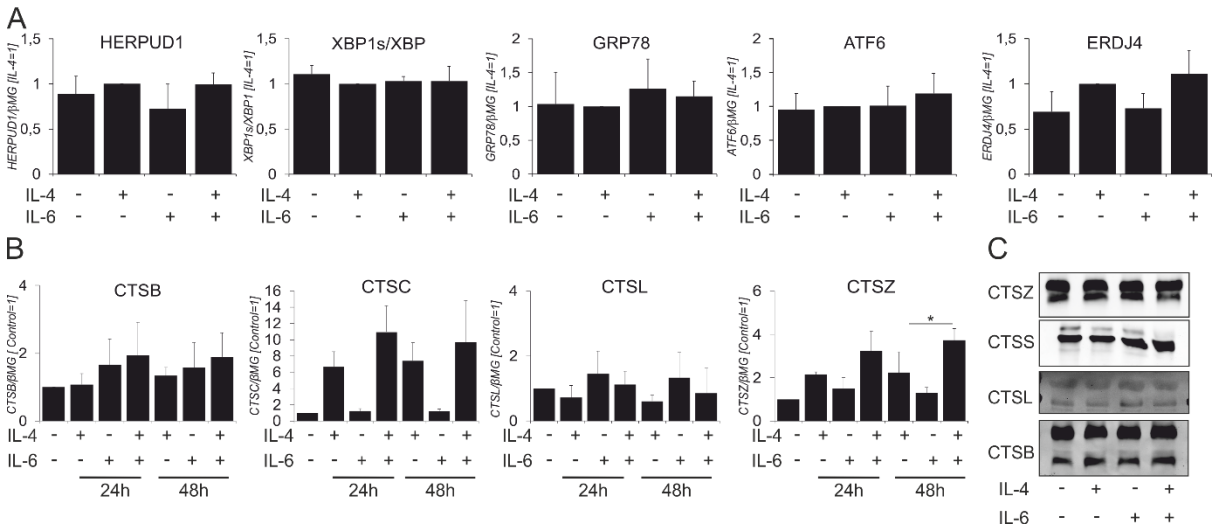

Figure 14: Expression levels of ER stress targets and cathepsins in hMDMs *(A, B) mRNA expression of ER stress markers and cathepsins and (C) cathepsin protein expression in macrophages treated for 24h (A, B) or 48 h (C) with IL-4 and IL-6 alone or in combination. Error bars indicate Mean±SD (*, p<0.05, **, p<0.01, ***, p<0.005).*

Neither did we observe mRNA or protein changes for the majority of cathepsin genes found upregulated in the murine system (Fig. 14B, C). Of 82 genes synergistically induced by IL-4/IL-6 in murine BMDMs only 2 (CCL8, CH25H) were present in the list of 292 IL-4/IL-6 synergistically induced genes in human macrophages (Table 35). Although gene sets co-induced in murine vs human systems are strikingly distinct, we do find similar classes of genes being upregulated, such as chemokines (Ccl8, Ccl7, Ccl24, Ccl12 in mBMDMs and CCL17, CCL18, CCL8, CCL23 in human macrophages) or C type lectin domain containing proteins (Clec10a vs CLEC4A, CLEC4G).

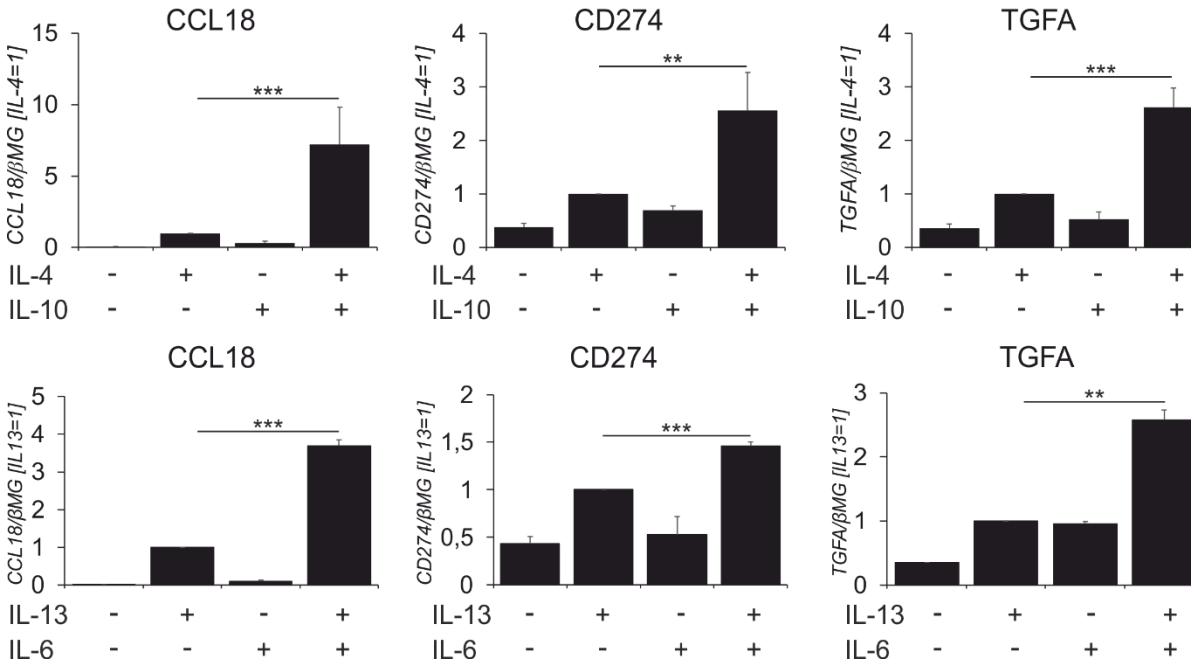

Figure 15. IL-4/IL-10 and IL-13/IL-6 co-stimulations induce similar changes in CCL18, TGFA and CD274 gene expression as IL-4/IL-6 co-treatment: *mRNA expression of indicated genes in hMDMs treated for 24h with indicated cytokines alone or in combination. Error bars indicate Mean±SD (*, p<0.05, **, p<0.01, ***, p<0.005).*

Since it was shown that IL-13 employs similar signaling as IL-4 whereas signaling by IL-6 may be partly mimicked by IL-10, we questioned whether IL-13 and IL-10 can substitute for IL-4 and IL-6 to induce IL-4/IL-6 co-regulated genes. Both IL-4/IL-10 and IL-13/IL-6 had similar effects on the induction of CCL18, TGFA and CD274 as compared to IL-4/IL-6 treatment (Fig. 15).

5.2. IL-6-induced upregulation of IL-4 target genes is STAT3-dependent

Signals by IL-4 and IL-6 are transduced, to a major part, by STAT6 and STAT3 phosphorylation respectively. Upon receptor activation, STAT6 and STAT3 undergo tyrosine phosphorylation and nuclear translocation activating downstream target genes. Analyzing tyrosine phosphorylation of STAT3 and STAT6 in whole cell lysates

(Fig. 16A) or nuclear extracts (Fig. 16B) upon IL-6 and IL-4 stimulation, we observed expected increases of STAT3 phosphorylation in IL-6-treated cells and STAT6 phosphorylation in IL-4-treated cells. However, neither changes in STAT6, nor STAT3 phosphorylation were detected after co-stimulation as compared to single cytokine treatments.

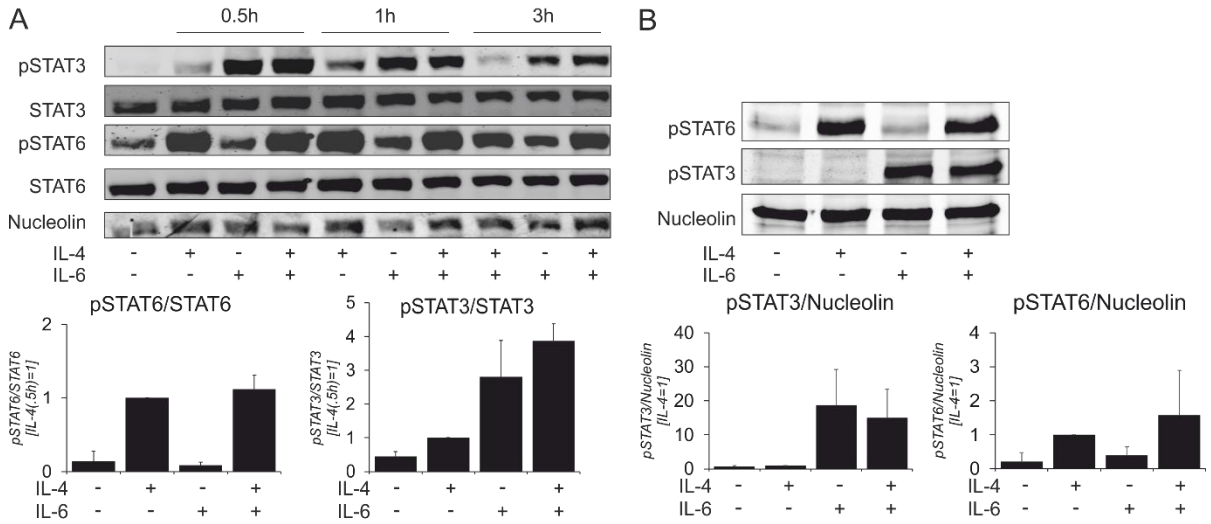

Figure 16: Effects of IL-4 and IL-6 on STAT3 and STAT6 phosphorylation *(A) Western blots of hMDMs total cell lysates treated for indicated times or (B) nuclear extracts for 1h (B) with indicated cytokines along with respective quantifications in the lower panel. Error bars indicate Mean±SD*

To assess the role of STAT3 in upregulating IL-4 target genes upon co-stimulation, we silenced STAT3 expression using siRNA, followed by single and dual cytokine treatments. A STAT3 knockdown reduced target gene expression in co-stimulated cells to levels observed in cells stimulated with IL-4 alone (Fig. 17 A, B), indicating that STAT3 is critical for the stimulatory effect of IL-6.

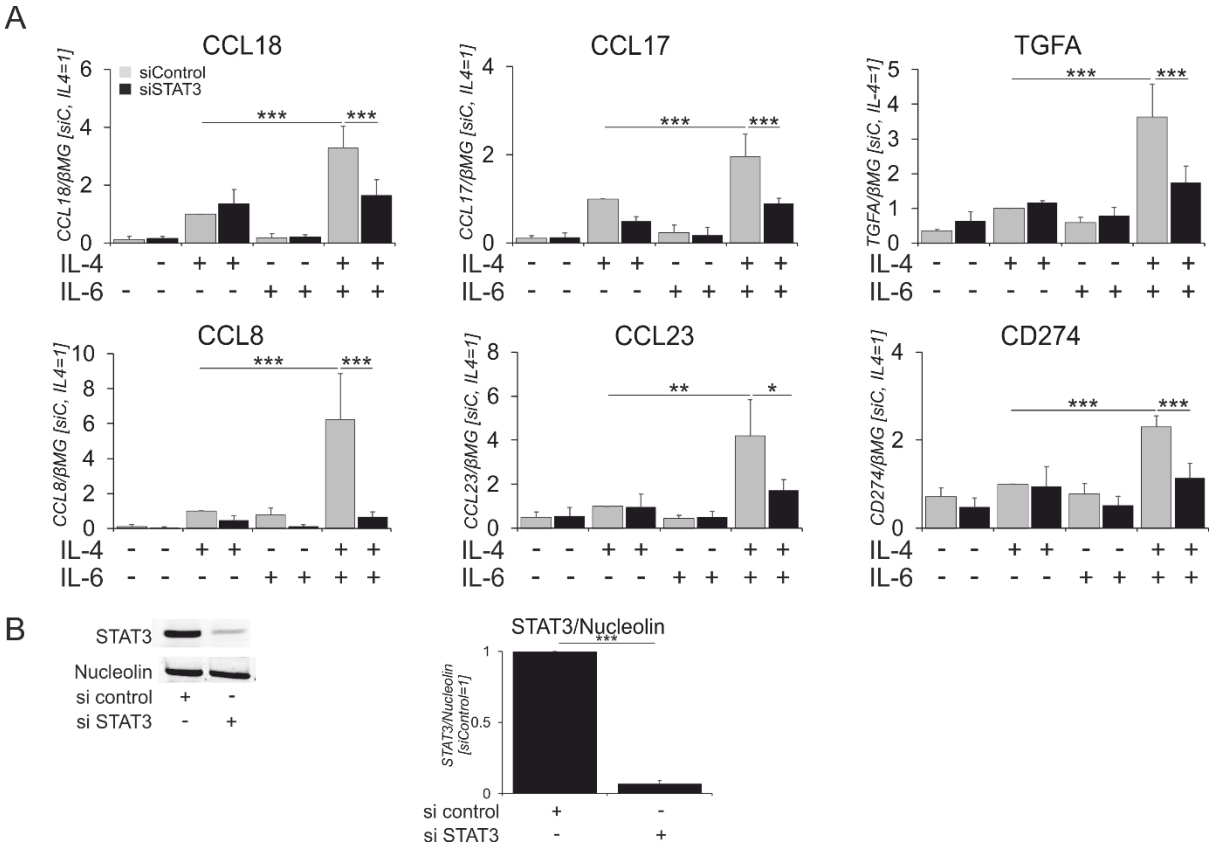

Figure 17: IL-6 synergy with IL-4 requires STAT3. *(A)mRNA expression of indicated genes in hMDMs transfected with control or STAT3 siRNAs for 72h prior to 24h-treatments with IL-4 and IL-6 alone or in combination. (B) STAT3 protein expression after STAT3 knockdown. Data are presented as mean±SD. *, p<0.05, **, p<0.01, ***, p<0.005.*

We next investigated STAT3 and STAT6 binding to cognate sites in target gene regulatory regions (GRRs) upon single and combined cytokine treatments. We explored the STAT3/STAT6 binding sites using existing ChIP-seq data across different cell lines [59-61], and the transcription factor binding site software JASPAR [62]. Of 109 genes differentially regulated between IL-4/IL-6 and IL-4, we focused on CD274 as a target involved in T cell immunosuppression, CCL18, a chemokine promoting tumor cell invasion and metastasis, and TGFA, a growth factor promoting tumor cell

proliferation. Testing several possible STAT3 and STAT6 binding sites in chromatin immunoprecipitation (ChIP) experiments, we found co-binding of STAT3 (Fig. 18A) and STAT6 (Fig. 18B) in GRRs of CCL18, TGFA, and CD274. STAT3 bound 8.1Kb upstream and STAT6 7.6Kb upstream of the transcription start site (TSS) in the CCL18 GRR, whereas STAT3 and STAT6 bound in close proximity (2-10bp apart) for CD274 (9Kb downstream of the TSS) and TGFA (37.6Kb downstream of the TSS).

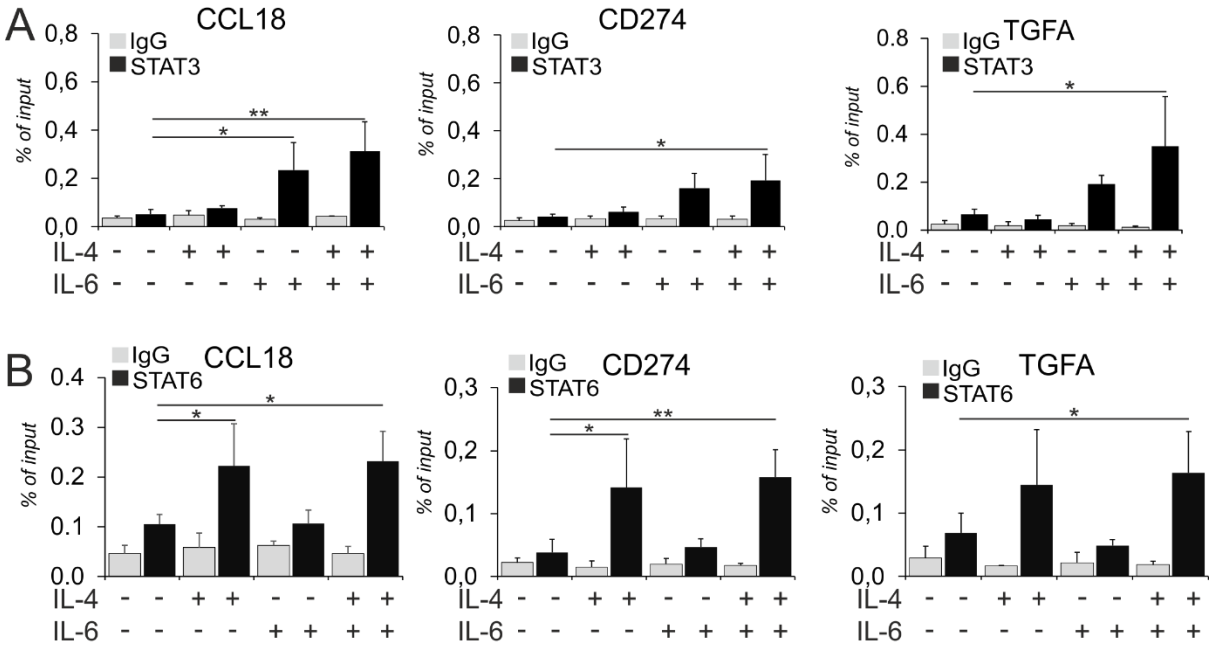

Figure 18: STAT3 and STAT6 bind the GRRs of co-induced target genes. *(A-B) HMDMs were treated for 1h with IL-4 and IL-6 alone or in combination for (A) STAT3 ChIP, (B) STAT6 ChIP. Data are presented as mean±SD. *, p<0.05, **, p<0.01, ***, p<0.005.*

Whereas IL-4 induced binding of STAT6 and IL-6 increased binding of STAT3 for some of the investigated targets, significantly increased co-binding of STAT3 and STAT6 to target GRRs was detected only in the presence of both, IL-4 and IL-6. We observed no increase in STAT6 or STAT3 binding upon co-stimulation as compared to single cytokine treatments.

The epigenetic landscape modulates transcription factor binding [63, 64], and previous studies [40] [38] highlighted the role of histone acetylation in transcription factor recruitment to chromatin in cytokine-treated macrophages. Therefore, we investigated changes of histone acetylation in the regulatory regions of co-induced genes after single and combined cytokine treatments. Analyzing levels of Lys9-acetylated histone H3 at STAT-binding sites of co-induced genes, we found increased H3 Lys9 acetylation upon co-treatment as compared to single treatments (Fig. 19).

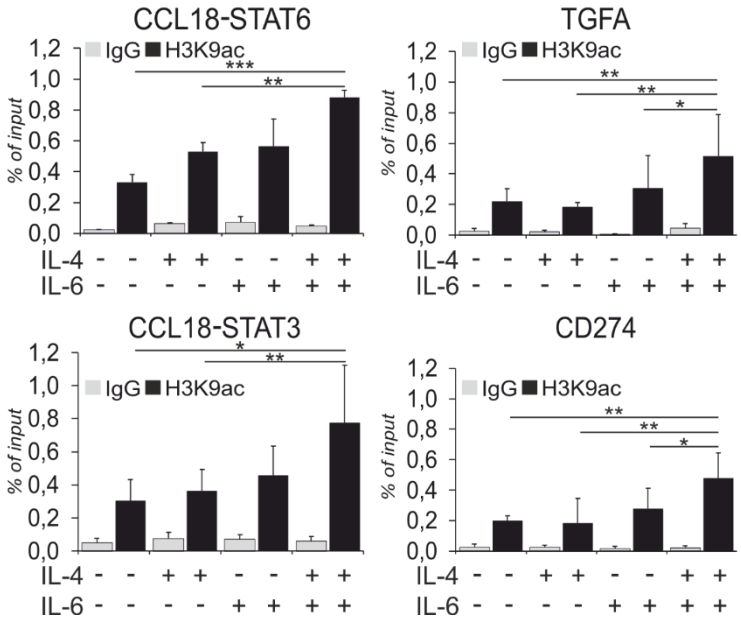

Figure 19: hMDMs were treated for 6h with IL-4 and IL-6 alone or in combination for H3K9ac ChIP for indicated genes at STAT3 and STAT6 binding sites. *Data are presented as mean±SD. *, p<0.05, **, p<0.01, ***, p<0.005.*

We further investigated if STAT3 and STAT6 binding at the enhancer sequence in CCL18 gene alone promotes enhanced gene expression. Therefore, we cloned the CCL18 core promoter (-147bp from TSS) with/without the enhancer binding sites in pGL3-basic luciferase reporter vector and measured firefly luciferase activity

normalized to activity of co-transfected renilla luciferase (SV40-pRL) as internal control.

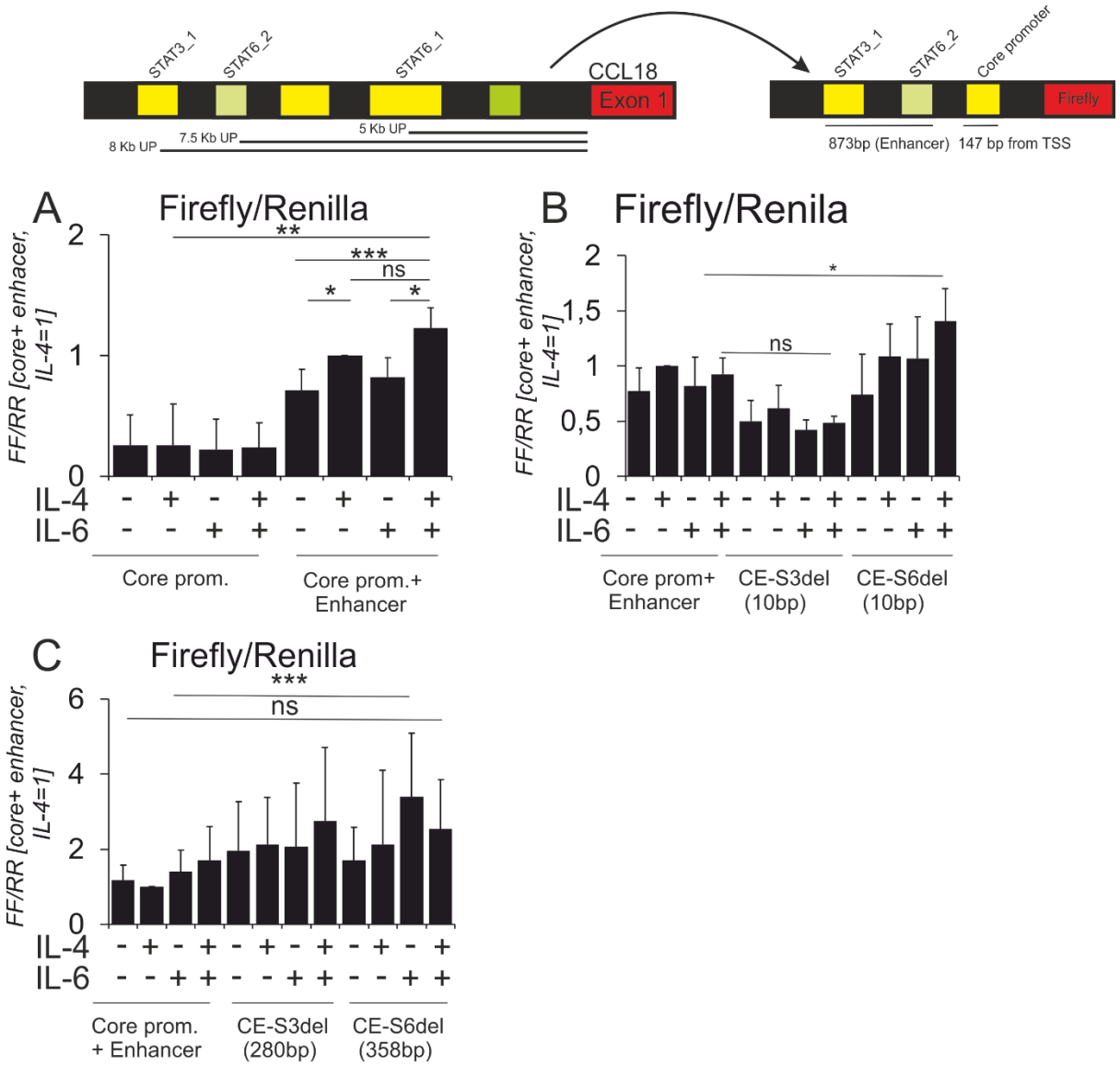

Figure 20: Quantification of firefly and renilla expression for cloned CCL18 enhancer sites with respective deletions in hMDMs. *Ratios of firefly to renilla luciferase activities in hMDMs transfected with (A) CCL18 core promoter and enhancer cloned in pGL3 basic luciferase reporter (B) same construct compared with constructs carrying 10bp deletions in STAT3/STAT6 binding sites or (C) constructs carrying deletions of 280bp in STAT3 and 358bp in STAT6 binding sites after 24hrs stimulation with IL-4 or/and IL-6.*

The firefly/renilla expression of enhancer binding sites (853bp long) along with CCL18 core promoter (20bp) was significantly increased relative to core promoter alone, implying that the enhancer sequences contribute to CCL18 gene expression. However, there was no increase in IL-4 vs IL-4/IL-6 stimulated condition (Fig. 20A). We speculate this is most likely due to failure of histone acetylation as observed in Fig. 19, since a cloned vector lacks the epigenetic machinery and represents the cloned DNA in a linear rather than a chromosome looping state (as occurring *in vivo*). We furthermore deleted either 10bp Fig. 20(B) or 200-400bp regions around STAT3 and STAT6 binding sites Fig. 20(C) using infusion-based plasmid deletions (Materials and methods for more detail), and unexpectedly there was no significant decrease in firefly activity. We assert the reason to failure of chromosome remodeling or binding of other transcription factors that might regulate the luciferase expression.

To validate that the STAT3/6 binding sites indeed regulate target gene expression, we used CRISPR interference (CRISPRi)[52, 53]. We prevented the binding of STAT3/STAT6 to their cognate sites at the CCL18 GRR by transfecting the cells with dCas9-KRAB (catalytically inactive Cas9 fused with KRAB repressor domain) and sgRNA plasmids targeting STAT3 and STAT6 binding sites (lying 500bp apart) individually.

As seen in Fig. 21A, in dCas9-KRAB and empty sgRNA vector (sg-RNA-MS2)-transfected cells IL-4 and IL-6 synergistically induced CCL18 expression. This effect was attenuated by blocking either the STAT6 or STAT3 binding sites individually.

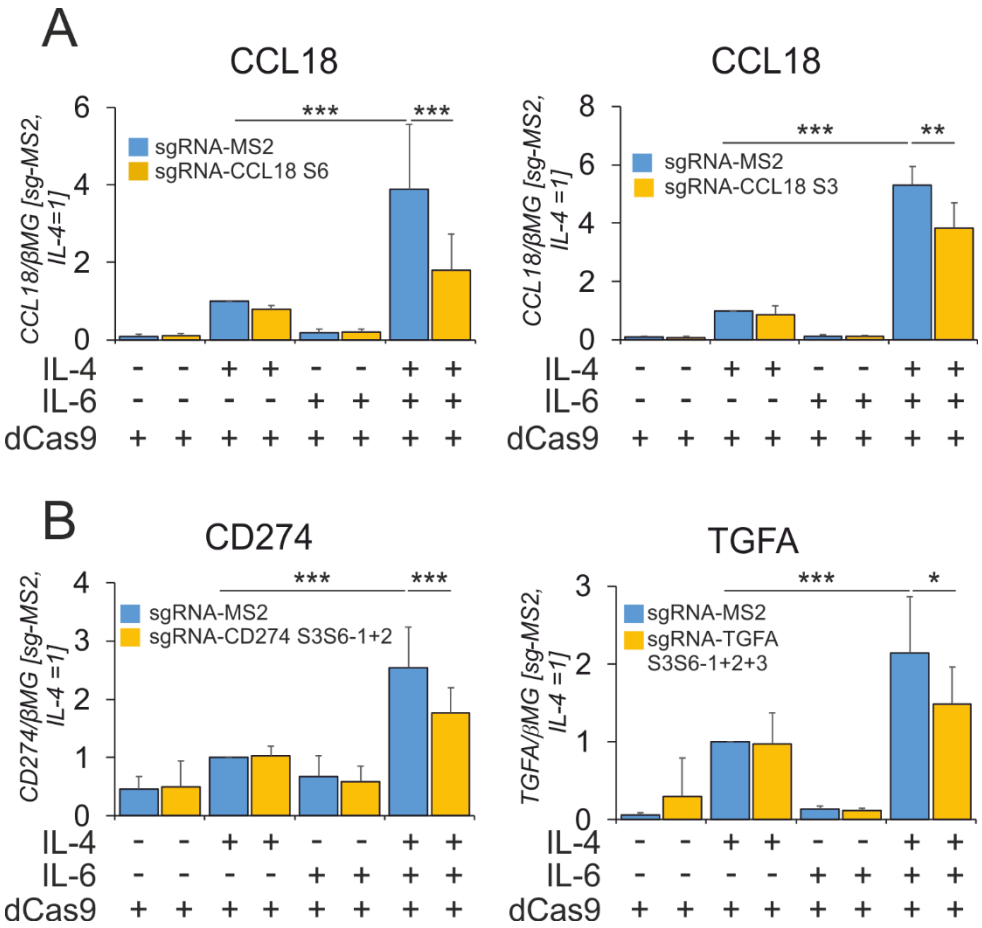

Figure 21: mRNA expression for target genes inhibited by blocking STAT3/STAT6 binding sites using CRISPRi. *mRNA expression for (A) CCL18 after blocking of STAT6- (left panel) and STAT3- (right panel) binding sites in CCL18 GRR (n=9) and (B) CD274 (left) and TGFA (right) expression after blocking two STAT3/STAT6 and three STAT3/STAT6 co-binding sites (n≥5-6) using CRISPRi-KRAB for 24h followed by stimulation with IL-4 and IL-6 for 24h. Data are presented as mean±SD. *, p<0.05, **, p<0.01, ***, p<0.005. mRNA expression is normalized to housekeeping gene β2-microglobulin (βMG). sg-RNA-MS2, sg-RNA-S3 or sg-RNA-S6 denote empty non-targeting control, sgRNA targeting STAT3 or STAT6 binding sites in CCL18 GRR. sgRNA S3S6-1+2 or S3S6-1+2+3 denote individual sgRNAs used to target different STAT3 or STAT6 co-binding (2-10bp apart) sites in the CD274 or TGFA GRRs. dCas9 denotes dead-Cas9 fused to KRAB repressor domain vector.*

We further tested our hypothesis for STAT3/STAT6 binding sites in GRRs of CD274 and TGFA. However, blocking STAT3 and STAT6 co-binding sites for the respective genes individually did not result in reduction of synergized target gene expression in dual stimulation (data not shown). Therefore, we blocked the binding sites in combinations i.e. 2 STAT3/-6 binding sites for CD274 (9 and 0.1Kb downstream of TSS, Fig. 21B, left) and 3 STAT3/-6 binding sites for TGFA (29.3Kb, 37.5Kb and 74.5Kb downstream of TSS, Fig.21B right). Collectively, these data suggest that binding of STAT3 and STAT6 in proximity to each other is required to mediate the synergism of IL-4 and IL-6 in inducing CCL18, CD274 and TGFA mRNA expression.

5.3. BATF cooperates with STAT3 and STAT6 to synergistically induce a subset of IL-4 target genes

We questioned whether co-treatment with IL-4 and IL-6 also induced transcription factors, which may cooperate with STAT3/STAT6, resulting in the increased expression of co-induced genes. Inspection of the IL-4/IL-6 co-stimulation transcriptome revealed increased expression of basic leucine zipper ATF-like transcription factor (BATF) upon IL-4/IL-6 co-treatment as compared to single treatments. To explore the role of BATF in more detail, we time-dependently tracked the changes of BATF mRNA (Fig. 22A) expression. BATF mRNA expression increased as early as 1h upon co-stimulation. Accordingly, we observed increased levels of BATF protein in nuclear fractions of IL-4/IL-6 co-stimulated within 1hr (Fig. 22B).

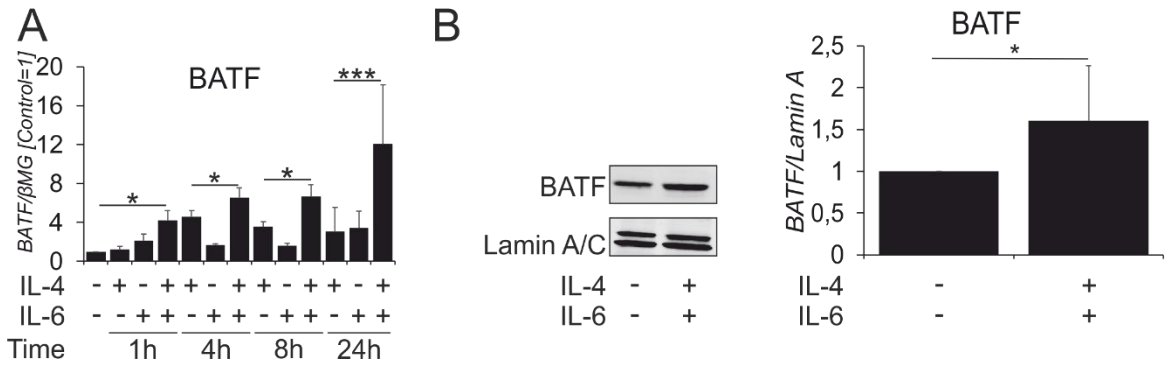

Figure 22: BATF gene and protein expression levels in hMDMs. *(A) Time course of BATF mRNA expression after treatments with IL-4 and IL-6 alone or in combination, n=5 (B) BATF protein in nuclear extracts of human macrophages treated with IL-4 and IL-6 for 1h., n=11*, **p<.05.*

We then investigated STAT3 and STAT6 binding to the BATF GRR using ChIP in cells stimulated with IL-4/IL-6 for 1h (Fig. 23). STAT3 and STAT6 binding sites were 1.2Kb downstream of the TSS and were only 5bp apart. We found no significant increase in STAT6 binding between IL-4 and IL-4/IL-6 stimulations. However, we found an increased STAT3 binding upon IL-4/IL-6 co-stimulation as compared to single cytokine treatments.

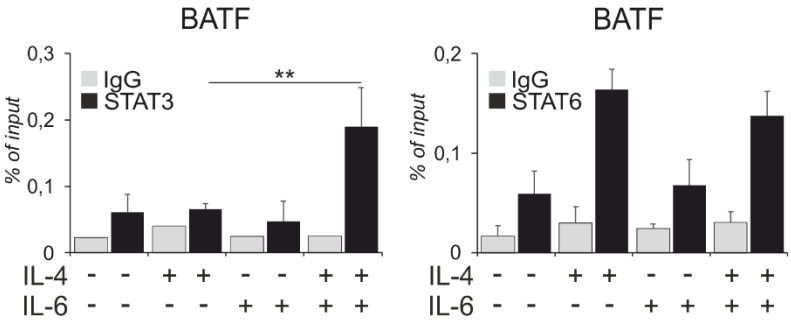

Figure 23: ChIP for STAT3 and STAT6 in hMDMs. *STAT3 and STAT6 binding in the GRRs of BATF 1h after cytokine treatments. Data are presented as mean±SD. *, p<0.05, **, p<0.01, ***, p<0.005*

STAT3 silencing abrogated the increase of BATF expression after co-stimulation, indicating that STAT3 along with STAT6 regulates BATF expression (Fig. 24).

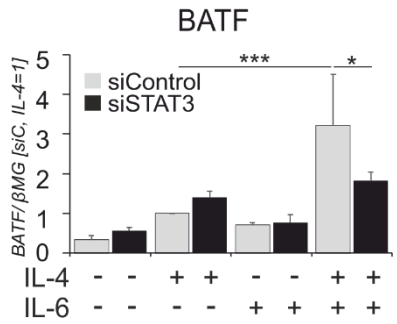

Figure 24: BATF mRNA expression in macrophages transfected with STAT3 siRNA 72h prior to 24h cytokine treatments*. Data are presented as mean±SD. *, p<0.05, **, p<0.01, ***, p<0.005*

To further investigate the impact of BATF on IL-4/IL-6-dependent gene expression we performed BATF silencing. Indeed, the mRNA expression of IL-4/IL-6 target genes (CCL18, CD274, TGFA, CCL8 and CCL23) was inhibited upon BATF knockdown (Fig. 25 A-B), indicating a possible role of BATF in cooperating with STAT3 and STAT6 to regulate co-induced target genes.

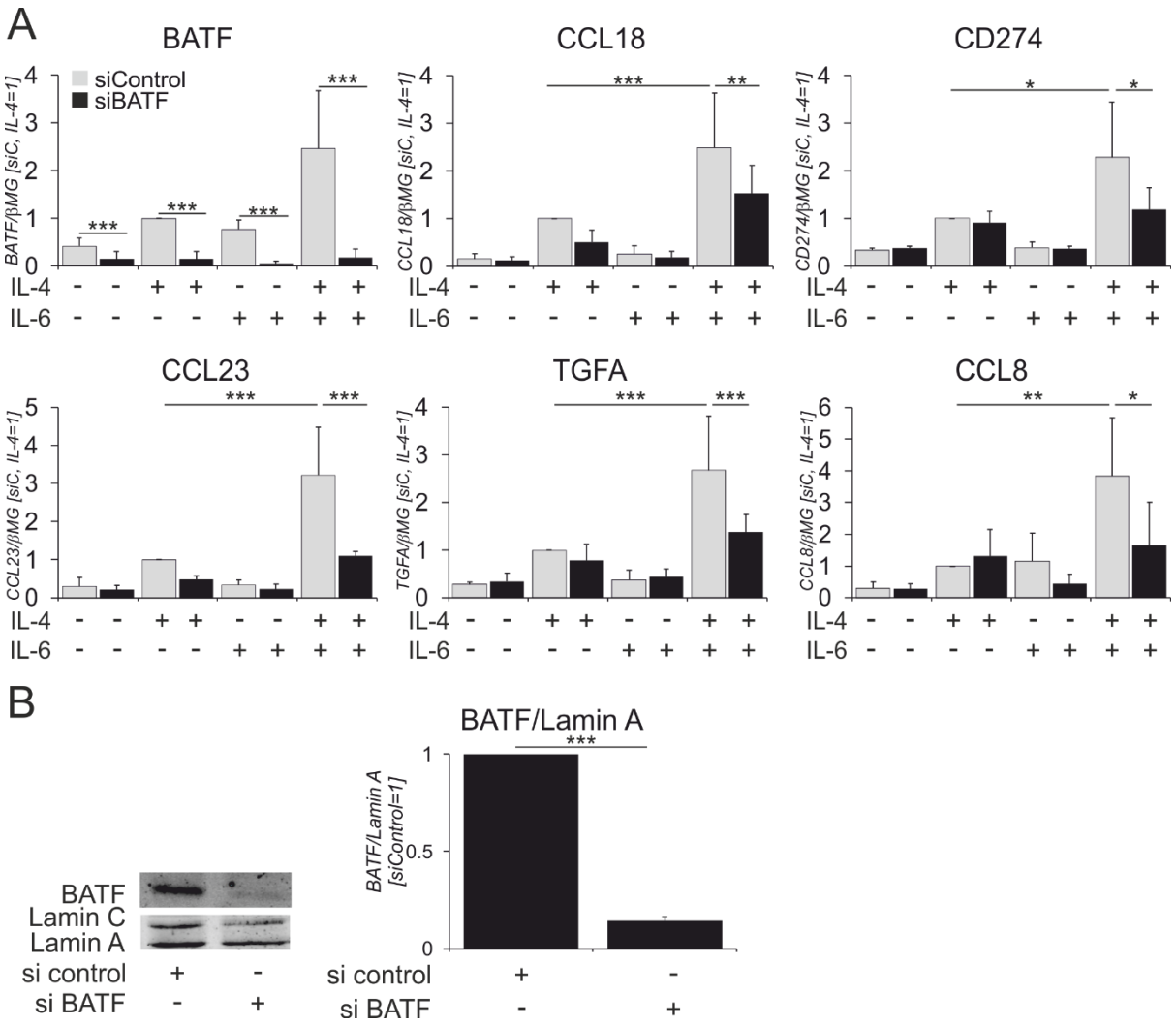

Figure 25: Expression levels after silencing BATF with siRNAs. *(A)* ***mRNA*** *expression of indicated genes in macrophages transfected with BATF siRNA 24h prior to 24h cytokine treatments. (B) Western blot analysis of BATF levels showing BATF siRNA knockdown efficiency for BATF. Error bars indicate (Mean±SD). (n=4, ***, p<0.005).*

Using BATF ChIP-seq data[65, 66] and JASPAR software we identified putative BATF binding sites in CCL18, TGFA and CD274 GRRs, 10, 29.5 and 37Kb downstream of respective TSS. Using ChIP, we further explored whether BATF binds to these elements. Fig. 26 shows that BATF binding to target gene GRRs increased in IL-4/IL-6 co-treated cells as compared to cells treated with IL-4.

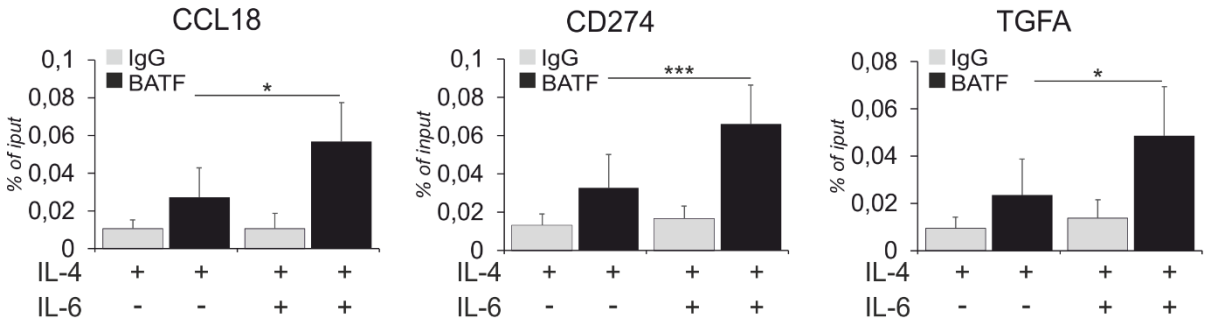

Figure 26: ChIP analysis of BATF binding at GRRs of indicated genes in macrophages treated for 6h with IL-4 and IL-6 alone and in combination. *Data are presented as mean±SD. *, p<0.05, **, p<0.01, ***, p<0.005*

We further analyzed the effects of histone acetylation at BATF binding sites (Fig. 27) and observed an increase of H3K9 acetylation upon co-stimulation, indicating increased chromatin accessibility at the BATF binding regions.

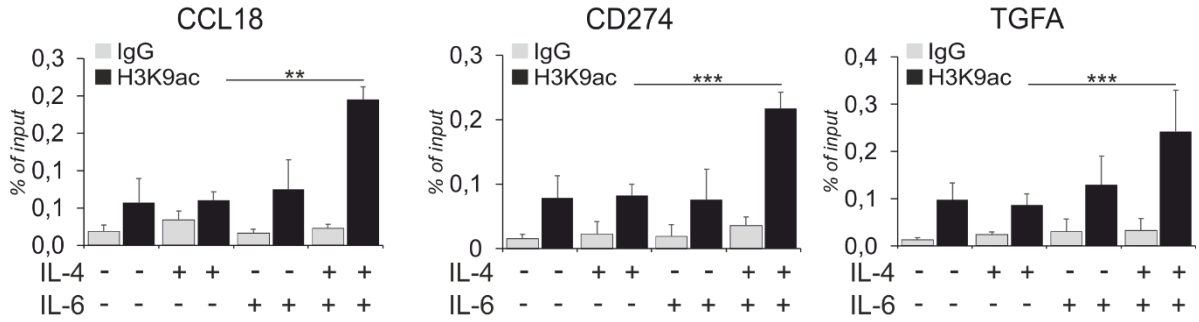

Figure 27: ChIP analysis of H3K9ac at GRRs of indicated genes in macrophages treated for 6h with IL-4 and IL-6 alone and in combination. *Data are presented as mean±SD. *, p<0.05, **, p<0.01, ***, p<0.005*

Blocking BATF binding sites in CCL18 GRR using CRISPRi, we detected decreased co-induction of CCL18 mRNA in cells transfected with sgRNA-BATF compared to cells transfected with empty sgRNA-vector, confirming that BATF binding functionally regulates STAT3 and STAT6 synergism (Fig. 28).

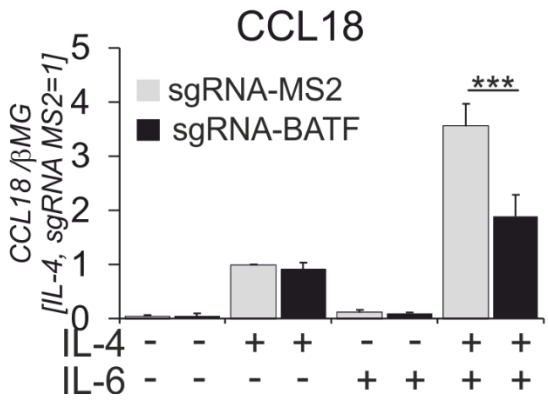

Figure 28: CCL18 mRNA expression in hMDMs transfected with CRISPRi against the BATF binding sites and treated for 24h with IL-4 and IL-6 alone and in combination. *Data are presented as mean±SD. *, p<0.05, **, p<0.01, ***, p<0.005.*

Investigating interaction partners of BATF, it was previously shown that BATF co-binds with IRF4 in a complex (Fig. 29) as represented in ChIP seq data showing co-localization of IRF4 and BATF binding peaks in CCL18 and TGFA GRR.

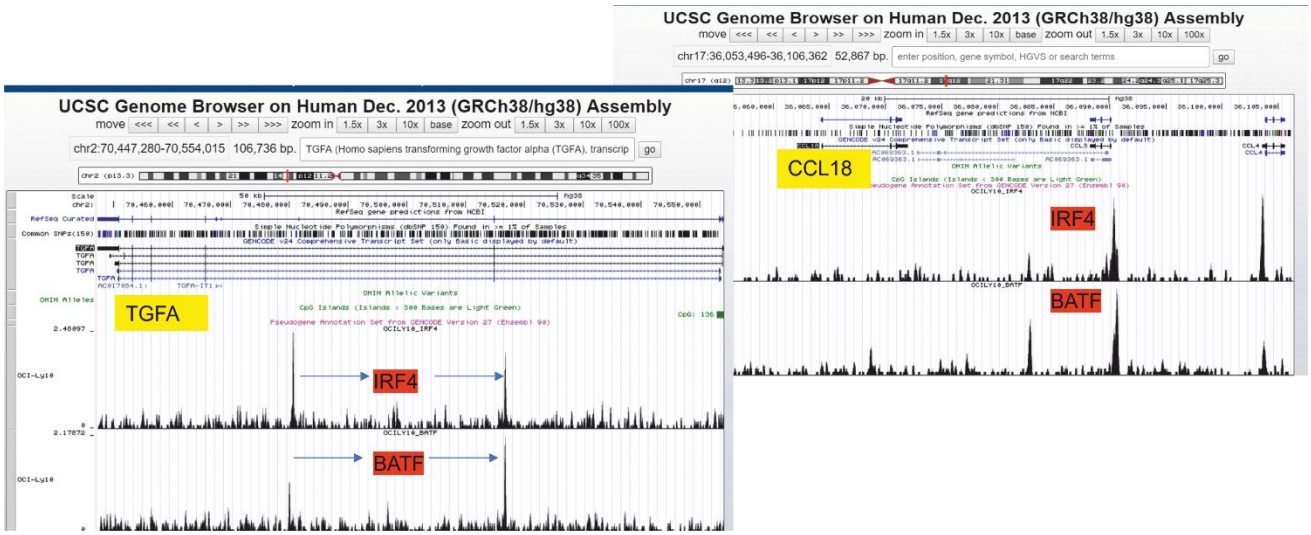

Figure 29: Binding sites for BATF and IRF4. *BATF (GSM2574766, GSM1370272, GSM1370277) and IRF4 (GSM803390, GSM1370274, GSM1370279) ChIP-seq data in B lymphocyte from blood (GM12878) show overlapping binding to TGFA and CCL18 GRRs.*

BATF and IRF4 co-binding was detected either within the gene (TGFA) or downstream (DS) of the TSS (30Kb DS CCL18) in the dataset [63]. It was also reported that the BATF and IRF act in a compensatory fashion to bind after IL-12 stimulation in conventional dendritic cells (cDCs). Moreover, BATF can replace the BATF3 functions as evidenced *in vitro* and *in vivo* by overexpressing BATF in in BATF3$^{-/-}$ mice, restoring the CD103^{+} Sirp-α^{-} cDC development in BATF3$^{-/-}$ bone marrow cultures[67]. We next summarized BATF interaction partners via *in silico* analysis using functional protein association networks (*STRING pathway)* (Fig. 30), and found among them ATF5 gene, which was uniquely present in our list of genes synergistically induced by IL-4/IL-6.

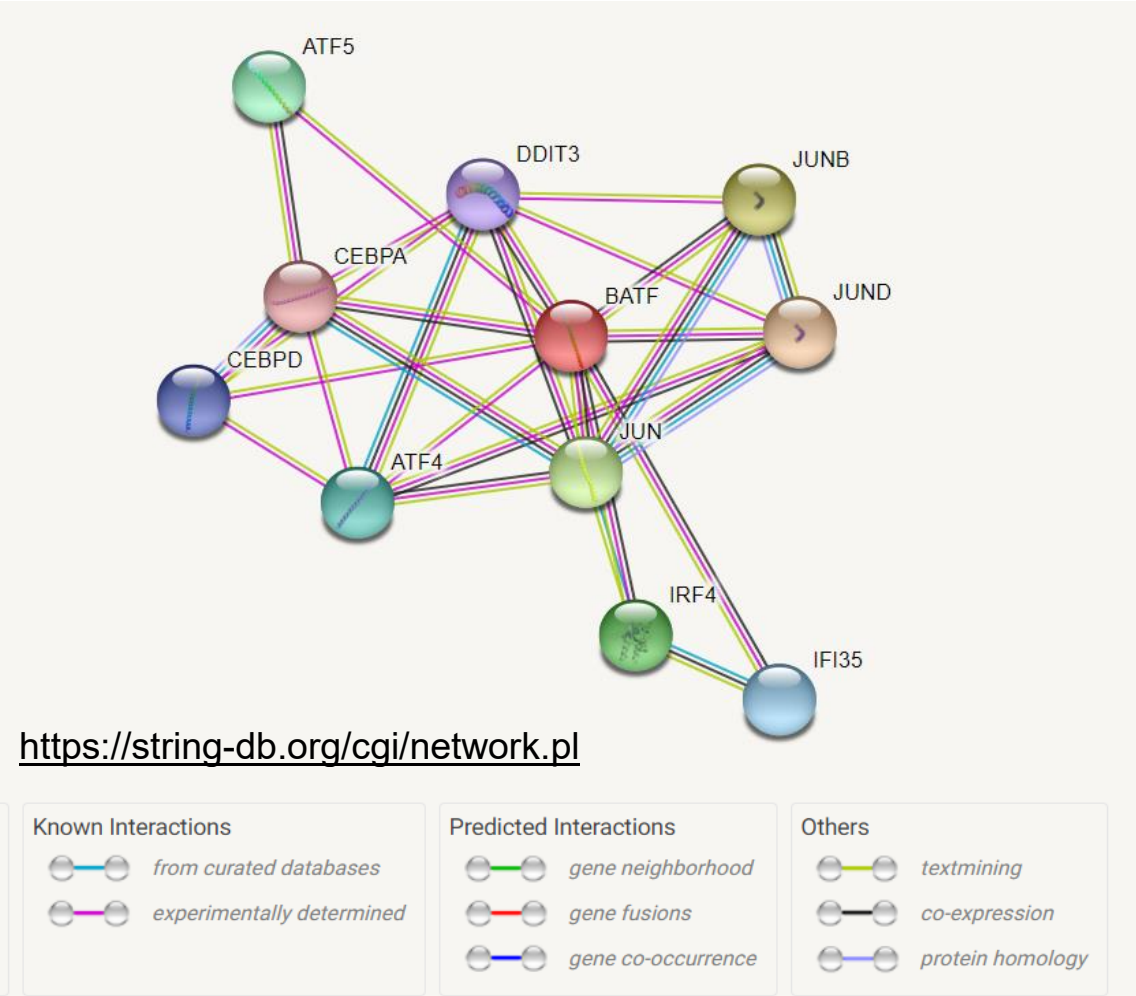

Figure 30: STRING network predicting BATF interaction partners

Interestingly, we found that dual cytokine stimulation significantly increased mRNA expression of BATF3, IRF4 and ATF5 compared to IL-4 stimulation alone (Fig. 31).

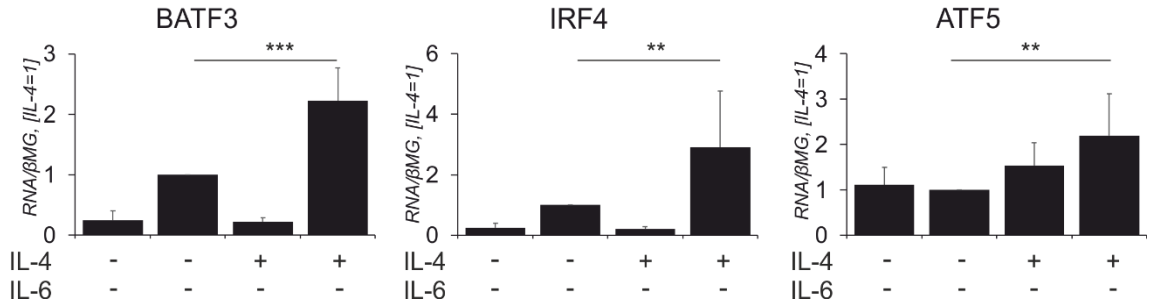

Figure 31: mRNA expression of BATF3, IRF4 and ATF5 measured 24hrs after cytokine treatments.

We then questioned if the synergistic induction of BATF3 and IRF4 by dual cytokine stimulation was STAT3- or BATF-dependent. Indeed, after silencing STAT3 and BATF, we found similar and significant reduction of BATF3 and IRF4 mRNA expression in IL-4/IL-6-treated cells as compared to control siRNA-transfected cells (Fig. 32).

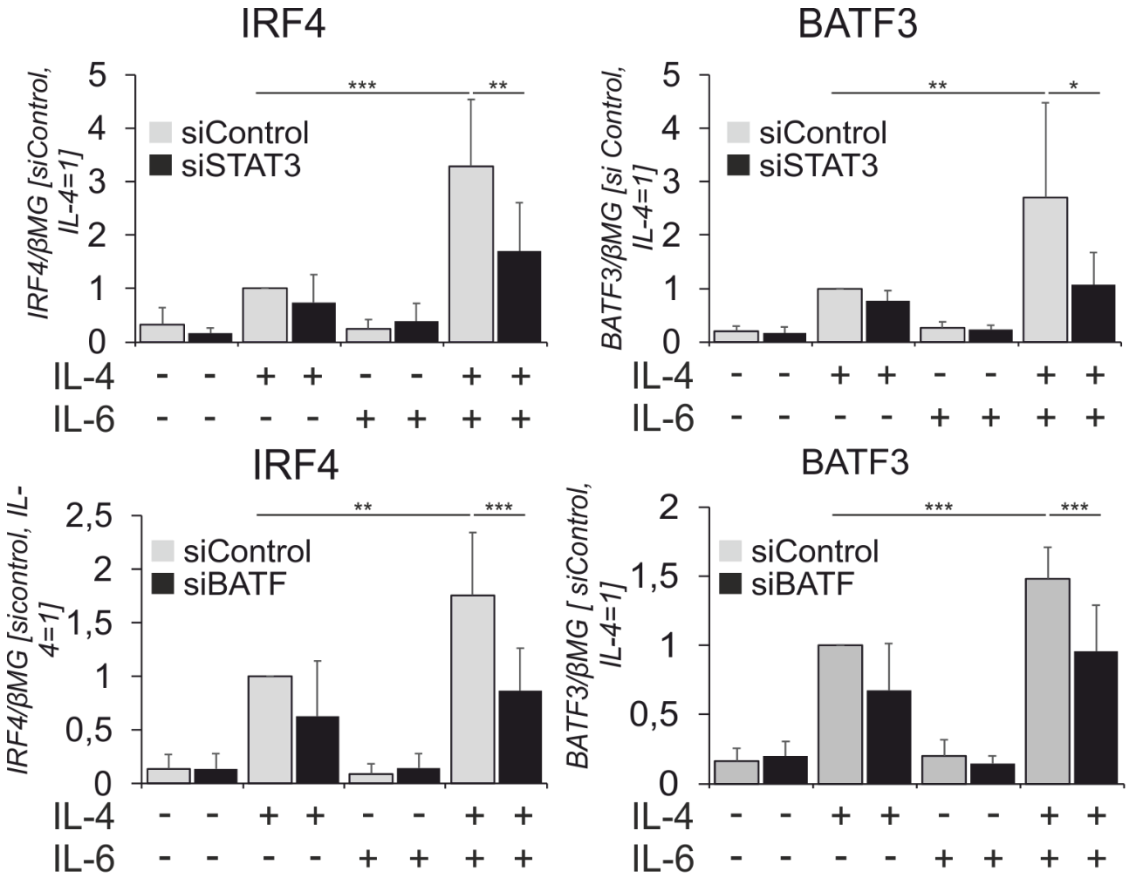

Figure 32: STAT3 and BATF knockdown suppresses synergistically induced BATF3 and IRF4 levels: *mRNA expression of indicated genes in macrophages transfected with STAT3 siRNA 72hr (upper) or BATF siRNA (lower) 24h prior to 24h cytokine treatments*

5.4. Functional analysis of IL-4/IL-6 co-stimulated macrophages

We explored functional implications of IL-4/IL-6 synergism for macrophage interactions with tumor and immune cells. As CCL18 was ascribed an important role in stimulating breast tumor cell migratory and pro-invasive phenotypes, we tested whether the secretome of cytokine-treated hMDMs promoted breast cancer cell migration. We tracked the migration of MCF-7 (ER^+, PR^+ $Her2^-$, luminal-like invasive ductal carcinoma (IDC)) and aggressive MDA-MB 231 (ER^-, PR^- $Her2^-$, basal like metastatic triple negative breast carcinoma (TNBC)) cells stimulated by conditioned

medium from hMDMs treated with IL-4 and IL-6 alone or in combination in 3D chemotaxis assays using Cell Observer technology. The motility of both MCF-7 (Fig. 33A) and MDA-MB 231 cells (Fig. 33B) increased upon stimulation with conditioned media from IL-4/IL-6-stimulated hMDMs as compared to cells incubated with conditioned media from single cytokine-treated cells. The extent of migratory response was highly similar in both MCF-7 and MDA-MB 231 cells treated with supernatants of stimulated hMDMs. Breast cancer cells treated with supernatants from dually stimulated hMDMs migrated twice the distance with a 2-fold higher velocity compared to cells exposed to supernatants of hMDMs stimulated with IL-4 alone.

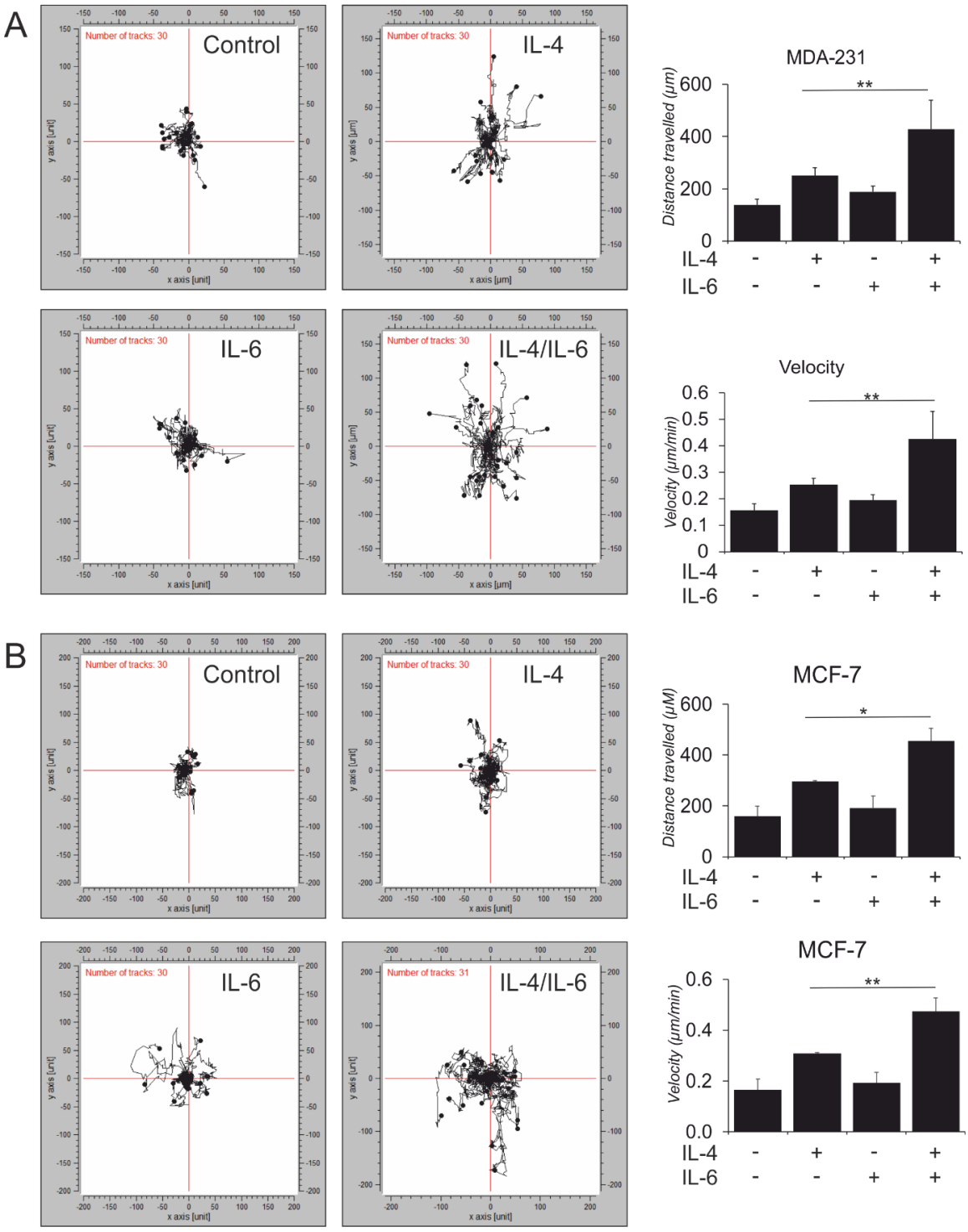

Figure 33: Activity assays investigating the downstream effects of IL-4/IL-6 co stimulation. *Representative tracks from 3D cell chemotaxis assays with (A) MDA-MB 231 and (B) MCF-7 cells incubated for 16h with conditioned media from polarized*

macrophages and quantified for accumulated distance travelled and velocity. (n≥3, 90 cells) in total were tracked

We found no difference in breast cancer cell proliferation for either MCF-7 or MDA-MB 231 cells after 72h of tracking (data not shown). We next investigated if viable cell conditioned media (VCM) from different mammary carcinoma cell lines (SKBR3, MCF-7 and MDA-MB 231) could induce a similar phenotype that we observe in hMDMs upon IL-4/IL-6 stimulations. Therefore, we incubated hMDMs for 24h with serum-free VCM generated from breast cancer cell lines. Surprisingly, we found that most of our target genes as well as CD206 and CD163 were induced only by VCM generated from MDA-MB 231 cells (Fig. 34A). Testing for levels of IL-4, IL-10, IL-13 or IL-6 in VCM we could detect only IL-6 released by MDA-MB 231 cells (Fig. 34B), suggesting that other factors released by the tumor cells, such as lactate, lipids or GM-CSF may substitute for IL-4/IL-13.

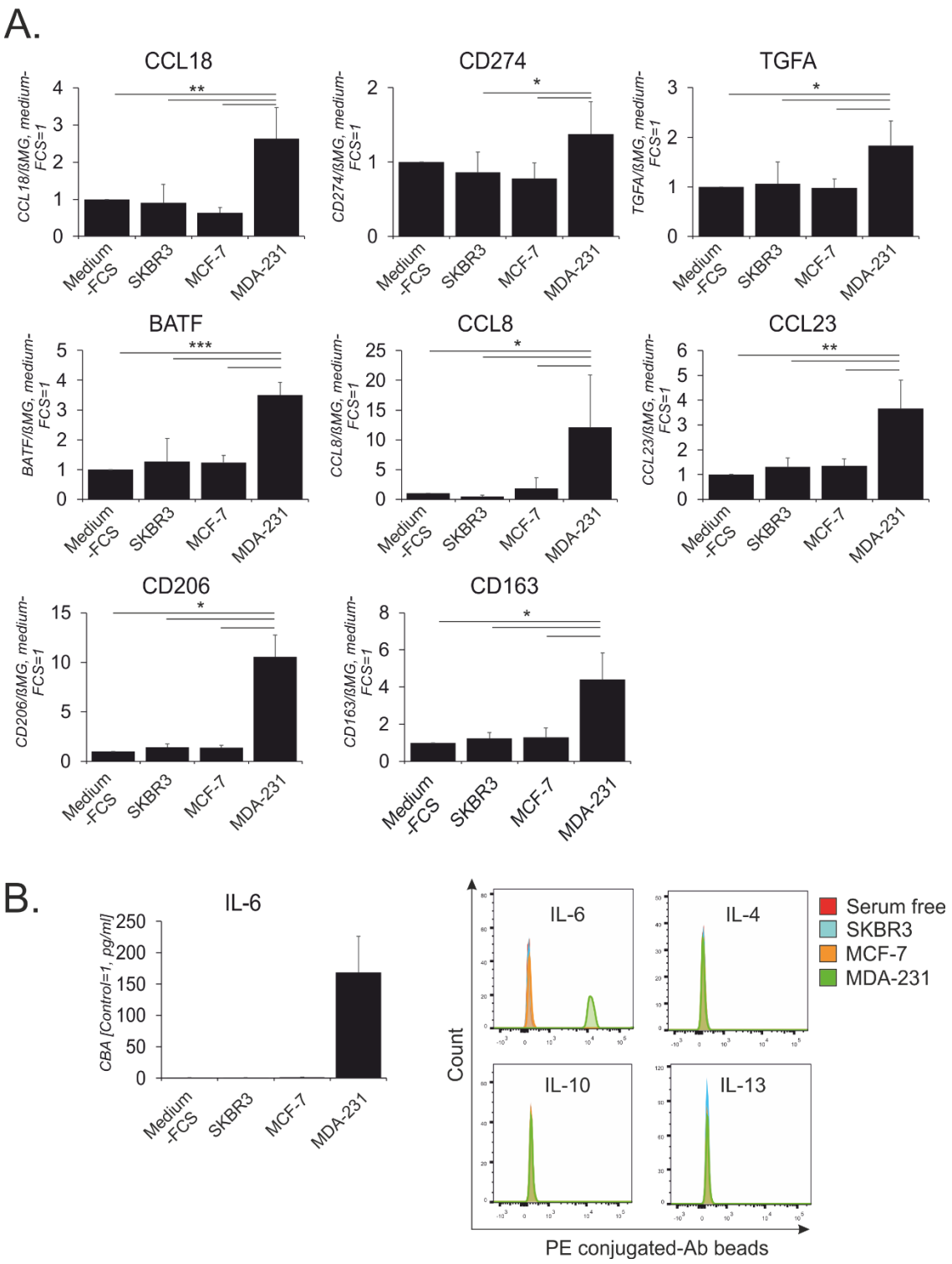

Figure 34: Expression levels after incubation of hMDMs with supernatants of breast cancer cell lines. *(A) mRNA expression of IL-4/IL-6 target genes in hMDMs after 24h incubation with supernatant from indicated breast cancer cell lines. (B) IL-6*

levels analyzed by CBA in tumor cell supernatants. Error bars indicate Mean±SD (, p<0.05, **, p<0.01, ***, p<0.005).*

Next, we validated the functionality of CD274 upregulation by performing a T cell activation assay with CD3/CD2/CD28 bead-activated T cells co-cultured for 3d in the presence of an isotype control (IgG) or an anti-CD274/PD-L1 antibody (Atezolizumab) with autologous hMDMs polarized with IL-4 and IL-6 individually or in combination for 48h prior to co-culture. A representative FACS panel (Fig. 35A) shows the gating scheme for analyzing T cell subsets distinguishing following subtypes: total T cells ($CD3^+$), $CD3^+CD4^+$ T helper cells, $CD3^+CD8^+$ cytotoxic T cells, $CD3^+CD4^+CD25^+CD127^-$ regulatory T cells (T_{reg}). We also quantified $CD3^+CD44^+CD25^-$ memory T cells (T_{mem})[68] , $CD3^+CD25^+CD44^+$ effector T cells (T_{eff}), $CD25^+CD44^-$ activated T cells ($T_{act.}$) for both $CD4^+$ and $CD8^+$ T cell subtypes.

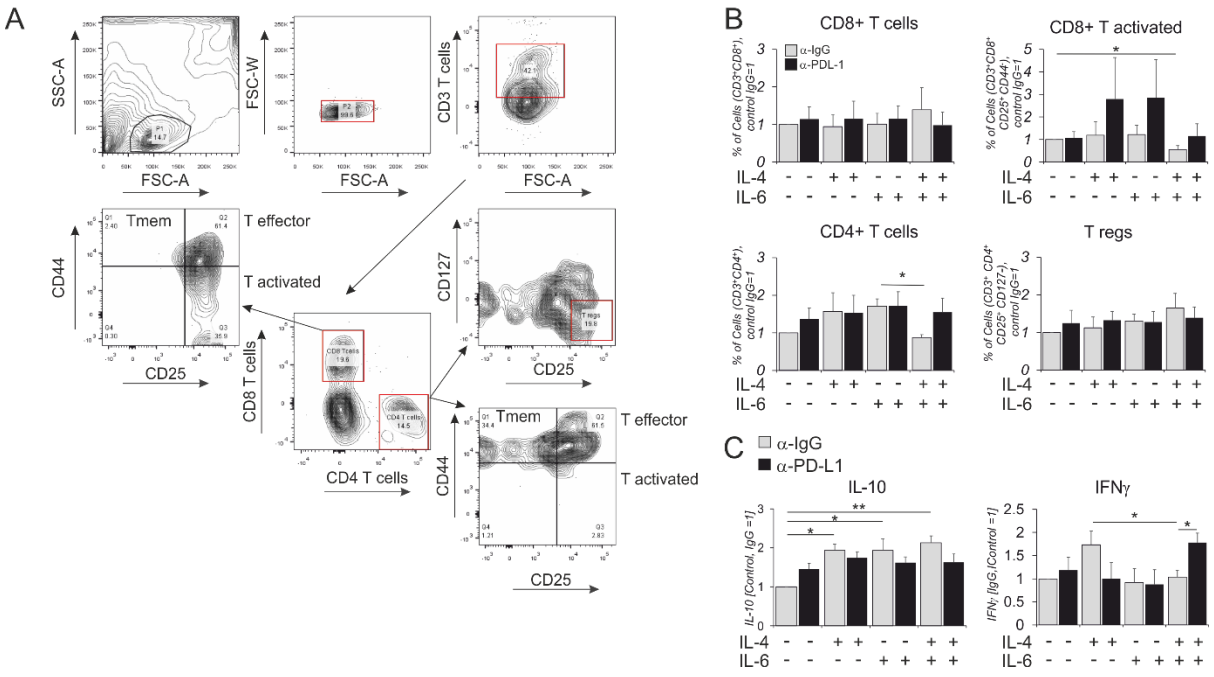

Figure 35: Quantification of T cell surface marker expression and cytokines released upon hMDMs-T cell co-culture. *(A-C) hMDMs were stimulated with indicated cytokines for 48h followed by co-culture with autologous CD3/2/28 bead-*

*activated T cells for the next 72h in the presence of isotype control IgG or anti-PD-L1 antibody. (n≥6-9) (A) FACS panel indicating different T cell markers profiled after co-culture along with respective fluorescent minus one (FMO) controls. (B) Percentages of T cell subtypes after the co-culture. (C) IL-10 and IFNγ secretion by total CD3$^+$T cells upon co-culture. Data are presented as mean±SD. *, p<0.05, **, p<0.01*

We found no major changes in relative cell abundance between the different treatment groups. There was a minor inhibition of percentages of CD8$^+$ T_{act} cells upon co-culture with IL-4/IL-6 stimulated hMDMs in the presence of isotype control antibody (Fig. 37B, upper panel). We also found 50% inhibition of total CD4+ T cells after co-culture with dually stimulated hMDMs as compared with hMDMs exposed to single IL-6 treatment (Fig. 35B, lower panel). The decreased percentages of CD8$^+$ T_{act} cells and CD4$^+$ T cells were partially rescued in the presence of anti-PD-L1 antibody. We observed a 1.5-fold yet non-significant increase in the percentage of T_{reg} after co-culture with dually stimulated vs. unstimulated hMDMs. We detected no significant changes in the percentages of CD4$^+$ or CD8$^+$ T_{eff} or T_{mem} cells (data not shown).

Although only minor changes in T cell surface marker expression were noticed, we observed altered cytokine production by T cells in co-cultures. Increased IL-10 levels, which may be produced by regulatory T cells, were detected upon treating macrophages with any of the cytokine combinations. However, this effect was PD-L1 independent (Fig. 35C, left panel). While levels of the TH2 cytokine IL-4 and the TH17 cytokine IL-17 were unaltered (data not shown), increased levels of IFNγ were observed after co-culture with IL-4 polarized hMDMs, an effect that was inhibited in dually stimulated hMDMs (Fig. 35C, right panel). This observation could be explained by decreased numbers of CD8$^+$ T_{act} cells or CD4$^+$ T cells, which might be TH1 polarized, in co-cultures with dually stimulated macrophages. Importantly, we

confirmed the role of increased CD274 in immunosuppression by dually stimulated hMDMs, since IFNγ levels in this group were markedly increased upon anti-PD-L1 treatment.

We also analyzed the expression of inhibitory T cell markers TIM3, LAG3, PD1 or CTLA4 either for $CD4^+$ or $CD8^+$ T cells, which showed no discernable changes after co-culture (Fig. 36A). However, TIM3, CTLA-4 and PD-1 expression on $CD4^+$T cells co-cultured with IL-4 polarized hMDMs increased in the presence of PD-L1 blocking antibody. This may occur as a compensatory mechanism to maintain increased expression of inhibitory receptors on $CD4^+$T cell surface.

The observed and unexpected increase in IFNγ expression after co-culture with IL-4 polarized hMDMs could be explained by increased expression of macrophage co-stimulatory receptors CD40, CD80 and CD86 (Fig. 36 B-D Table 32).

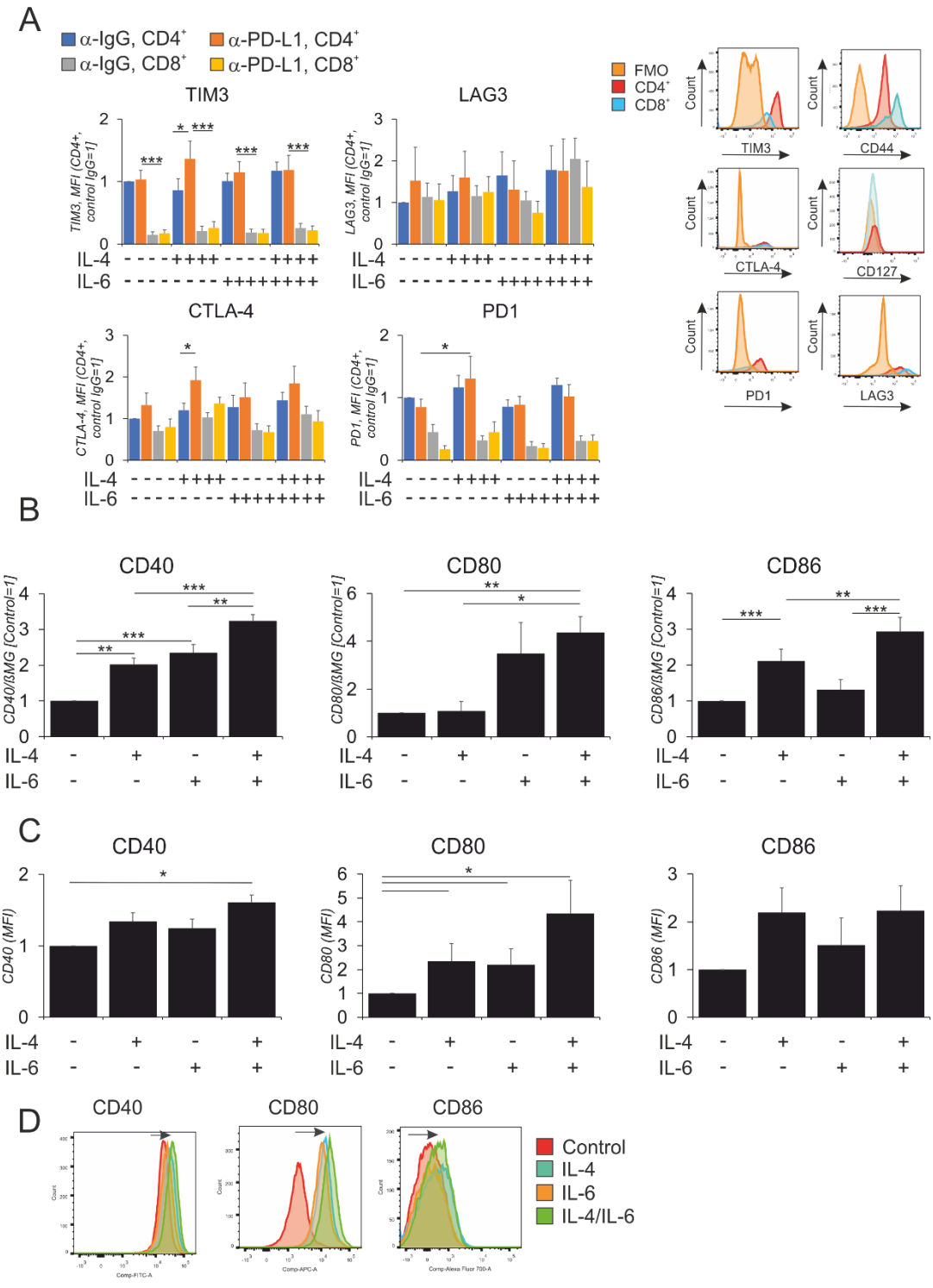
A
α-IgG, CD4+
α-PD-L1, CD4+
α-IgG, CD8+
α-PD-L1, CD8+
TIM3
LAG3
CTLA-4
PD1
TIM3, MFI (CD4+, control IgG=1]
LAG3, MFI (CD4+, control IgG=1]
CTLA-4, MFI (CD4+, control IgG=1]
PD1, MFI (CD4+, control IgG=1]
IL-4
IL-6
FMO
CD4+
CD8+
Count
CD44
CD127
B
CD40
CD80
CD86
CD40/ßMG [Control=1]
CD80/ßMG [Control=1]
CD86/ßMG [Control=1]
C
CD40 (MFI)
CD80 (MFI)
CD86 (MFI)
D
Control
IL-4
IL-6
IL-4/IL-6

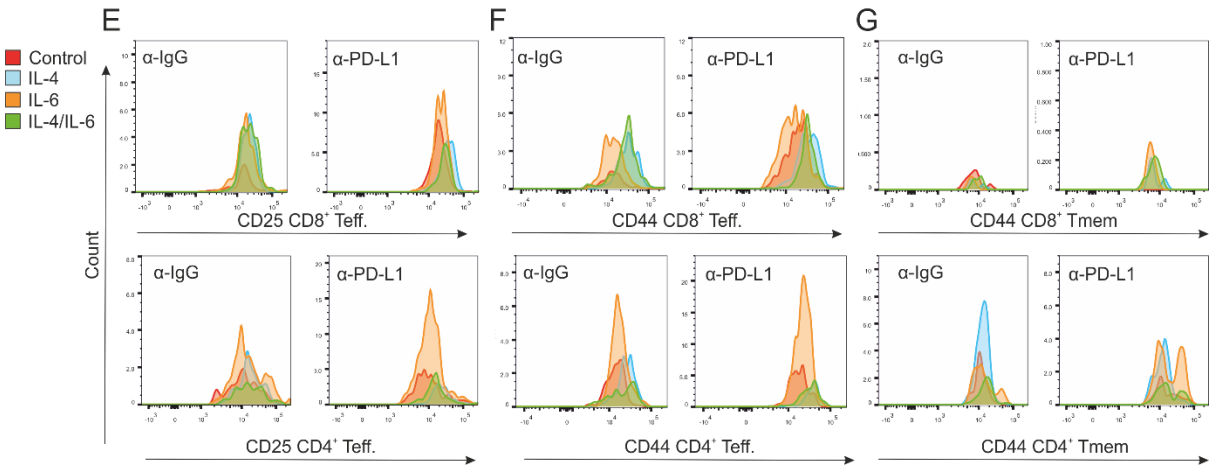

Figure 36: Expression of genes quantified via FACS on T cells after co-culture with hMDMs. *(A) Cell surface expression of inhibitory receptors on T cell surface after co-culture with polarized hMDMs for $CD4^+$ or $CD8^+$ T cells expressed as Mean fluorescent Intensity (MFI) represented (left) and Fluorescent minus one (FMO) controls (right) (B) mRNA normalized to β2-microglobulin and (C) cell surface expression for co-stimulatory CD40/80/86 markers on polarized hMDMs along with their respective (D) histograms. (E, F) Histograms showing surface expression for $CD25^+CD44^+$ T effector cells (T_{eff}) and (G) $CD25^-CD44^+$ T memory (T_{mem}) cells for $CD4^+$ and $CD8^+$ T cells. Error bars indicate Mean±SD with p value calculated by One-way ANOVA analysis with matched pair and Bonferroni post multiple correction test, 95% confidence interval (*, p<0.05, **, p<0.01, ***, p<0.005).*

Our experiments functionally validated that hMDMs co-treated with IL-4 and IL-6 released factors enhanced breast tumor cell motility. Furthermore, dual stimulated hMDMs augmented immunosuppressive molecules (PD-L1) inhibiting $CD8^+$ T cell activation, as well as total $CD4^+$ T cell percentages and likely IFNγ production. Through these mechanisms, hMDMs stimulated with IL-4 and IL-6 in combination potentially act in a pro-tumorigenic manner.

5.5. BATF expression is elevated in primary breast tumor stroma

We investigated the relevance of our findings for human cancer by analyzing BATF mRNA expression levels in breast tumor stroma using GEO2R analysis. Exploring publicly available breast cancer datasets for tumor stroma BATF expression, we found significantly increased BATF expression in tumor stroma compared to normal tissue stroma in ductal carcinoma in situ (DCIS/IDC)[48] (Fig. 37A) or Triple negative breast carcinoma (TNBC) (Fig. 37B)[49] or Her2+ breast carcinoma (Fig. 37C)[50] or Invasive breast carcinoma (Fig. 37D)[51].

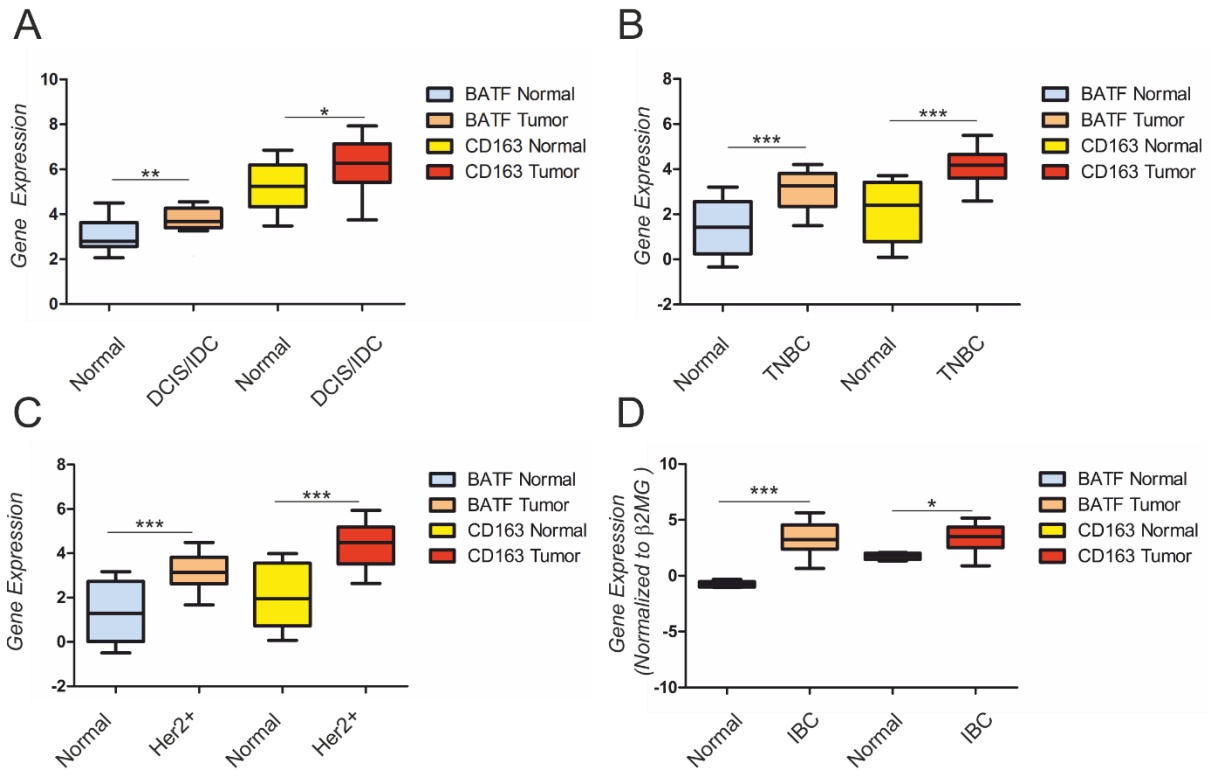

Figure 37: BATF expression in tumor stroma correlates with IL-4/IL-6 target genes. *Datasets from previously published studies by Ma et al. (A), Saleh et.al (B), Liu et.al (C), and Finak et al. (D-F) were analysed using GEO2R. (A-C) Box and whiskers plots with 10-90 % error bars for BATF, macrophage marker (CD163)*

expression in normal tissue (A, n=14; B, n=12; C, n=14; D, n=6) versus tumor stroma (A, n=18; B, n=58; C, n= 39; D, n =53) in breast carcinoma samples.

BATF expression was induced along with synergistically induced IL-4/IL-6 target genes (CCL18, CCL8, CCL23, CD274, FCGR2B) in breast tumor versus normal tissue stroma (Fig. 38A). Analysis of sample-matched expression of BATF and CCL18 in tumor stroma revealed significant positive correlation (Fig. 38B). We further asses the BATF expression in different grades of breast tumor and normal stromas and observed increased expression with increase in tumor stage (Fig. 38C). Since, macrophages closely relate to myeloid cell origin cells, we speculated if BATF expression could also be correlated to poor patient survival in myeloid origin neoplasms (Fig.38D). We observed poor patient survival in patients expressing high levels of BATF. This data indicates that cells in tumor stroma express high levels of BATF that can potentially contribute to tumor progression, suggesting that BATF may be a potential cancer biomarker. candidate.

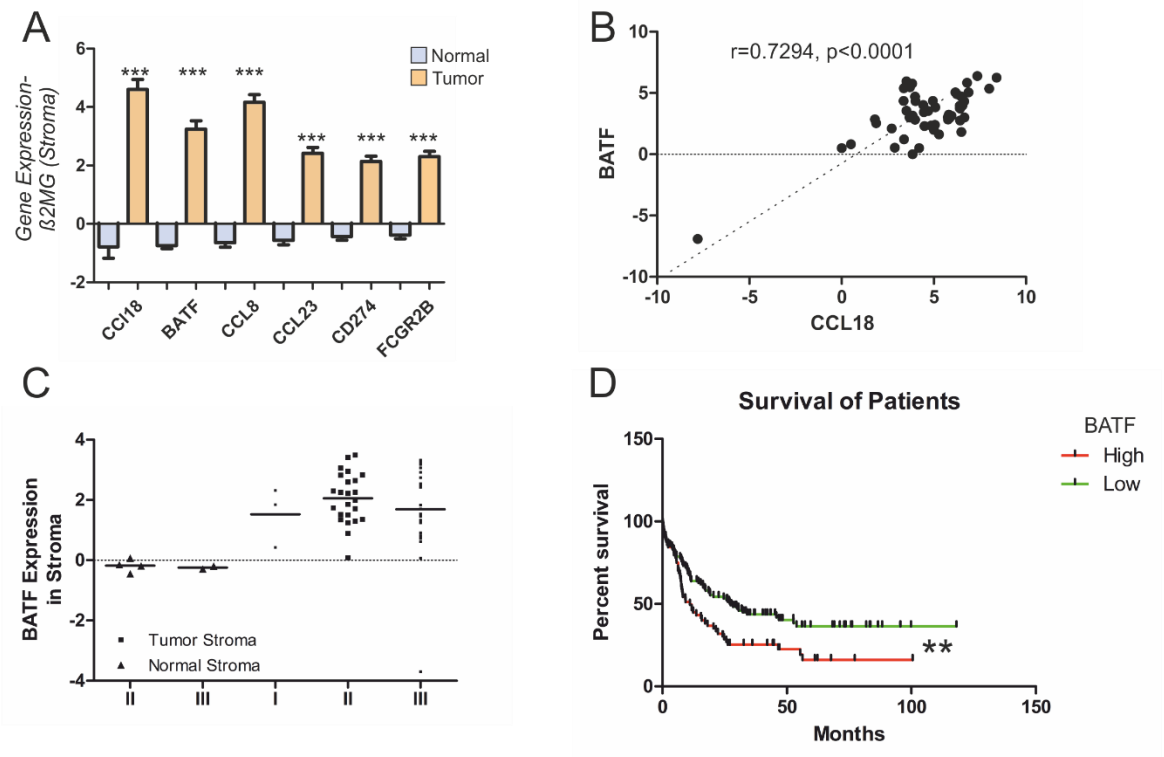

Figure 38: Correlation of BATF with different tumor grades and cell type *(A) Gene expression for indicated genes in tumor versus normal stroma. Two tailed, 95% confidence, non-parametric t-test was used for statistical analysis (B) Pearson correlation analysis for BATF and CCL18 expression in tumor stroma shows a positive correlation (R=.7294, p<.0001, n= 53). (C) BATF expression in breast and normal stroma in different tumor grades from Finak et.al. (D) Kaplan–Meier survival curve correlating poor prognosis for patient survival associated with high expression levels of BATF (n=173). Data are presented as mean± 10-90% SEM. *, p<0.05, **, p<0.01. ***, p<0.005.*

6. Discussion

TAMs are subjected to a variety of cytokines promoting their tumor-supportive phenotype. Here we carried out mechanistic and functional analyses to elucidate how two cytokines of the tumor microenvironment, IL-4 and IL-6, cooperate in altering the transcriptome of human macrophages. Comparing our data with a previously published analysis of IL-4/IL-6 co-stimulated transcriptome of murine macrophages [37] revealed an explicit non-redundancy in synergistic responses upon IL-4 and IL-6 stimulation in human versus mouse systems. Thus, whereas synergistic effects of IL-6 and IL-4 on gene expression in murine BMDMs were suggested to depend on the activation of the unfolded protein response (UPR)-mediating enzyme IRE-1α [37], we found no evidence involving UPR and its IRE-1α branch in the human macrophage transcriptome response to IL-4/IL-6 co-stimulation. In contrast to mouse data, IL-4/IL-6 co-stimulation elicited no change of mRNA or protein expression for the majority of cathepsins in human macrophages. In fact, only 2 genes were synergistically induced both in murine and human data sets. However, similar classes of genes were induced, e.g. chemokines or C-type lectins. These discrepancies are reminiscent of previously acknowledged differences between human and murine macrophages regarding IL-4 stimulation [69, 70].

We explored the mechanism of IL-6 mediated synergism and find neither increased differences in STAT3 or STAT6 nuclear translocation, nor the increase in IL-4 receptor expression as suggested earlier [29]. STAT3 silencing confirmed its central role in the synergistic effects of IL-4/IL-6 co-stimulation. Speculating that STAT6/STAT3 co-binding in the regulatory regions of target genes upon IL-4 and IL-6 co-stimulation drives increased gene expression [29], we found and validated closely spaced STAT6/STAT3 binding sites in GRRs of co-induced genes. Furthermore, increased

H3K9 acetylation in these GRRs was detected upon co-stimulation, indicating enhanced chromatin accessibility for transcription factor binding [71, 72]. Using CRISPRi, we validated functionality of STAT3/STAT6 binding sites for CCL18, CD274 and TGFA co-induction wherein the dCas9 fused KRAB repressor domain blocks the binding of transcription factors in 20bp regions. Individual or combined blocking of STAT6 binding sites in CCL18 GRR alleviates synergistic induction of CCL18 in IL-4/IL-6 polarized hMDMs. For CD274 and TGFA, where the STAT3 and STAT6 binding sites were only 2-10bp apart, we used a common sg-RNA for different co-binding sites. Unlike CCL18, blocking STAT3/STAT6 binding sites in GRR of CD274 and TGFA individually did not inhibit the synergistic gene induction, necessitating blocking 2 STAT3 and STAT6 co-binding sites for CD274 and 3 co-binding sites for TGFA in combination to observe reduced synergistic induction. This could be explained by multiple STAT3/STAT6 binding sites mediating induction of CD274/TGFA and compensation by other STAT6/STAT3 sites upon individual transcription factor blocking.

Investigating whether STAT6/STAT3 co-binding induced transcription factors that cooperated in transmitting synergistic effects of IL-4/IL-6 co-treatment, we identified BATF as one such factor. BATF is a pivotal transcription factor shown to control IL-4 production by T follicular helper cells [73], to function as an early $CD8^+$ T cell differentiation checkpoint [74], or to regulate IL-23-driven colitis by acting on Th17 cells [75]. However, the function and roles of BATF are largely unexplored in myeloid settings. Synergistic induction of BATF was STAT3-dependent as confirmed by STAT3 knockdown and STAT3 and STAT6 binding to the BATF GRR as revealed by ChIP experiments. Silencing BATF repressed synergistically induced IL-4/IL-6 target genes analogous to STAT3 knockdown. Furthermore, these genes harbored BATF binding sites showing increased BATF occupancy and H3K9 acetylation upon co-stimulation.

Using CRISPRi to block BATF binding in the CCL18 GRR we found decreased CCL18 induction, further supporting BATF involvement in target gene regulation. Therefore, we suggest that STAT3 and STAT6 binding induces BATF, which binds the GRR along with STAT3/STAT6 and thus cooperates in synergistic upregulation of IL-4/IL-6 co-induced genes.

IL-4 and IL-6 co-induced BATF transcription factor that synergizes with STAT3 and STAT6, could be compensated by BATF3 or IRF4 binding in *in vivo* conditions. We base this hypothesis on our observation that BATF3 and IRF4 are not only synergistically induced by dual cytokine stimulation, but also regulated by STAT3 and BATF as evidenced by siRNA knockdowns. Also, BATF and IRF4 were previously shown to co-bind in a complex.

To functionally characterize the role of differentially regulated genes, we performed a series of activity assays, observing increased motility of MCF-7 and MDA-MB 231 cells incubated with conditioned media from IL-4/IL-6-treated hMDMs. This increase could be due to the enhanced chemokine release by co-stimulated macrophages. One such potential chemokine could be CCL18 as it was previously described to bind the PITPNM3 receptor and induce motility in MCF-7 and MDA-MB 231 cells[13].

We further noticed that hMDMs upon dual stimulation inhibit $CD8^+$T cell activation as evidenced by reduced IFNγ secretion and reduced percentages of $CD8^+$ activated T cells from autologous CD3/2/28 bead-activated T cell in co-culture assays. We found this effect to be PD-L1 dependent as using PD-L1 blocking antibody rescued the above phenotypes. Of interest was increased IFNγ release upon co-culture of T cells with IL-4 polarized hMDMs. We speculate that the increased expression of immune co-stimulatory receptors (CD40, CD80, CD86) and modest induction of PD-L1 in IL-4-

polarized hMDMs shifts the macrophage phenotype towards immune/T cell activation. This effect is reversed after dual cytokine treatments through synergistic induction of PD-L1, whose immunosuppressive effects override the co-stimulatory hMDMs cell surface phenotype, leading to reduced IFNγ secretion by $CD8^+$ T_{act} cells and TH1 cells.

Analysis of GEO datasets revealed elevated expression of BATF together with CD163 macrophage marker in breast tumor versus normal stroma, which positively correlated with CCL18 and several other IL-4/IL-6 target genes. While this may suggest that BATF levels increase because of enhanced macrophage infiltrates, other immune cells express BATF as well, and as our study indicates BATF levels may increase in macrophage upon activation. Nevertheless, these data suggest that macrophages expressing BATF may be of clinical relevance in the progression of breast cancer.

7. Conclusion

In summary, our study provides evidence for a pro-tumorigenic polarization of human macrophages by IL-4/IL-6. Our data support the central role of STAT3 as a transcription factor driving IL-6-elicited alterations of the macrophage transcriptome and reveal a novel role of BATF transcription factor in shaping the transcriptional response of co-stimulated macrophages, suggesting its potential importance as a target to suppress pro-tumorigenic properties of TAMs.

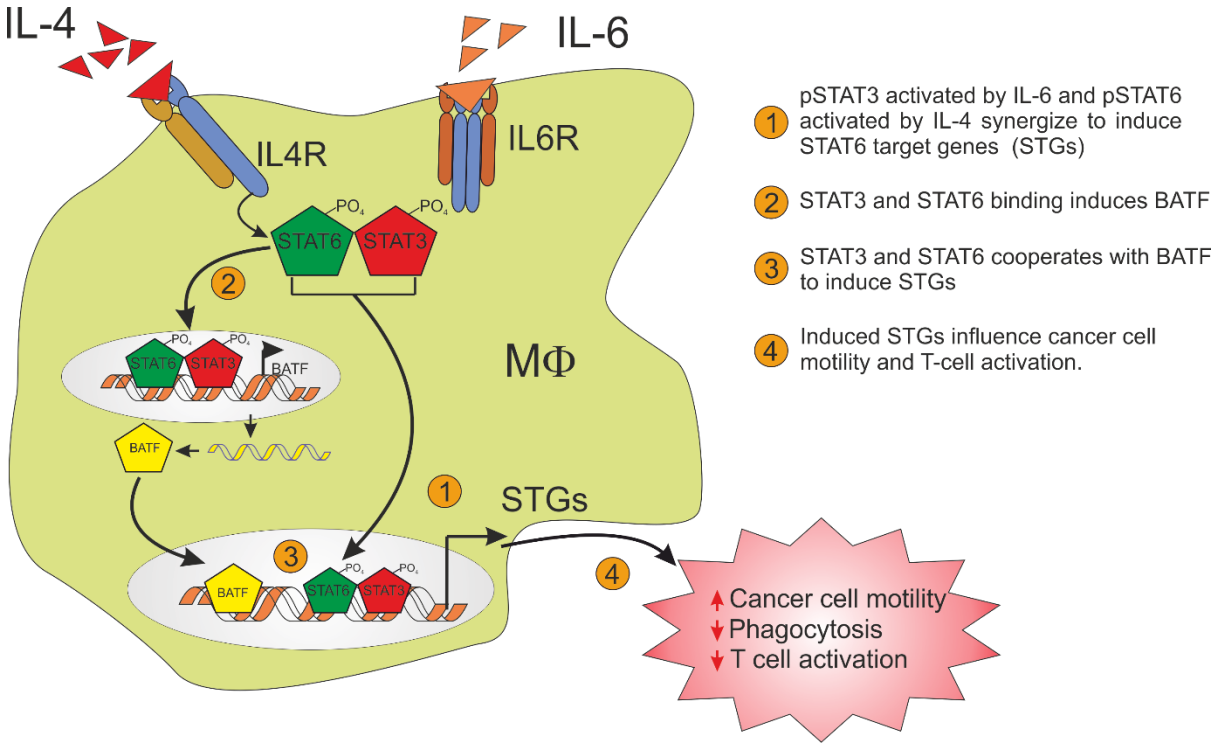

Figure 39: Graphical Summary of our finding depicting STAT3, STAT6 and BATF synergy and the functional outcome.

8. List of Figures

9. List of Tables

Project II

1. Introduction

30,000 genes were identified in human genome project, however, most of them remain unannotated. MTFR1L (Mitochondrial fission regulator-1 like) or Fam54b (Family With Sequence Similarity 54b), is one such factor that was identified as AMPK substrate in two recent proteomic studies [76, 77]. The first screen by Hoffman et.al employed a global phospho-proteomic analysis in muscle biopsies in untrained males before and after exercise, identifying 1004 novel exercise-regulated phosphosites on 562 proteins. Among these 562 proteins were annotated targets of exercise-regulated kinases, including AMPK, PKA, CaMK, MAPK, and mTOR. The authors next performed a parallel phosphor-peptide mass-spectrometric analysis of rat L6 myotubes stimulated with AMPK activator 5-aminoimidazole-4-carboxamide ribonucleotide (AICAR) and used the data for machine learning algorithms based on the fold induction and primary amino acid motif surrounding the phosphosites post AICAR treatment to predict AMPK targets in human muscle biopsies. Based on this prediction model and in vitro AMPK binding assay, they identified novel AMPK substrates, including MTFR1L.

The second study by Schaffer BE et.al [77]employed a more direct approach where the authors overexpressed in HEK293T and U2OS cells a mutant AMPK kinase (α1 and α2) accepting N^6-(phenethyl) ATPγS (bulky ATP) that tags direct substrates with thiophosphate moiety followed by thioP antibody capture and LC-MS/MS. The authors identified 57 novel AMPK phosphorylation sites with targets involved in cell motility, adhesion and invasion.

In both screens, MTFR1L was phosphorylated on serine residues S103 and S238. These sites were found to be phosphorylated in several other large proteomic screens (www.phosphosite.org). MTFR1L is a member of a MTFR protein family, and

expression data suggest its ubiquitous expression across different cell types. However, until now no literature data exists on function and role of MTFR1L. Two closely related paralogues of the same gene family are MTFR1 (FAM54A2/CHPPR (Chondrocyte protein with a poly-proline region)) and MTFR2 (DUFD1/FAM54A).

MTFR1 is a novel mitochondrial protein predominantly localized in the inner mitochondrial membrane (IMM) and first identified as being potentially relevant in late stages of chondrocyte differentiation[78, 79]. Studies of Mtfr1$^{-/-}$ mice show that MTFR1 is required to maintain defence against ROS-mediated stress in adult mice spermatids and Leydig cells. The KO mice had enhanced oxidative DNA damage due to reduced expression of enzymes involved in ROS detoxification (e.g. *Akr1b7, Atx1, Cox7c, Gpx3/4/5, Txn1, Tnrdx1*) with highest disparity in glutathione peroxidase 3 *(Gpx3)* expression[80, 81].

Recently, MTFR1 was reported to induce mitochondrial fission, cardiomyocyte apoptosis and myocardial infarction that was regulated by nuclear factor of activated T-cells 4 (NFAT4) -dependent miR-324-5p [82]. miR-324-5p attenuates MTFR1 translation and miR-342-5p is in turn inhibited by NFAT4 as shown in Fig. 40. NFAT4 is modulated by Ca^{2+}/calmodulin signalling through its import into the nucleus following dephosphorylation by Ca^{2+}/calmodulin-dependent protein phosphatase calcineurin[83, 84] and is implicated to reduce voltage gated K^+ currents after myocardial infraction[85, 86]. Therefore, targeting NFAT4 could potentially block MTFR1 induced mitochondrial fission and prevent cardiomyocytes from cell death.

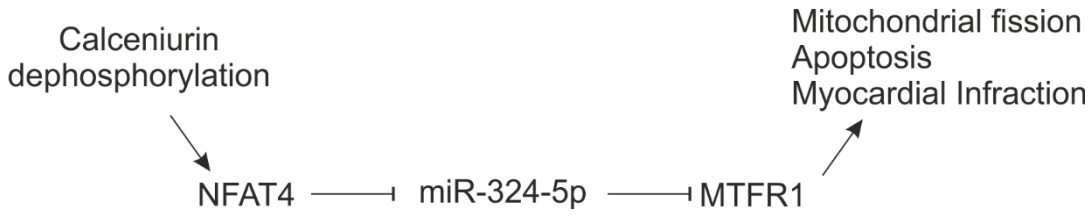

Figure 40: *MTFR1L-induced mitochondrial fission, apoptosis and thereby myocardial infraction can be inhibited via miR-324-5p that is in turn inhibited by NFAT4* [82].

MTFR1 and MTFR2 are suggested to play similar functional roles. MTFR2 was shown to be expressed in seminiferous tubules by middle-late pachytene spermatocytes and spermatids and shared mitochondrial fission phenotype with MTFR1. MTFR2 and MTFR1 regulate mitochondrial dynamics and cellular respiration (O_2 consumption and ATP synthesis)[87].

Interestingly, MTFR2 was identified as a candidate gene for obesity in the GWAS study of around 250,000 people based on body mass index (BMI)[88-90]. The authors further curated the existing gene expression profiles of obese patients and performed Ingenuity pathway analysis. Strikingly, pathway analysis of BMI regulated genes identified Glutathione Redox Reactions and MTFR2 were highly enriched terms in the obese cohort population. This is reminiscent to the glutathione peroxidase genes being downregulated in Mtfr1$^{-/-}$ mice [81]. In another study, MTFR2 was implicated in transcriptional regulation of the expression of a dual specificity protein kinase (TTK) in glioma stem-like cells (GSCs), since MTFR2 silencing reduced the activity of TTK promoter-based luciferase reporter [91]. Through TTK regulation, MTFR2 was suggested to contribute to maintenance of GSCs population in glioblastoma. *Keysar S et.al* identified a novel NFIB-MTFR2 fusion in relapsing adenoid cystic carcinoma of salivary gland[92]. . Furthermore, patient-derived xenograft models validated a more aggressive cancer stem cell CD44^{hi} and ALDH-expressing population in tumor sphere formation assays in NFIB-MTFR2-fused adenoid cystic carcinoma.

Based on previous literature data on MTFR1L paralogues, we tried to investigate the role of a novel substrate for AMPK, MTFR1L and its interaction partners.

2. Materials and methods

2.1. Plasmids

2.1.1. AMPK KO CRISPR plasmids: AMPK sgRNA cloned plasmids for CRISPR KO were purchased from Addgene (pX462-hPRKAA1-gRNA and pX462-hPRKAA1-gRNA, addgene#74374-74377), targeting exon 1 of AMPK α1 and α2. Plasmids were transfected into one 6 well plate with 0.5µg each of forward and reverse oligo for sgRNA-PRKAA1 and sgRNA-PRKAA2 in U2OS cells using HiPerFect transfection reagent (Qiagen# 301704) for 6h. Cells were seeded in 10 cm dish the next day and cultured for further 24h. On day3, cells were selected under puromycin pressure for 3 days and single cell clones were sorted and expanded in a 96-well format. Once the clones were confluent, theexpression of AMPK was analyzed by western blotting of total cell lysates using AMPKα1 (Eurogentech, rabbit) and AMPKα2 (CST#2757T).

2.1.2 MTFR1L mutant constructs

A plsmid containing MTFR1L cDNA with C-terminal Myc-DDK tag under control of CMV-driven promoter and containing neomycin mammalian resistance cassette was purchased from Origene (Origene#PS100001). The cDNA was then mutated using PfuII ultra and Quickchange site-directed mutagenesis protocol (Agilent, according to manufacturer's instructions), to introduce S103A, S238A, S103D and S238D mutations.

2.2 Cells

U2OS cells were cultured in DMEM supplemented with 10%FCS and 1%P/S. Stably expressing MTFR1L mutant S103AS238A and S103DS238D constructs were

maintained in 600µg/ml of neomycin (G418, Geniticin, InVivoGen), determined by U2OS kill curve in AMPK$^{-/-}$ cells.

2.3. Immunofluorescence

Cells were rinsed with PBS, followed by fixation in freshly prepared 4%PFA for 15mins at room temperature. The fixed cells were then washed with PBS twice and permeabilized with PBST (0.1% Triton-X) for 15 mins at room temperature, washed with PBS and blocked for 1hr with blocking solution (5%BSA/0.01% Triton-X/PBS, PBST) followed by incubation with primary antibodies in 1% BSA/PBST (1% Triton-X) overnight at 4 °C. Cells were then further washed thrice with PBST (0.01% Triton-X), incubated with secondary antibodies (Thermo Scientific) in 1%BSA/PBST (0.01% Triton-X) for 2 h and Hoechst 33342 for 10mins. Cells were then washed with PBS and imaged using Plan-Apochromat 20X and 40X oil objectives on a Zeiss LSM 510 confocal microscope.

2.4 Xcelligence cell proliferation

Gold plated Xcelligence plates were measured for blank with 1%FCS/DMEM. 5000 cells were incubated in 1% FCS/DMEM and allowed to seed for 20mins. RTCA measurement program was then run for 72h to measure cell proliferation based on electron changes/current measurement via XCELLigence x96 machine according to manufacturer's instructions.

3.1 Results

3.1. MTFR1L is ubiquitously but variably expressed across different cells

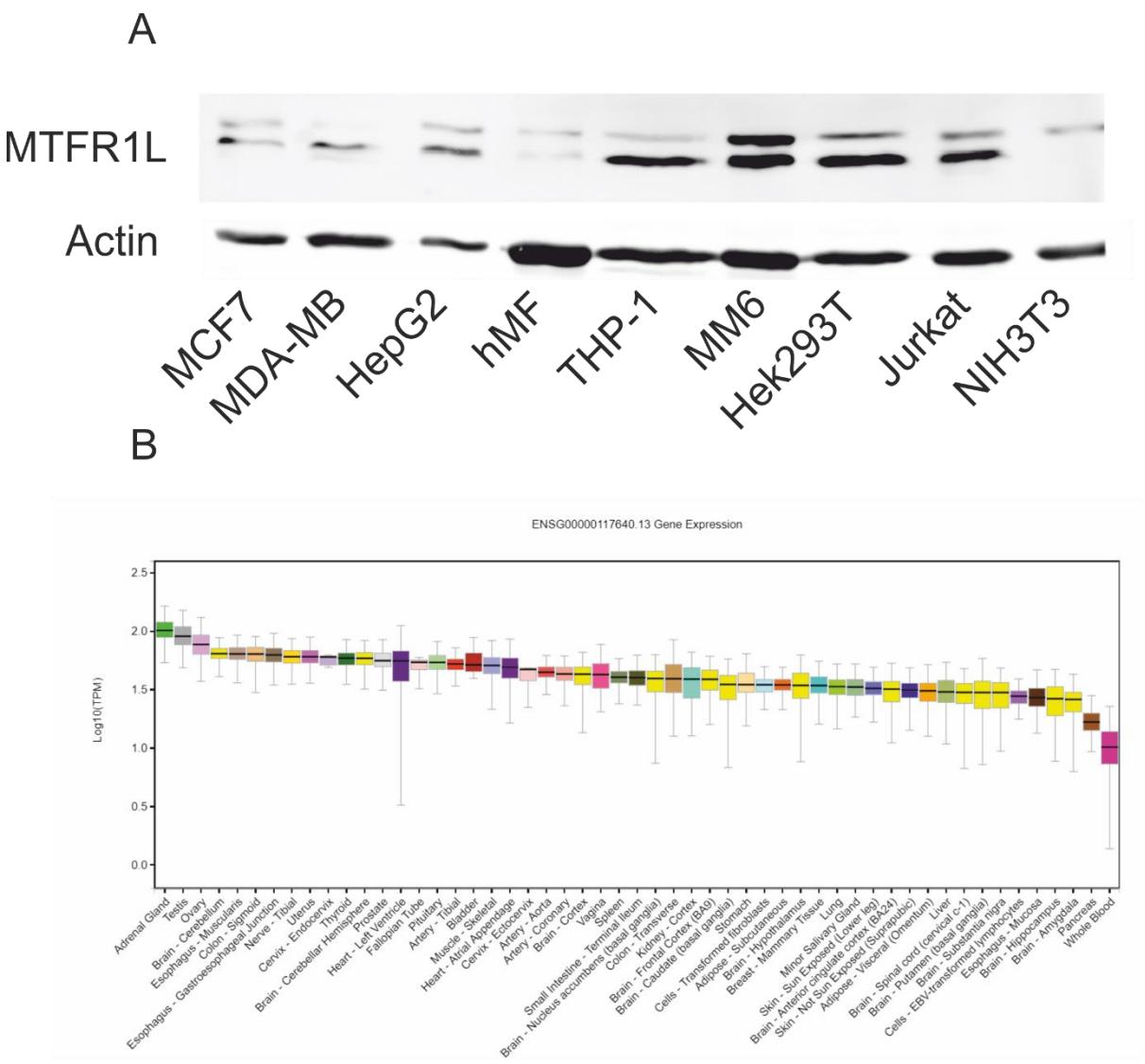

Figure 41: *(A) MTFR1L protein expression compared across different cell lines or human macrophages (hMF) by western blotting. (B) log10 gene expression Transcript per million expression (TPM) profile of MTFR1L across different organs in normal human samples (analysed using GTEx plugin)* https://portals.broadinstitute.org/ccle/page?gene=MTFR1L

We observed ubiquitous yet variable expression pattern of MTFR1L protein across different cells with highest expression levels in HEK293T and myeloid (THP-1 and MM6) and lymphoid (Jurkat) cancer cell lines) (Fig. 41A). We further analysed MTFR1L expression across different tissue types through *in silico* GTEx plugin from Broad institute (Fig. 41B). MTFR1L has highest expression in the heart, testis and adrenal gland and lowest in pancreas, bone marrow, salivary glands and skin.

3.2. Characterization of MTFR1L expression pattern in U2OS cells

To understand the mechanism and function of MTFR1L, we separated nucleus, mitochondria and cytosol of U2OS upon AMPK activation using combination of A-769 and phenformin (Fig. 42) and concluded that MTFR1L is localized in the nucleus and cytoplasm but not in mitochondria. We did not observe an overall change in MTFR1L distribution in different cellular fractions upon AMPK activation.

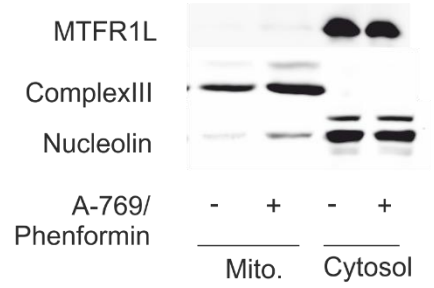

Figure 42: *Cellular fractionation of U2OS cells after stimulation with AMPK activators A-769 (250µM)/phenformin (100µM)*

3.3. MTFR1L subcellular localization analysed by microscopy

We further studied the subcellular localization of MTFR1L via immunofluorescence using confocal microscopy. We used MTFR1L overexpression constructs using TrueORF gold DDK-Myc-tagged expression plasmids carrying neomycin resistance gene. We further mutated the cDNA to generate constructs S103A/S238A (SS→AA)

representing phosphorylation-deficient and S103D/S238D (SS→DD) as phosphomimetic using site-directed mutagenesis. We chose these sites based on AMPK substrate phosphorylation screens as mentioned in the introduction.

3.3.1 MTFR1L response to nutrient withdrawal

Since AMPK as an energy sensor is activated upon withdrawal of nutrients, we used Hank's balanced salt solution (HBSS) to induce starvation for 4h. Thus, we transfected U2OS cells with MTFR1L wild type and mutant SS→AA and SS→DD constructs for 24h and next day starved cells for further 4h. Phosphorylation-deficient SS→AA mutant overexpressed in U2OS cells shows similar distribution in the cell cytoplasm as wild type MTFR1L. Surprisingly yet quite evidently MTFR1L localized to what appeared to be the cell cytoskeletal network i.e. microtubules, actin filaments, and intermediate filaments. The structures showing MTFR1L expression were reminiscent of microtubules, astral tubes and plausibly kinetochore. These data suggested that MTFR1L may interact or be even part of the cytoskeletal machinery. The SS→DD phosphomimetic mutant construct on the other hand had a diffused localization upon overexpression (Fig. 43).

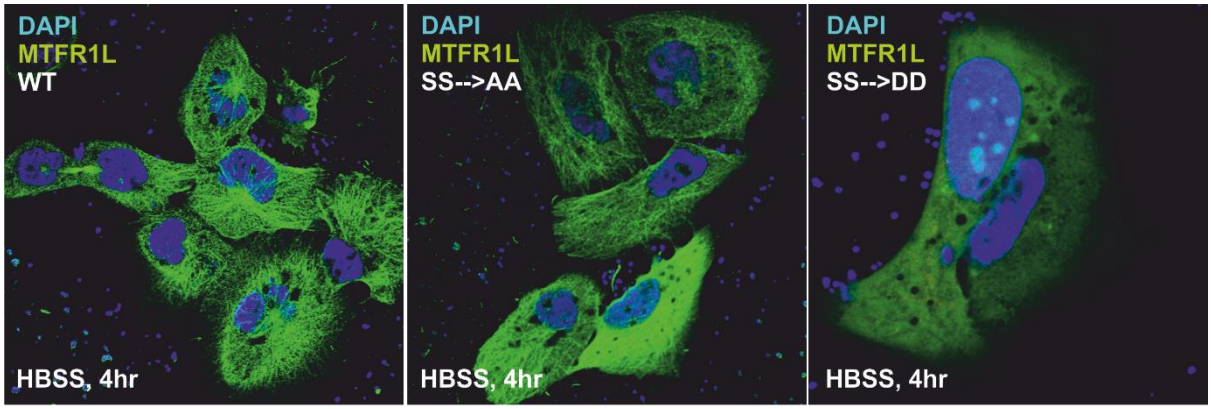

Figure 43: *MTFR1L OE constructs localization after 4h nutrient withdrawal.*

Therefore, based on our above hypothesis that MTFR1L is expressed in cytoskeletal proteins, we overexpressed our MTFR1L constructs and stained the cells for tubulin, a marker for microtubules. MTFR1L OE constructs partially co-localize with tubulin, suggesting a possible involvement of MTFR1L in maintaining cytoskeletal structure (Fig. 44). We postulate the partial localization might be due to MTFR1L association with other cytoskeletal markers e.g. double helix microfilaments from F-actin strand (actin) or intermediate filaments or oversaturation of MTFR1L overexpression constructs' expression.

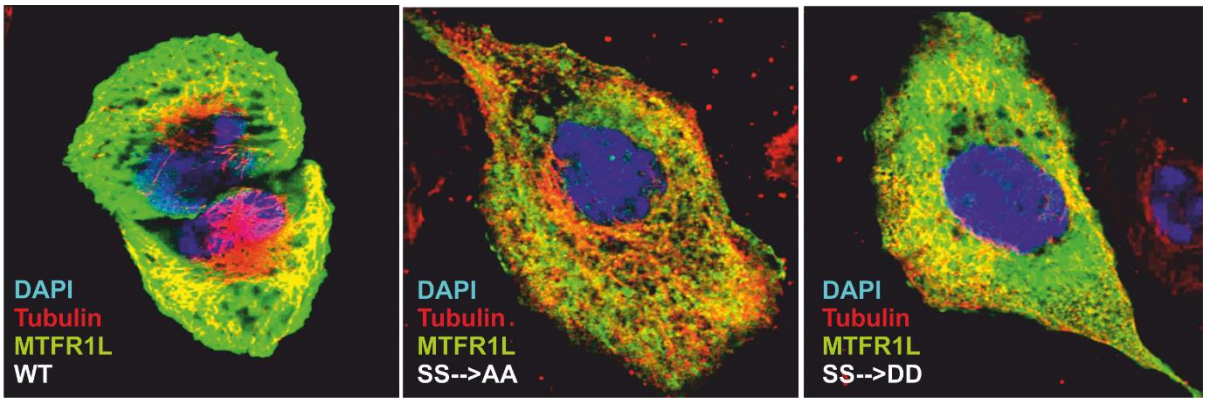

Figure 44: *MTFR1L OE mutant constructs expressed in U2OS and stained with tubulin and MTFR1L antibodies.*

3.3.2. MTFR1L does not affect mitochondrial morphology

Since, MTFR1L paralogues, MTFR1 and MTFR2 were shown to be involved with mitochondrial fission phenotype, we tested if MTFR1L overexpression had any morphological effect on mitochondrial fission/fusion properties. We overexpressed MTFR1L wild type and mutant constructs for 24h and performed immunohistochemistry for complex V (mitochondria) and MTFR1L. We observed no major changes in mitochondrial morphology after MTFR1L overexpression (Fig. 45).

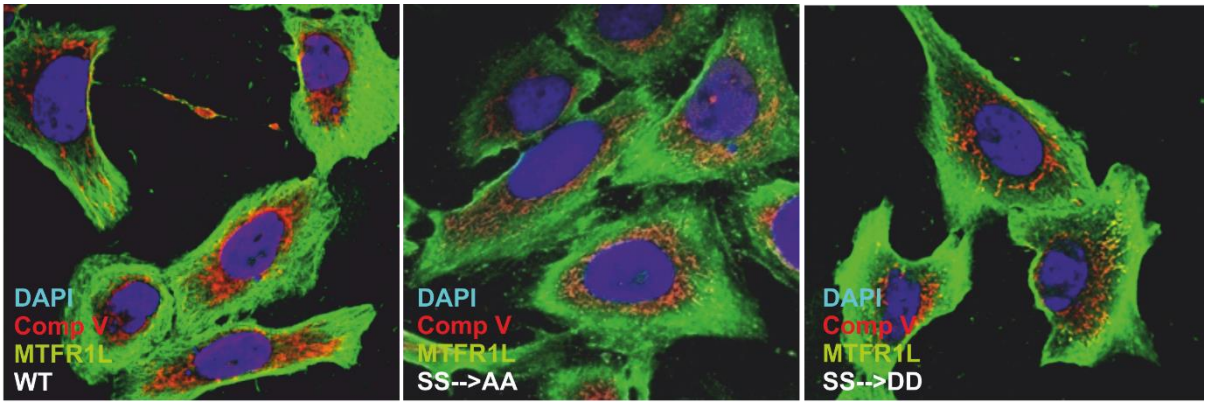

Figure 45: *Mitochondrial morphology in U2OS cells overexpressing indicated MTFR1L constructs determined by staining with Complex V antibody.*

3.4. Characterization of MTFR1L mutant constructs in AMPK$^{-/-}$ background

To study the function of MTFR1L, we tried to generate MTFR1L KO U2OS cells using CRISPR-Cas9. We were only able to generate cells that showed lower MTFR1L expression as compared to wild type cells, whereas no knockouts were obtained (data not shown). We postulated, given the ubiquitous expression of MTFR1L, that a knockout might be lethal. As an alternative strategy, we created AMPK$^{-/-}$ cells asserting that the endogenous phosphorylation levels of MTFR1L, an AMPK substrate would be lower compared to wt AMPK expressing cells, while comparing its function in the context of AMPK.

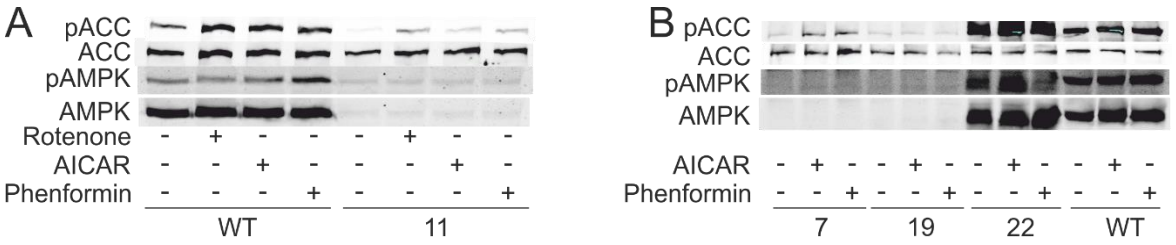

Figure 46*: Analysis of AMPK and ACC expression and phosphorylation in U2OS wild type and AMPK KO cells created via CRISPR-Cas9 and treated with AMPK activators rotenone, AICAR and phenformin.*

Therefore, we created AMPK U2OS KO cells (Fig. 46 A-B). Out of the three candidate clones, 7, 11 and 19, only clone 19 showed no ACC phosphorylation upon AMPK activation. Moreover, there was no total AMPK in this clone. We further overexpressed phosphorylation-deficient S103A/S238A and phosphomimetic S103D/S238D MTFR1L mutant constructs in U2OS AMPK$^{-/-}$ cells. We selected the clones for neomycin resistance, since the MTFR1L mutant plasmid harboured neomycin resistance gene. Thereby, the mutant cDNA is stably integrated in AMPK$^{-/-}$ U2OS cell's genome. As evidenced by Fig. 47, we show no AMPK in KO cells and high expression of mutant MTFR1L constructs.

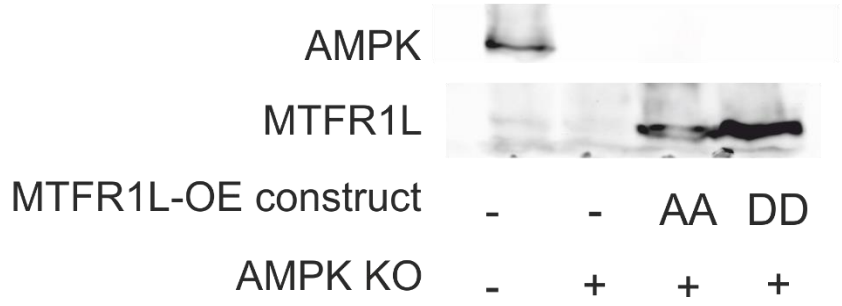

Figure 47: *MTFR1L expression in AMPK$^{+/+}$ and AMPK$^{-/-}$ background.*

We further characterized our cell populations by performing cell proliferation assay and observed that AMPK$^{-/-}$ cells grew significantly slower compared to AMPK$^{+/+}$ (WT) U2OS with active AMPK (Fig.48). Stably overexpressing MTFR1L phosphonegative mutant partially rescued the stalled growth in AMPK$^{-/-}$ U2OS cells compared to phospho-mimic MTFR1L DD mutant in AMPK$^{-/-}$ U2OS, which had comparable proliferation as AMPK$^{-/-}$ cells.

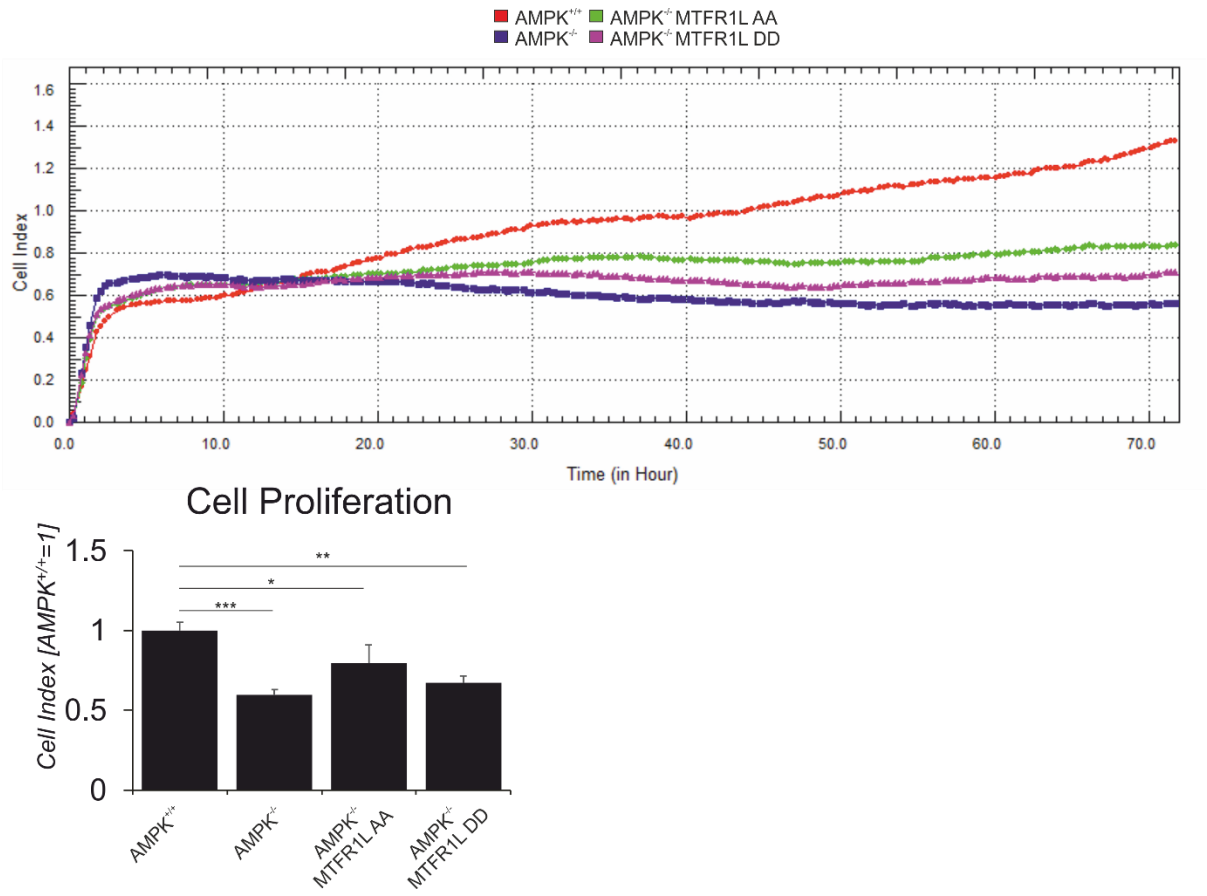

***Figure 48**: proliferation for AMPK$^{-/-}$, AMPK$^{+/+}$ and MTFR1L mutant-expressing U2OS cells, as measured by xCELLigence RTCA DP software. Data are presented as mean± 10-90% SEM. *, p<0.05, **, p<0.01. ***, p<0.005.*

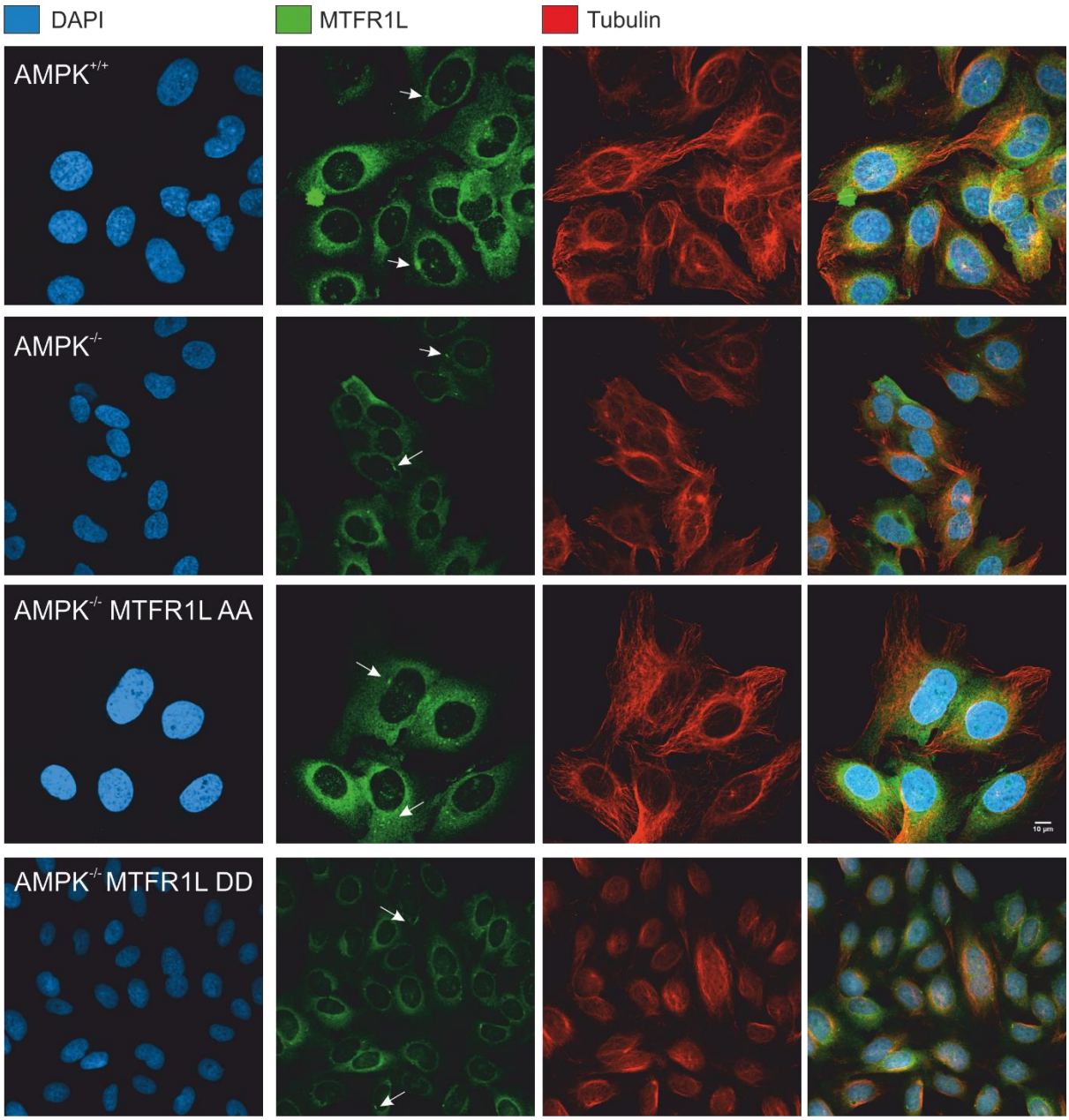

***Figure 49**: Immunofluorescence imaging for MTFR1L and tubulin in AMPK+/+ (WT), AMPK -/- (KO) and stable MTFR1L mutant OE in U2OS cells.*

We further checked the co localization of MTFR1L with tubulin in stably expressing MTFR1L mutant constructs via immunofluorescence (Fig.49). We could only observe partial and inconclusive co-localization of MTFR1L with tubulin. However, we did observe paranuclear specks specific to MTFR1L in each cell type.

3.5. MTFR1L expression across tumor cells

In cancer cell lines, MTFR1L is shown to have the highest expression in normal cells compared to tumor subtypes. We validated MTFR1L expression via firebrowser, online TCGA portal that sums up gene expression in tumor vs normal tissues. The datasets are a cumulative assembly of mRNA expression quantified via RNA sequencing or microarray analysis. Surprisingly, MTFR1L was either unchanged or mostly downregulated in tumors compared to normal cells (Fig. 50). This suggested MTFR1L could be a potential tumor suppressor unlike MTFR1 which was reported to have pro-tumorigenic potential.

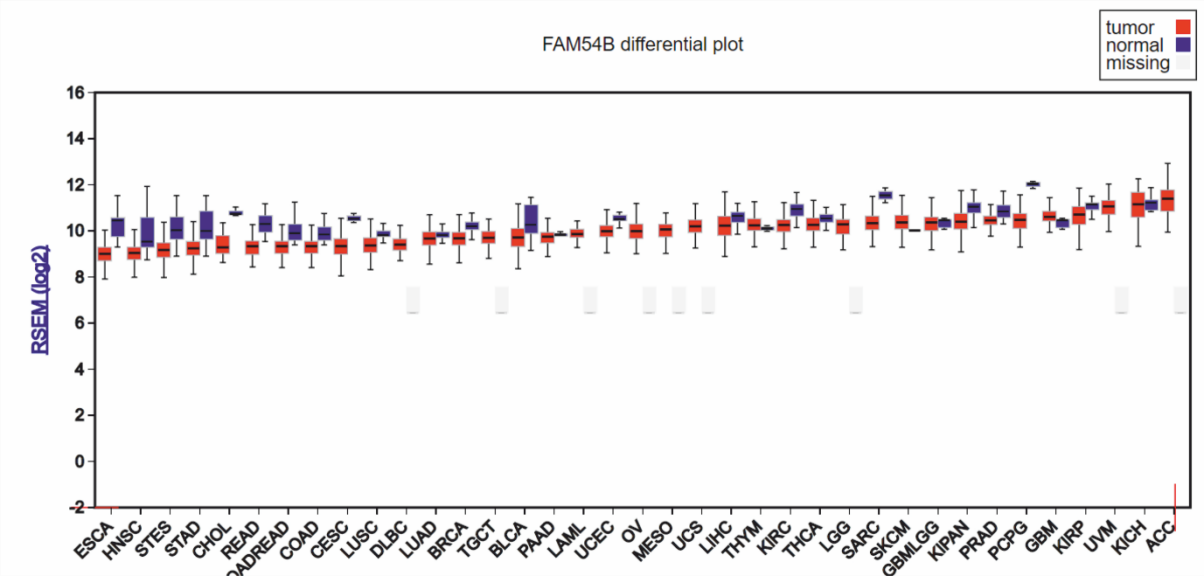

Figure 50: *MTFR1L expression in cancer (red) versus normal (blue) or grey (missing normal) cells with RSEM (RNA-Seq by Expectation-Maximization) on the Y axis and cancer type on the X-axis. (adapted from Firebrowser plugin, http://firebrowse.org/viewGene.html?gene=fam54b)*

We further explored existing TCGA datasets to understand if MTFR1L is a potential tumor suppressor, a rationale supported by low or unaltered expression levels in tumor compared to normal tissues. We looked at breast invasive cancer datasets

(http://www.cbioportal.org/study?id=brca_tcga#summary), since our preliminary analysis (Fig. 43, 50) showed low levels of MTFR1L in cell lines derived from niche-dependent solid tumors compared to suspension culture neoplasms (where MTFR1L levels were high or unaltered relative to normal tissue). As expected we found high levels of MTFR1L associated with overall patient survival and low expression with poor outcome (Fig. 51). Therefore, we speculate that MTFR1L could be a potential tumor suppressor gene that is downregulated in most tumors. Nevertheless, further work is required to confirm the MTFR1L anti-tumorigenic phenotype as summed up in Section 3.1.

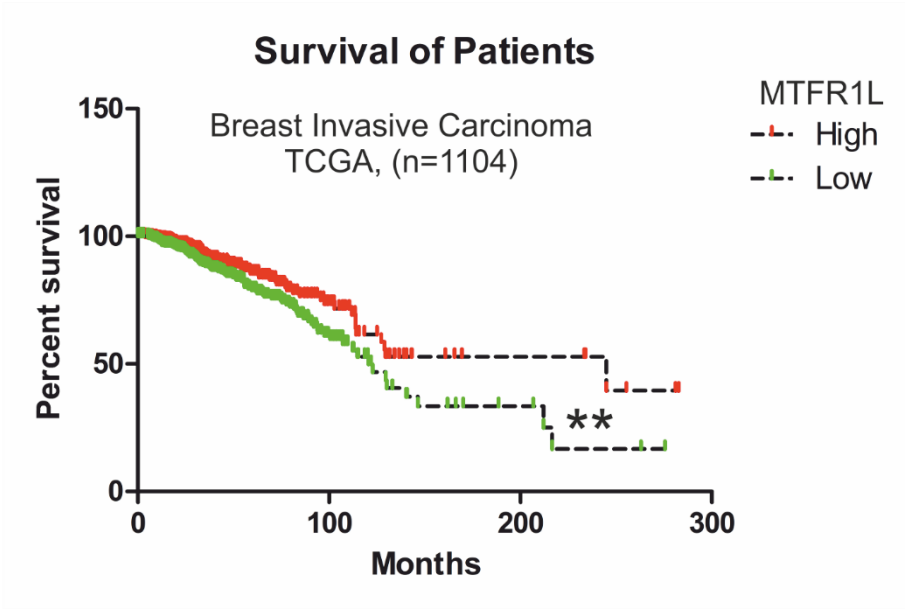

Figure 51: *Kaplan-Meier median-Survival curve for MTFR1L expression in invasive breast carcinoma (TCGA, MTFR1L$_{high}$= 515, MTFR1L$_{low}$=579)*

4. Discussion

The function of MTFR1L protein remains unknown since its first identification as a downstream AMPK target. We show through the initial parts of our study that MTFR1L is a cytoskeletal localized protein which could probably be a tumor suppressor gene since almost all different cancer types have lower expression of MTFR1L compared to patient matched normal cell samples.

We observed that wt MTFR1L OE was expressed in a cytoskeletal arrange pattern. To confirm this hypothesis, we stained our cells with cytoskeletal marker tubulin. MTFR1L was partially co-localized with MTFR1L in WT and phospho-negative MTFR1L AA mutant construct but appeared to have a diffused morphology for phosphor-mimetic MTFR1L DD OE construct. We observed a similar diffused MTFR1L cytoplasmic expression for MTFR1L DD mutant construct upon serum withdrawal with HBSS. Since, MTFR1 and MTFR2 were confirmed to cause mitochondrial fission, we observed no obvious phenotypes regarding mitochondrial morphology upon either MTFR1L wt or mutant OE constructs.

To study the function of MTFR1L we tried to design MTFR1L KO U2OS cells for overexpressing MTFR1L mutant constructs but were unsuccessful, probably because MTFR1L KO might be lethal given its ubiquitous expression. Therefore, we designed AMPK$^{-/-}$ U2OS cells and generated stable MTFR1L OE mutant construct cell lines in AMPK KO background, hoping the endogenous MTFR1L phosphorylation might be lower compared to wild type counterpart.

AMPK$^{-/-}$ U2OS took significantly longer to proliferate compared to cells with WT AMPK. Nevertheless, stably expressing MTFR1L mutant AA rescued the stalled proliferation partially yet non-significantly compared to WT U2OS. However, MTFR1L mutant DD

had similar proliferation cycle like AMPK$^{-/-}$. We next characterized via immunofluorescence imaging MTFR1L expression across different cell types but could find significant differences between four cell types. Further work in MTFR1L characterization needs to be performed to get mechanistic insights to MTFR1L interaction partners via MS analysis and further validation of MTFR1L targets.

6. Conclusion

MTFR1L is an AMPK target protein of unknown function that is not only ubiquitously expressed, but its expression is also deregulated in cancer. We show here the preliminary data on MTFR1L expression, as a potential gene involved in cytoskeletal network and carcinogenesis.

7. List of Figures

8. References

1. Hanahan D, Weinberg Robert A. Hallmarks of Cancer: The Next Generation. Cell; 144:646-74.
2. Hanahan D, Weinberg RA. Hallmarks of cancer: the next generation.
3. Elpek KG, Cremasco V, Shen H, Harvey CJ, Wucherpfennig KW, Goldstein DR, et al. The tumor microenvironment shapes lineage, transcriptional, and functional diversity of infiltrating myeloid cells. Cancer immunology research 2014; 2:655-67.
4. Qian B, Pollard JW. Macrophage Diversity Enhances Tumor Progression and Metastasis. Cell 2010; 141:39-51.
5. Kitamura T, Qian B-Z, Pollard JW. Immune cell promotion of metastasis. Nature reviews Immunology 2015; 15:73-86.
6. Ugel S, De Sanctis F, Mandruzzato S, Bronte V. Tumor-induced myeloid deviation: when myeloid-derived suppressor cells meet tumor-associated macrophages. The Journal of Clinical Investigation 2015; 125:3365-76.
7. Condamine T, Ramachandran I, Youn J-I, Gabrilovich DI. Regulation of Tumor Metastasis by Myeloid-Derived Suppressor Cells. Annual Review of Medicine 2015; 66:97-110.
8. Markowitz J, Wesolowski R, Papenfuss T, Brooks TR, Carson WE. Myeloid Derived Suppressor Cells in Breast Cancer. Breast cancer research and treatment 2013; 140:13-21.
9. Gantt S, Gervassi A, Jaspan H, Horton H. The Role of Myeloid-Derived Suppressor Cells in Immune Ontogeny. Frontiers in Immunology 2014; 5:387.
10. Draghiciu O, Lubbers J, Nijman HW, Daemen T. Myeloid derived suppressor cells—An overview of combat strategies to increase immunotherapy efficacy. Oncoimmunology 2015; 4:e954829.
11. Condamine T, Mastio J, Gabrilovich DI. Transcriptional regulation of myeloid-derived suppressor cells. Journal of Leukocyte Biology 2015; 98:913-22.
12. Marvel D, Gabrilovich DI. Myeloid-derived suppressor cells in the tumor microenvironment: expect the unexpected. The Journal of Clinical Investigation 2015; 125:3356-64.
13. Chen J, Yao Y, Gong C, Yu F, Su S, Liu B, et al. CCL18 from tumor-associated macrophages promotes breast cancer metastasis via PITPNM3. Cancer cell 2011; 19:541-55.
14. Nagarsheth N, Wicha MS, Zou W. Chemokines in the cancer microenvironment and their relevance in cancer immunotherapy. Nature Reviews Immunology 2017; 17:559-72.
15. Petricevic B, Laengle J, Singer J, Sachet M, Fazekas J, Steger G, et al. Trastuzumab mediates antibody-dependent cell-mediated cytotoxicity and phagocytosis to the same extent in both adjuvant and metastatic HER2/neu breast cancer patients. Journal of Translational Medicine 2013; 11:307-.
16. Garcia-Diaz A, Shin DS, Moreno BH, Saco J, Escuin-Ordinas H, Rodriguez GA, et al. Interferon Receptor Signaling Pathways Regulating PD-L1 and PD-L2 Expression. Cell reports; 19:1189-201.
17. Abiko K, Matsumura N, Hamanishi J, Horikawa N, Murakami R, Yamaguchi K, et al. IFN-γ from lymphocytes induces PD-L1 expression and promotes progression of ovarian cancer. British Journal Of Cancer 2015; 112:1501-9.
18. Mandai M, Hamanishi J, Abiko K, Matsumura N, Baba T, Konishi I. Dual Faces of IFNγ in Cancer Progression: A Role of PD-L1 Induction in the Determination of Pro- and Antitumor Immunity. Clinical Cancer Research 2016; 22:2329-34.
19. Caldwell C, Johnson CE, Balaji VN, Balaji GA, Hammer RD, Kannan R. Identification and Validation of a PD-L1 Binding Peptide for Determination of PDL1 Expression in Tumors. Scientific reports 2017; 7:13682.
20. Elsegood CL, Tirnitz-Parker JEE, Olynyk JK, Yeoh GCT. Immune checkpoint inhibition: prospects for prevention and therapy of hepatocellular carcinoma. Clin Trans Immunol 2017; 6:e161.
21. Saha D, Martuza RL, Rabkin SD. Macrophage Polarization Contributes to Glioblastoma Eradication by Combination Immunovirotherapy and Immune Checkpoint Blockade. Cancer cell; 32:253-67.e5.

22. Zhu H, Bengsch F, Svoronos N, Rutkowski Melanie R, Bitler Benjamin G, Allegrezza Michael J, et al. BET Bromodomain Inhibition Promotes Anti-tumor Immunity by Suppressing PD-L1 Expression. Cell reports; 16:2829-37.
23. Su S, Liu Q, Chen J, Chen F, He C, Huang D, et al. A positive feedback loop between mesenchymal-like cancer cells and macrophages is essential to breast cancer metastasis. Cancer cell 2014; 25:605-20.
24. Mauer J, Denson JL, Brüning JC. Versatile functions for IL-6 in metabolism and cancer. Trends in Immunology; 36:92-101.
25. Matthes T, Manfroi B, Zeller A, Dunand-Sauthier I, Bogen B, Huard B. Autocrine amplification of immature myeloid cells by IL-6 in multiple myeloma-infiltrated bone marrow. Leukemia 2015; 29:1882-90.
26. Rosean TR, Tompkins VS, Olivier AK, Sompallae R, Norian LA, Morse HC, 3rd, et al. The tumor microenvironment is the main source of IL-6 for plasma cell tumor development in mice. Leukemia 2015; 29:233-7.
27. Rattigan YI, Patel BB, Ackerstaff E, Sukenick G, Koutcher JA, Glod JW, et al. Lactate is a mediator of metabolic cooperation between stromal carcinoma associated fibroblasts and glycolytic tumor cells in the tumor microenvironment. Experimental cell research 2012; 318:326-35.
28. Li J, Lan T, Zhang C, Zeng C, Hou J, Yang Z, et al. Reciprocal activation between IL-6/STAT3 and NOX4/Akt signalings promotes proliferation and survival of non-small cell lung cancer cells. Oncotarget 2015; 6:1031-48.
29. Mauer J, Chaurasia B, Goldau J, Vogt MC, Ruud J, Nguyen KD, et al. Signaling by IL-6 promotes alternative activation of macrophages to limit endotoxemia and obesity-associated resistance to insulin. Nature immunology 2014; 15:423-30.
30. Yu H, Pardoll D, Jove R. STATs in cancer inflammation and immunity: a leading role for STAT3. Nature reviews Cancer 2009; 9:798-809.
31. Gaggianesi M, Turdo A, Chinnici A, Lipari E, Apuzzo T, Benfante A, et al. IL4 Primes the Dynamics of Breast Cancer Progression via DUSP4 Inhibition. Cancer research 2017; 77:3268-79.
32. Hu J, Jo M, Eastman BM, Gilder AS, Bui JD, Gonias SL. uPAR Induces Expression of Transforming Growth Factor β and Interleukin-4 in Cancer Cells to Promote Tumor-Permissive Conditioning of Macrophages. The American Journal of Pathology 2014; 184:3384-93.
33. De Palma M. Partners in crime: VEGF and IL-4 conscript tumour-promoting macrophages. The Journal of Pathology 2012; 227:4-7.
34. Chen J, Yao Y, Gong C, Yu F, Su S, Chen J, et al. CCL18 from Tumor-Associated Macrophages Promotes Breast Cancer Metastasis via PITPNM3. Cancer cell 2011; 19:541-55.
35. Gocheva V, Wang H-W, Gadea BB, Shree T, Hunter KE, Garfall AL, et al. IL-4 induces cathepsin protease activity in tumor-associated macrophages to promote cancer growth and invasion. Genes & Development 2010; 24:241-55.
36. De Palma M, Lewis Claire E. Macrophage Regulation of Tumor Responses to Anticancer Therapies. Cancer cell; 23:277-86.
37. Yan D, Wang HW, Bowman RL, Joyce JA. STAT3 and STAT6 Signaling Pathways Synergize to Promote Cathepsin Secretion from Macrophages via IRE1alpha Activation. Cell reports 2016; 16:2914-27.
38. Piccolo V, Curina A, Genua M, Ghisletti S, Simonatto M, Sabò A, et al. Opposing macrophage polarization programs show extensive epigenomic and transcriptional cross-talk. Nature immunology 2017; 18:530-40.
39. Kang K, Park SH, Chen J, Qiao Y, Giannopoulou E, Berg K, et al. Interferon-gamma Represses M2 Gene Expression in Human Macrophages by Disassembling Enhancers Bound by the Transcription Factor MAF. Immunity 2017; 47:235-50 e4.
40. Goldstein I, Paakinaho V, Baek S, Sung MH, Hager GL. Synergistic gene expression during the acute phase response is characterized by transcription factor assisted loading. Nature communications 2017; 8:1849.

41. Fernando MR, Reyes JL, Iannuzzi J, Leung G, McKay DM. The pro-inflammatory cytokine, interleukin-6, enhances the polarization of alternatively activated macrophages.
42. S. A. FastQC: a quality control tool for high throughput sequence data. Available online 2010; http://www.bioinformatics.babraham.ac.uk/projects/fastqc.
43. Bolger AM, Lohse M, Usadel B. Trimmomatic: a flexible trimmer for Illumina sequence data. Bioinformatics 2014; 30:2114-20.
44. Grabherr MG, Haas BJ, Yassour M, Levin JZ, Thompson DA, Amit I, et al. Trinity: reconstructing a full-length transcriptome without a genome from RNA-Seq data. Nature biotechnology 2011; 29:644-52.
45. Dobin A, Davis CA, Schlesinger F, Drenkow J, Zaleski C, Jha S, et al. STAR: ultrafast universal RNA-seq aligner. Bioinformatics 2013; 29:15-21.
46. Liao Y, Smyth GK, Shi W. featureCounts: an efficient general purpose program for assigning sequence reads to genomic features. Bioinformatics 2014; 30:923-30.
47. Love MI, Huber W, Anders S. Moderated estimation of fold change and dispersion for RNA-seq data with DESeq2. Genome Biology 2014; 15:550.
48. Ma X-J, Dahiya S, Richardson E, Erlander M, Sgroi DC. Gene expression profiling of the tumor microenvironment during breast cancer progression. Breast Cancer Research : BCR 2009; 11:R7-R.
49. Saleh SMI, Bertos N, Gruosso T, Gigoux M, Souleimanova M, Zhao H, et al. Identification of Interacting Stromal Axes in Triple-Negative Breast Cancer. Cancer Research 2017; 77:4673-83.
50. Liu H, Dowdle JA, Khurshid S, Sullivan NJ, Bertos N, Rambani K, et al. Discovery of Stromal Regulatory Networks that Suppress Ras-Sensitized Epithelial Cell Proliferation. Developmental Cell 2017; 41:392-407.e6.
51. Finak G, Bertos N, Pepin F, Sadekova S, Souleimanova M, Zhao H, et al. Stromal gene expression predicts clinical outcome in breast cancer. Nature Medicine 2008; 14:518-27.
52. Konermann S, Brigham MD, Trevino AE, Joung J, Abudayyeh OO, Barcena C, et al. Genome-scale transcriptional activation by an engineered CRISPR-Cas9 complex. Nature 2015; 517:583-8.
53. Kearns NA, Genga RMJ, Enuameh MS, Garber M, Wolfe SA, Maehr R. Cas9 effector-mediated regulation of transcription and differentiation in human pluripotent stem cells. Development (Cambridge, England) 2014; 141:219-23.
54. Konishi T. Principal component analysis for designed

experiments. BMC Bioinformatics 2015; 16(Suppl 18).
55. Abdi H, Williams Lynne J. Principal component analysis. Wiley Interdisciplinary Reviews: Computational Statistics 2010; 2:433-59.
56. Jura J, Węgrzyn P, Korostyński M, Guzik K, Oczko-Wojciechowska M, Jarząb M, et al. Identification of interleukin-1 and interleukin-6-responsive genes in human monocyte-derived macrophages using microarrays. Biochimica et Biophysica Acta (BBA) - Gene Regulatory Mechanisms 2008; 1779:383-9.
57. Mi H, Dong Q, Muruganujan A, Gaudet P, Lewis S, Thomas PD. PANTHER version 7: improved phylogenetic trees, orthologs and collaboration with the Gene Ontology Consortium. Nucleic acids research 2010; 38:D204-D10.
58. Thomas PD, Campbell MJ, Kejariwal A, Mi H, Karlak B, Daverman R, et al. PANTHER: A Library of Protein Families and Subfamilies Indexed by Function. Genome Research 2003; 13:2129-41.
59. Tripathi SK, Chen Z, Larjo A, Kanduri K, Nousiainen K, Aijo T, et al. Genome-wide Analysis of STAT3-Mediated Transcription during Early Human Th17 Cell Differentiation. Cell reports 2017; 19:1888-901.
60. Czimmerer Z, Nagy ZS, Nagy G, Horvath A, Silye-Cseh T, Kriston A, et al. Extensive and functional overlap of the STAT6 and RXR cistromes in the active enhancer repertoire of human CD14+ monocyte derived differentiating macrophages. Molecular and Cellular Endocrinology 2017; pii: S0303-7207:30414-8.

61. Fleming JD, Giresi PG, Lindahl-Allen M, Krall EB, Lieb JD, Struhl K. STAT3 acts through pre-existing nucleosome-depleted regions bound by FOS during an epigenetic switch linking inflammation to cancer. Epigenetics & Chromatin 2015; 8:7.
62. Mathelier A, Zhao X, Zhang AW, Parcy F, Worsley-Hunt R, Arenillas DJ, et al. JASPAR 2014: an extensively expanded and updated open-access database of transcription factor binding profiles. Nucleic acids research 2014; 42:D142-7.
63. Hutchins AP, Diez D, Takahashi Y, Ahmad S, Jauch R, Tremblay ML, et al. Distinct transcriptional regulatory modules underlie STAT3's cell type-independent and cell type-specific functions. Nucleic Acids Res 2013; 41:2155-70.
64. Saeed S, Quintin J, Kerstens HHD, Rao NA, Aghajanirefah A, Matarese F, et al. Epigenetic programming during monocyte to macrophage differentiation and trained innate immunity. Science (New York, NY) 2014; 345:1251086-.
65. Care MA, Cocco M, Laye JP, Barnes N, Huang Y, Wang M, et al. SPIB and BATF provide alternate determinants of IRF4 occupancy in diffuse large B-cell lymphoma linked to disease heterogeneity. Nucleic acids research 2014; 42:7591-610.
66. Gertz J, Savic D, Varley KE, Partridge EC, Safi A, Jain P, et al. Distinct properties of cell-type-specific and shared transcription factor binding sites. Molecular cell 2013; 52:25-36.
67. Tussiwand R, Lee W-L, Murphy TL, Mashayekhi M, Wumesh KC, Albring JC, et al. Compensatory dendritic cell development mediated by BATF-IRF interactions. Nature 2012; 490:502-7.
68. Wu F, Zhang W, Shao H, Bo H, Shen H, Li J, et al. Human effector T cells derived from central memory cells rather than CD8+T cells modified by tumor-specific TCR gene transfer possess superior traits for adoptive immunotherapy. Cancer Letters 2013; 339:195-207.
69. Martinez FO, Helming L, Milde R, Varin A, Melgert BN, Draijer C, et al. Genetic programs expressed in resting and IL-4 alternatively activated mouse and human macrophages: similarities and differences. Blood 2013; 121:e57.
70. Spiller KL, Wrona EA, Romero-Torres S, Pallotta I, Graney PL, Witherel CE, et al. Differential gene expression in human, murine, and cell line-derived macrophages upon polarization. Experimental cell research 2016; 347:1-13.
71. Nagy Z, Tora L. Distinct GCN5/PCAF-containing complexes function as co-activators and are involved in transcription factor and global histone acetylation. Oncogene 2007; 26:5341-57.
72. Ramsey SA, Knijnenburg TA, Kennedy KA, Zak DE, Gilchrist M, Gold ES, et al. Genome-wide histone acetylation data improve prediction of mammalian transcription factor binding sites. Bioinformatics 2010; 26:2071-5.
73. Sahoo A, Alekseev A, Tanaka K, Obertas L, Lerman B, Haymaker C, et al. Batf is important for IL-4 expression in T follicular helper cells. 2015; 6:7997.
74. Kurachi M, Barnitz RA, Yosef N, Odorizzi PM, DiIorio MA, Lemieux ME, et al. The transcription factor BATF operates as an essential differentiation checkpoint in early effector CD8+ T cells. Nature immunology 2014; 15:373-83.
75. Punkenburg E, Vogler T, Büttner M, Amann K, Waldner M, Atreya R, et al. Batf-dependent Th17 cells critically regulate IL-23 driven colitis-associated colon cancer. Gut 2016; 65:1139-50.
76. Hoffman Nolan J, Parker Benjamin L, Chaudhuri R, Fisher-Wellman Kelsey H, Kleinert M, Humphrey Sean J, et al. Global Phosphoproteomic Analysis of Human Skeletal Muscle Reveals a Network of Exercise-Regulated Kinases and AMPK Substrates. Cell Metabolism; 22:922-35.
77. Schaffer BE, Levin RS, Hertz NT, Maures TJ, Schoof ML, Hollstein PE, et al. Identification of AMPK phosphorylation sites reveals a network of proteins involved in cell invasion and facilitates large-scale substrate prediction. Cell metabolism 2015; 22:907-21.
78. Tonachini L, Monticone M, Di Marco E, Zerega B, Cancedda R, Castagnola P. Chondrocyte protein with a poly-proline region is a novel protein expressed by chondrocytes in vitro and in vivo. Biochimica et Biophysica Acta (BBA) - Gene Structure and Expression 2002; 1577:421-9.

79. Tonachini L, Monticone M, Puri C, Tacchetti C, Pinton P, Rizzuto R, et al. Chondrocyte protein with a poly-proline region (CHPPR) is a novel mitochondrial protein and promotes mitochondrial fission. Journal of Cellular Physiology 2004; 201:470-82.
80. Monticone M, Tonachini L Fau - Tavella S, Tavella S Fau - Degan P, Degan P Fau - Biticchi R, Biticchi R Fau - Palombi F, Palombi F Fau - Puglisi R, et al. Impaired expression of genes coding for reactive oxygen species scavenging enzymes in testes of Mtfr1/Chppr-deficient mice.
81. Monticone M, Tonachini L Fau - Tavella S, Tavella S Fau - Degan P, Degan P Fau - Biticchi R, Biticchi R Fau - Palombi F, Palombi F Fau - Puglisi R, et al. Impaired expression of genes coding for reactive oxygen species scavenging enzymes in testes of Mtfr1/Chppr-deficient mice. Reproduction 2007; 134:483-92.
82. Wang K, Zhang Dl, Long B, An T, Zhang J, Zhou LY, et al. NFAT4-dependent miR-324-5p regulates mitochondrial morphology and cardiomyocyte cell death by targeting Mtfr1. Cell Death &Amp; Disease 2015; 6:e2007.
83. Kar P, Mirams Gary R, Christian Helen C, Parekh Anant B. Control of NFAT Isoform Activation and NFAT-Dependent Gene Expression through Two Coincident and Spatially Segregated Intracellular Ca(2+) Signals. Molecular Cell 2016; 64:746-59.
84. Sompol P, Furman JL, Pleiss MM, Kraner SD, Artiushin IA, Batten SR, et al. Calcineurin/NFAT Signaling in Activated Astrocytes Drives Network Hyperexcitability in Aβ-Bearing Mice. The Journal of Neuroscience 2017; 37:6132.
85. Nieves-Cintrón M, Hirenallur-S D, Nygren PJ, Hinke SA, Dell'Acqua ML, Langeberg LK, et al. AKAP150 participates in calcineurin/NFAT activation during the down-regulation of voltage-gated K(+) currents in ventricular myocytes following myocardial infarction. Cellular signalling 2016; 28:733-40.
86. Cai B, Wang G, Chen N, Liu Y, Yin K, Ning C, et al. Bone marrow mesenchymal stem cells protected post-infarcted myocardium against arrhythmias via reversing potassium channels remodelling. Journal of Cellular and Molecular Medicine 2014; 18:1407-16.
87. Monticone M, Panfoli I, Ravera S, Puglisi R, Jiang MM, Morello R, et al. The nuclear genes Mtfr1 and Dufd1 regulate mitochondrial dynamic and cellular respiration. Journal of Cellular Physiology 2010; 225:767-76.
88. Hägg S, Ganna A, Van Der Laan SW, Esko T, Pers TH, Locke AE, et al. Gene-based meta-analysis of genome-wide association studies implicates new loci involved in obesity. Human Molecular Genetics 2015; 24:6849-60.
89. Locke AE, Kahali B, Berndt SI, Justice AE, Pers TH, Day FR, et al. Genetic studies of body mass index yield new insights for obesity biology. Nature 2015; 518:197-206.
90. Speliotes EK, Willer CJ, Berndt SI, Monda KL, Thorleifsson G, Jackson AU, et al. Association analyses of 249,796 individuals reveal eighteen new loci associated with body mass index. Nature genetics 2010; 42:937-48.
91. Wang J, Xie Y, Bai X, Wang N, Yu H, Deng Z, et al. Targeting dual specificity protein kinase TTK attenuates tumorigenesis of glioblastoma. Oncotarget 2018; 9:3081-8.
92. Keysar S, Eagles J, Miller B, Jackson BC, Chowdhury FN, Reisinger J, et al. Salivary gland cancer patient-derived xenografts enable characterization of cancer stem cells and new gene fusions associated with tumor progression. Clinical Cancer Research 2018.

9. Acknowledgements

I would like to thank many people that helped me during my last 3.5 years of PhD and contributed to the successful to completion of my PhD projects.

I would like to thank my PhD Supervisor PD. Dr. Dmitry Namgaladze for financing my PhD project and conference travels along with his invaluable recommendations, care, support and trust in me. From the day I joined the lab to this day where I saw ends meet, I have evolved in not only my scientific aptitude but also my research vision and career goals. Dr. Dmitry Namgaladze played a major part in shaping the prospective path for my research, for which I am eternally grateful.

Prof. Dr. Bernhard Brüne for his suggestions, comments, scientific criticism and finally the opportunity to learn in his laboratory at the Institute of Biochemistry I. Our weekly Institute seminars were a key for PhD students like me to expand their scientific knowledge.

The entire Institute of Biochemistry I for their daily help, guidance and healthy working atmosphere. I would also like to thank my friends and family, without whose support, this would be hard to achieve.

Prof. Dieter Steinhilber for the supervision and assessment of my dissertation.

This study was supported by grants from Deutsche Forschungsgemeinschaft [NA429/2-2].

10. Curriculum Vitae

SAHIL GUPTA

sahilgupta@inbox.com

MOBILE [redacted]

PERSONAL

Born: 17.10.1990, Dehradun, India

[redacted]

Languages: English, German, Hindi

STRENGTHS

Enthusiastic, Curious, Persistent, Analytical

PUBLICATIONS

- ***Gupta S et.al*** , IL-6 augments IL-4-induced polarization of primary human macrophages through synergy of STAT3, STAT6 and BATF transcription factors, Oncoimmunology, 2018:1-17
- *Snodgrass RG, Zezina E, Namgaladze D,**Gupta S***, Angioni C, Geißlinger G, Lütjohann Dand Brüne B,* (2018), A Novel Function for 15-Lipoxygenases in Cholesterol Homeostasis and CCL17 Production in Human Macrophages, Frontiers in Immunolog, doi: 10.3389/fimmu.2018.01906
- *Boß M, Newbatt Y, **Gupta S*,** Collins I, Brüne B, Namgaladze D.,* AMPK-independent inhibition of human macrophage ER stress response by AICAR, Sci Rep. 2016 ;6:32111
- *Atale N*, **Gupta S***, Yadav UC, Rani V. (*equal contribution)* Cell-death assessment by fluorescent and nonfluorescent cytosolic and nuclear staining techniques., J Microsc. 2014 ; 255(1):7-19.
- *Dey B*, Thukral S*, Krishnan S*, Chakrobarty M*, **Gupta S***, Manghani C*, Rani V*., (*all authors contributed equally)* DNA-protein interactions: methods for detection and analysis., Mol Cell Biochem. 2012 ;365(1-2): 279-99

EDUCATION

PhD, Cell signaling in Macrophages and Tumor microenvironment
Goethe University Frankfurt
1.12.2014-31.07.2018 *Frankfurt*

- Guidance towards independent investigation with an interdisciplinary approach

Masters in Biology
Ludwig Maximilian University
GPA 1.8/5 (1: best)
1.10.2012-1.09.2014 *Munich*

- Five research internships and six months masters thesis, helped me troubleshoot and develop analytical thinking

Bachelors in Biotechnology
Jaypee Institute of Information Technology
GPA 7.4/10 (10: best)
Jul 2008- Jun 2012 *Noida, India*

- One year Bachelor thesis and determination to make significant contribution in the scientific community in prospective future.

High school Diploma, CBSE
N.K.Bagrodia Public School Rohini, Sec-9
82.2/100 100: Best
Jul 2006- Jul 2008 *Delhi, India*

- Graduated in Physics, Biology, Chemistry, English and Mathematics

TECHNICAL SKILLS

In Vitro	
In Vivo	
Bioinformatics	
Ex Vivo	
RNA Sequencing	

Molecular Biology

- CRISPR/Cas9 KO in cell lines, Chromatin Immunoprecipitation
- Next generation sequencing library prepration (RNA)
- Luciferase (Firefly/Renilla) Assay, Gene Expression Analysis
- High-throughput cloning, site directed mutagenesis
- T cell, Monocyte extraction (Dyna magnetic beads)

In Vitro

- Cell culture: Cell lines and primary cell cultures (macrophages)
- Functional and activity assays (Generation of 3D tumor spheroids, tumor killing assay, Chemotaxis, Migration and Invasion assays)

*Continued on next page

LONG TERM GOAL

Leading team in multi-disciplinary studies defining the role of aneuploidy and immune cells in cancer cells crosstalk.

INTERESTS

Aneuploidy and Cancer immunology

TIMELINE

- *1.08-1.12 2018* Programming in R,Department for Applied Bioinformatics, Frankfurt
- *1.12.2014-31.07.2018* PhD, Goethe University Frankfurt Germany (DE)
- *1.03-30.08 2014* Master Thesis, Max Planck Institute of Heart & Lung Research, Bad Nauheim, DE
- *1.10-30.12 2013* Internship, Adolf-Butenandt-Institute, Munich, DE
- *1.07-31.09 2013* Internship, Max Planck Institute of Psychiatry, Munich, DE
- *1.05-30.06 2013* Internship, Gene Zentrum Munich, DE
- *1.02-31.03 2013* Internship, Clinic for Radiotherapy & Radiooncology Munich, DE
- *1.12.2012-31.01.2013* Internship, Zoology State Collection, Munich, DE
- *1.10.2012-31.09.2014* Masters in Biology Ludwig Maximilian University Munich, DE
- *1.06.2011-30.08.2012* Bachelor Thesis, JIIT, Noida, India (IND)
- *1.06-31.07 2011* Internship, Sir Gangaram Hospital (SGRH), Centre of Medical Genetics, New Delhi, IND
- *1.12.2010-31.01.2011* Internship, All India Institute of Medical Sciences, Transplant Immunology & Immunogenetics Department, New Delhi, IND
- *1.06.2008-30.08.2012* Bachelors in Biotechnology Jaypee Institute of Information Technology (JIIT), Noida, India

In Vivo/ex Vivo

- Handling/Disecting mice and chicken embryos
- Isolation of various organs like liver, spleen, lung, thymus,heart, bone marrows
- Ex vivo culture (BMDMs differentiation)

Protein Purification & Characterization

- ELISA: Serum immunoglobulins, secreted cytokines
- Chromatography (Size Exclusion Chromatography, Gel Filtration S200 GL10/300 ,S75 GL10/300, HiTrap HPQ Ion exchange)
- Protein pulldown and Protein Expression (Baculovirus Expression System), Periplasmic extraction in BL-21
- Protein Extraction (Ni-NTA, His Tag)
- Spectroscopy (Fluoresence (Qubit), UV-Vis (Nanodrop), Bradford Assay (Bio-Rad)

Cell Biology

- Bacterial culture and characterization, yeast culture, etc.
- FACS of different immune cells populations
- Immuno-fluorescence assays, Immunohistochemistry Confocal microscopy (LSM series), Live cell imaging

Bioinformatics & Softwares

- Functional Genomics (Sequence analysis, Gene Expression Analysis, Pathway Analysis),
- Practicing coding for NGS data analysis
- Protein prediction, Gene Annotation, Data Mining, 3D Reconstruction software (Amira, Image J, Fiji) Imaris, Chimera

CONFERENCES

- Poster presentation at *'Turning molecular information into novel cancer therapies on* 'IL-6 augments IL-4-induced polarization of primary human macrophages through STAT3, STAT6 and BATF' from 25-27.09.2018 at Frankfurt Cancer conference, Germany.
- Poster presentation at *'Macrophage Biology in single cell era'* organized by Prof. Dr. Martin Guilliams and Jo Van Ginderachter, VIB - U Gent Center for Inflammation Research, Belgium from 26-27 Oct.17.
- Attended RMU-RNA Salon "*Genomics approaches in RNA biology*" 3rd Mini Symposium on "Medical RNomics" on September 11'2017 at Natural Science Campus of Justus-Liebig University Gießen, Germany
- Poster presentation at *Myeloid Cells (D3) Keystone Conference* on '*Mechanism of IL-4/-6 synergism in regulating CCL18*' from April 10-14, 2016 in Killarney Ireland.
- Attended 7th *University Cancer Centre Science Day* on October 7 , 2016 in Frankfurt, Germany.
- Attended 2nd Symposium on *Tumor microenvironment crosstalk* organized by Prof. Dr. Florian Greeten from Oct 13-14, 2016 in Frankfurt, Germany.
- Attended GE Healthcare Life Sciences conference on '*Evolving solutions in Protein Interaction Analysis*' on December 8, 2011 at JIIT, Noida, India.

JOBS

- Employed at Max Planck Institute of Neurobiology in Structure of Neocortical Circuits Group for Brain cell neuron tracking from electron microscopic data from Jan - Mar 2013.
- Employed at Helmholtz Zentrum, Neuherberg, Oberschleißheim at Prof Dr. Magdelina Gotz lab as a Student Assistant for genotyping from Aug - Oct 2013

ACHIEVEMENTS

- **Turning five years' lab experience into project proposals**

  I have designed two complete projects for my prospective future in research, which Ibelieve would be groundbreaking and novel.

- Secured GATE Biotechnology **All India Rank 82 with 99.4 percentile** (BT 3043152) among 14638 candidates on February 12, 2012.

THESIS

PhD Thesis, PD Dr. Dmitry Namgaladze

- Mechanism and physiological relevance of IL-4 and IL-6 mediated transcriptome changes in human macrophages
- Role of MTFR1L and it's mechanism of action upon AMPK activation (ongoing second project)

Master Thesis, Prof. Dr. Didier Stainier

- Forward genetic screen: Identification of regulators in cell type differentiation of early postnatal respiratory system of p7 pups (F3) in ENU mutagenized mice
  - Experimental Design and in vivo mice work

http://www.mpi-hlr.de/en/forschung/dept-iii.html

Bachelor Thesis, Assoc. Prof. Vibha Rani

- Cloning of Developmentally Regulated Protein Target sites in 13 day old Chick embryo
  - First exposure into long term practical lab experience and troubleshooting

http://www.jiit.ac.in/faculty_jiit.php?id=18341722&dep=bt&page=0

INTERNSHIPS

- Assembly studies of the MSL complex and characterization of the human ortholog of the MSL's protein MLE (RHA)
  Adolf-Butenandt-Institute, Prof. Dr.Peter Becker
  http://www.molekularbiologie.abi.med.uni-muenchen.de/ueber_uns/becker/index.html
- Quantification of Gene expression (SLPI, MMP-9, OSM) in corticosteroid and TNF-α induced PBMC and granulocytes in Multiple Sclerosis (MS) patients.
  Max Planck Institute of Psychiatry, Prof. Dr. F. Weber
  http://www.psych.mpg.de/135251/research_report_411133?c=2007220
- Cloning, expression and binding assays for sirpa-16-33 triplebody variants against Acute myeloid Leukemia (AML) with mutated sirp alpha binding site
  Gene Zentrum, Prof. Dr. Karl Peter Hopfner
  http://w/ww.hopfner.genzentrum.lmu.de
- Comparison of the pattern of DNA damage,induced by Hydrogen Peroxide and Hydroxy- urea,to the replication structure of CV-1 cells
  Klinik und Poliklinik für Strahlentherapie und Radioonkologie, PD Dr. Friedl
  http://www.klinikum.uni-muenchen.de/Klinik-und-Poliklinik-fuer-Strahlentherapie-und-Radioonkologie/de/direktion/bereichsleitungen/friedl_anna/index.html
- Soft Part 3D visualization by serial sectioning and reconstruction of internal anatomy of mollusc Wirenia argentea and Otis
  ZSM Munich, Dr. Bernhard Ruthensteiner
  https://www.zsm.mwn.de/eve/staff.htm

11. List of Publications

1. **Gupta S** et.al., IL-6 augments IL-4-induced polarization of primary human macrophages through synergy of STAT3, STAT6 and BATF transcription factors, Oncoimmunology, 2018: 1-17, https://doi.org/10.1080/2162402X.2018.1494110
2. Snodgrass RG, Zezina E, Namgaladze D,**Gupta S***, Angioni C, Geißlinger G, Lütjohann D and Brüne B, A Novel Function for 15-Lipoxygenases in Cholesterol Homeostasis and CCL17 Production in Human Macrophages, 2018, doi: 10.3389/fimmu.2018.01906

3. Boß M, Newbatt Y, **Gupta S**, Collins I, Brüne B, Namgaladze D., AMPK-independent inhibition of human macrophage ER stress response by AICAR, Sci Rep. 2016 ;6:32111
4. Atale N*, **Gupta S***, Yadav UC, Rani V. (*equal contribution) Cell-death assessment by fluorescent and nonfluorescent cytosolic and nuclear staining techniques., J Microsc. 2014 ;255(1):7-19. (* equal contribution)
5. Dey B*, Thukral S*, Krishnan S*, Chakrobarty M***, Gupta S***, Manghani C*, Rani V*., (*all authors contributed equally), 'DNA-protein interactions: methods for detection and analysis', Molecular and Cellular Biochemistry, 2012 ;365(1-2):279-99 (* equal contribution)
6. **Gupta S** *and Rachana. "Respiratory Distress Syndrome and Surfactant Therapy", The Pharma Review, vol. 10, 46, pp. 64-67, Mar –Apr. 2012. (* equal contribution)

12. Poster Presentations

1. Poster presentation at ‘Turning molecular information into novel cancer therapies’ on ‘IL-6 augments IL-4-induced polarization of primary human macrophages through STAT3, STAT6 and BATF’ from 25-27.09.2018 at Frankfurt Cancer conference, Germany.
2. Poster presentation at Merck GmbH, Darmstadt on 5.06.2018 on ‘IL-6 augments IL-4-induced polarization of primary human macrophages through synergy of STAT3, STAT6 and BATF transcription factors’
3. Poster presentation at ‘Macrophage Biology in single cell era’ organized by Prof. Dr. Martin Guilliams and Jo Van Ginderachter, VIB - U Gent Center for Inflammation Research, Belgium from 26-27 Oct.17
4. Poster presentation at Myeloid Cells (D3) Keystone Conference on 'Mechanism of IL-4/-6 synergism in regulating CCL18' from April 10-14, 2016 in Killarney Ireland.

13. Erklärung

D E C L A R A T I O N

I herewith declare that I have not previously participated in any doctoral examination procedure in a mathematics or natural science discipline.

Frankfurt am Main, ….....(Date) …….

(Signature)

Author’s Declaration

I herewith declare that I have produced my doctoral dissertation on the topic of **‘Functional and mechanistic insights into cytokine induced macrophage polarization’**

independently and using only the tools indicated therein. In particular, all references borrowed from external sources are clearly acknowledged and identified. I confirm that I have respected the principles of good scientific practice and have not made use of the services of any commercial agency in respect of my doctorate.

Frankfurt am Main, ...(Date)……

(Signature)